

EVALUATION OF NATURAL DRAUGHT WET-COOLING TOWER PERFORMANCE UNCERTAINTIES

by

Daniël van der Merwe

Thesis presented in partial fulfilment of the requirements for the degree Master of Science in Engineering
at Stellenbosch University



Thesis supervisor: Mr H.C.R. Reuter
Thesis co-supervisor: Prof. D.G. Kröger

Department of Mechanical Engineering
Stellenbosch University
March 2007

DECLARATION

I, Daniël van der Merwe, the undersigned, hereby declare that the work contained in this thesis is my own original work and has not previously, in its entirety or in part, been submitted at any university for a degree.

Signature

Date

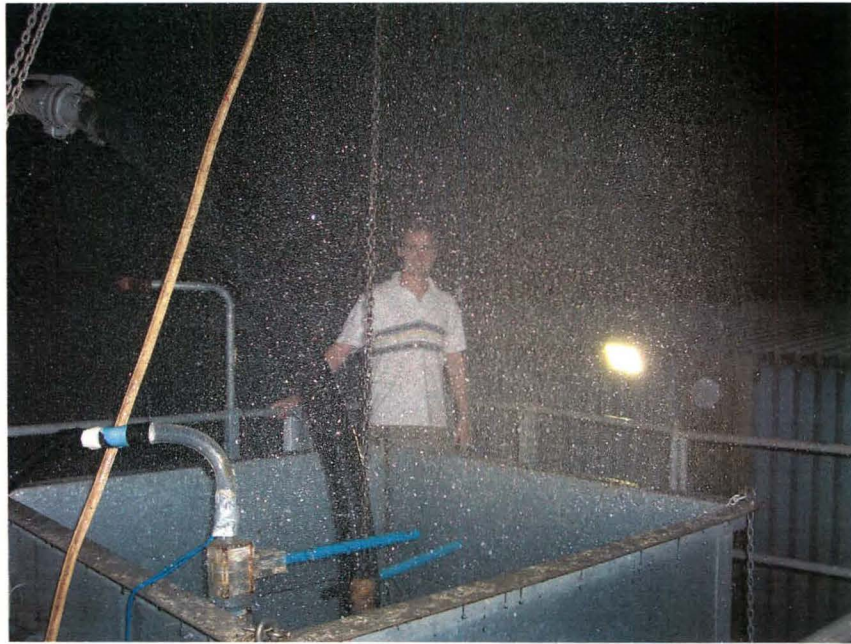
ABSTRACT

A natural draught wet-cooling tower (NDWCT) was modelled using the Merkel method with an improved energy equation as recommended by Kloppers and Kröger (2005a) – referred to as the Improved Merkel method. The improved energy equation is used for calculating the heat rejection rate of the tower and includes the energy associated with water evaporation. The sensitivity indexes of a NDWCT were calculated numerically with the Improved Merkel method model. It was found that the performance of a NDWCT is most sensitive to the fill Merkel number. The “Natklos” fill test facility at Stellenbosch University was used to estimate typical uncertainties found in fill performance characteristics. The zeroth order uncertainty for the Merkel number and loss coefficient was calculated to be 0.2100 m^{-1} and 0.4248 m^{-1} , respectively, while the first order uncertainty for the Merkel number and loss coefficient was calculated to be 0.1933 m^{-1} and 0.2008 m^{-1} , respectively. ASME requires that the uncertainty in tower capability has to be less than 6 % for a NDWCT performance test to be deemed ASME approved. Propagating typical measurement uncertainties found in NDWCT test standards and experimental data into the tower capability showed that the 6 % uncertainty limit imposed by ASME is unrealistic and too stringent. Performance curve generator (PCG) is a software package developed that generates NDWCT performance curves. With these performance curves it is possible to easily and effectively adjust the off-design test results in order to determine whether the NDWCT has met its guarantee or not.

SAMEVATTING

Die werksverrigting van 'n natuurlike trek nat koeltoring (NTNT) is gemodelleer deur gebruik te maak van die Merkel metode met 'n verbeterde energie vergelyking, soos aanbeveel deur Kloppers en Kröger (2005a) –Verbeterde Merkel metode. Die energie vergelyking word gebruik om die toring se tempo van warmteoordrag te bereken en sluit die energieverlies as gevolg van verdamping in. Die Verbeterde Merkel metode model was gebruik om die sensitiwiteits-indekse van 'n NTNT te bepaal. Dié analise toon dat die toring se werksverrigting die sensitiefste is vir die pakking se Merkel getal. Die Natklos pakkings-toetsfasiliteit aan die Universiteit van Stellenbosch was gebruik om tipiese onsekerheid in die pakkings-prestasielkarakteristieke te bepaal. Die zero-orde onsekerheid in die Merkel getal en verlieskoëffisiënt was bereken as 0.2100 m^{-1} en 0.4248 m^{-1} , onderskeidelik, terwyl die eerste-orde onsekerhede bereken was as 0.1933 m^{-1} en 0.2008 m^{-1} , onderskeidelik. Die toelaatbare onsekerheid in toringvermoë vir 'n NTNT aanvaardingstoes volgens ASME is 6 %. Deur tipes meetonsekerhede, soos gegee deur NTNT aanvaardings-toesstandaarde sowel as eksperimentele data, deur te propageer, word 'n onsekerheid veel groter as die toelaatbare 6 % gegenereer. 'n Renekaarpakket, genaamd Performance Curve Generator (PCG), is ontwikkel om werksverrigtinginskurwes vir 'n NTNT te genereer. PCG se werksverrigtinginskurwes maak dit moontlik om maklik te bepaal of a NTNT sy ontwerpseriteria bereik het of nie.

Aan Ma en Pa



ACKNOWLEDGMENTS

Thanks to my heavenly Father, Jesus Christ for giving me the strength and will to complete this thesis.

My mom and dad, who always believed and encouraged me during the last two years.

Dawie Viljoen (a.k.a. Dangerous Dave) and Darren Pierce, for their friendship, invaluable inputs and willingness to always help with the performance tests.

To Mr. Cobus Zietsman, whom without I would have been totally lost during the performance tests.

The Bester family for housing me during the last part of my thesis.

My supervisors, Mr. H.C.R. Reuter and Prof. D.G. Kröger for their guidance and support.

My friends for their support and interest in my project.

TABLE OF CONTENTS

Declaration	i
Abstract	ii
Samevatting	iii
Dedication	iv
Acknowledgements	v
Table of contents	vi
List of figures	ix
List of tables	xi
List of symbols	xii
CHAPTER 1. INTRODUCTION	1-1
1.1. General overview	1-1
1.2. Motivation	1-3
1.3. Objectives	1-5
1.4. Approach and layout of thesis	1-6
CHAPTER 2. MODELLING OF NDWCT PERFORMANCE	2-1
2.1. Introduction	2-1
2.2. Merkel method with an improved energy equation	2-1
2.3. NDWCT modelling with and without inclusion of evaporation	2-6
2.4. Poppe method	2-8
2.5. Comparison of the Improved Merkel and Poppe method	2-8
2.6. Conclusion	2-9
CHAPTER 3. FILL PERFORMANCE TEST FACILITY	3-1
3.1. Introduction	3-1
3.2. Presenting fill performance characteristics	3-2
3.3. Experimental setup and test procedure	3-3
3.4. Evaluation of experimental setup and test procedure	3-7
3.5. Combined water trough and spray zone performance test	3-9
3.6. Fill performance test	3-12
3.7. Uncertainty analysis	3-14
3.8. Conclusion	3-16
CHAPTER 4. FILL PERFORMANCE STANDARD TEST PROCEDURE	4-1
4.1. Introduction	4-1
4.2. Pipe and instrument diagram	4-1
4.3. Check list	4-3
4.4. Photographs of equipment	4-7

4.5.	Conclusion	4-9
CHAPTER 5. NDWCT PERFORMANCE EVALUATION		5-1
5.1.	Introduction	5-1
5.2.	NDWCT sensitivity indexes	5-1
5.3.	Performance test code comparative study	5-2
5.4.	Conclusion	5-8
CHAPTER 6. CONCLUSION AND RECOMMENDATIONS		6-1
6.1.	Conclusion	6-1
6.2.	Recommendations	6-3
CHAPTER 7. REFERENCES		7-1
APPENDIX A. THERMOPHYSICAL PROPERTIES		A-1
A.1.	Introduction	A-1
APPENDIX B. UNCERTAINTY ANALYSIS		B-1
B.1.	Introduction	B-1
B.2.	Basic concepts and definitions	B-1
B.3.	Propagation of uncertainty into the result	B-5
APPENDIX C. PROCESSING OF EXPERIMENTAL DATA		C-1
C.1.	Introduction	C-1
APPENDIX D. FILL PERFORMANCE UNCERTAINTY ANALYSIS		D-1
D.1.	Introduction	D-1
D.2.	Sensitivity indexes	D-1
D.3.	Zeroth order analysis, $i = 0$	D-2
D.4.	First order analysis, $i = 1$	D-5
D.5.	N'th order analysis	D-7
APPENDIX E. AIR PRESSURE DROP EQUATION		E-1
E.1.	Introduction	E-1
E.2.	Pressure drop over the fill	E-1
E.3.	Using a pressure transducer	E-2
APPENDIX F. CALIBRATION OF MEASUREMENT EQUIPMENT		F-1
F.1.	Introduction	F-1
F.2.	Pressure transducers	F-1
F.3.	Water mass flow rate	F-2
F.4.	Air-vapour mass flow rate	F-4

F.5.	Water trough catchment ratio	F-6
APPENDIX G. WATER TROUGH AND SPRAY ZONE PERFORMANCE TEST DATA		G-1
G.1.	Introduction	G-1
APPENDIX H. FILL PERFORMANCE TEST DATA		H-1
H.1.	Introduction	H-1
APPENDIX I. PERFORMANE CURVE GENERATOR (PCG)		I-1
I.1.	Introduction	I-1
I.2.	Generating performance curves	I-1
I.3.	PCG	I-3
APPENDIX J. CONFIGURATION OF NDWCT'S		J-1
J.1.	Introduction	J-1
APPENDIX K. AMBIENT TEMPERATURE GRADIENT		K-1
K.1.	Introduction	K-1
K.2.	Derivation of the pressure difference between ground level and a point at an elevation z external to the tower	K-1
K.3.	Ambient temperature gradient as independent input parameter	K-3

LIST OF FIGURES

Figure 1-1: Schematic of a simplified vapour power cycle	1-1
Figure 1-2: Schematic of a NDWCT	1-2
Figure 1-3: Layout of power plant developing process	1-4
Figure 2-1: Application of Merkel numbers in NDWCT modelling	2-3
Figure 2-2: Simplified psychrometric chart showing properties of air exiting the fill	2-9
Figure 3-1: Fill types, (a) Film , (b) Splash, (c) Trickle pack	3-1
Figure 3-2: Layout of fill test facility, all dimensions in mm	3-3
Figure 3-3: Picture of fill test facility	3-3
Figure 3-4: Pipe and instrument diagram of fill test facility	3-4
Figure 3-5: Nozzle air pressure drop measurement used to determine air-vapour mass flow rate	3-5
Figure 3-6: Layout of thermocouples upstream of nozzles	3-5
Figure 3-7: Pipe and instrument diagram of counter flow fill test section	3-6
Figure 3-8: Schematic side view of water troughs	3-7
Figure 3-9: Inlet velocity profile, $v_{avi} = 1.822$ m/s,	3-8
Figure 3-10: Inlet velocity profile, $v_{avi} = 3.658$ m/s,	3-8
Figure 3-11: Pipe and instrument diagram of water troughs and spray zone performance test	3-10
Figure 4-1: Pipe and instrument diagram of fill test facility	4-2
Figure 4-2: Pipe and instrument diagram of counter flow fill test section	4-3
Figure 4-3: Photographs of equipment	4-7
Figure B-1: Random and systematic errors	B-1
Figure B-2: Hypothetical distribution of data and experimental setup.	B-4
Figure B-3: Propagation of uncertainty into a result	B-6
Figure E-1: Elementary control volume in the vertical fill test section	E-1
Figure E-2: Setup for measuring Δp_{fi}	E-2
Figure F-1: Calibration curves of pressure transducers	F-2
Figure F-2: Calibration tank for orifice plate, all dimensions in mm	F-3
Figure F-3: Water mass flow rate determined with orifice plate and calibration tank.	F-3
Figure F-4: Nozzle pressure drop measurement used to determine air-vapour mass flow rate	F-4
Figure F-5: View of nozzles when looking upstream	F-5
Figure F-6: Water trough catchment ratio with WDS 200 mm above troughs	F-6
Figure F-7: Water trough catchment ratio with 1.524 m of fill installed	F-6
Figure G-1: Water trough and spray zone performance characteristic data compared to Equation (3.8) and (3.9)	G-2
Figure G-2: Water trough and spray zone performance characteristic data compared to Equation (3.11) to (3.14)	G-3
Figure G-3: Effect on water trough and spray zone Merkel number using Equation (G.2) and (G.3) to determine T_{wo}	G-4
Figure G-4: Air pressure drop over water troughs – dry test with WDS at 200 + 1524 mm above water troughs	G-5

Figure G-5: Air pressure drop over water troughs – dry test with WDS at 200mm above water troughs	G-5
Figure H-1: Fill performance characteristic data compared to Equation (3.15) and (3.16)	H-2
Figure H-2: Fill performance characteristic data compared to Equation (3.20) to (3.23)	H-3
Figure H-3: Effect on fill Merkel number using Equation (H.2) and (H.3) to determine T_{wo}	H-4
Figure H-4: Air pressure drop over fill only – dry test	H-4
Figure I-1: Step 1 of generating performance curves	I-1
Figure I-2: Step 2 of generating performance curves	I-2
Figure I-3: Step 3 of generating performance curves	I-2
Figure I-4: Histogram for difference in T_{wo} values	I-2
Figure I-5: PCG – Cooling tower dimensions tab	I-3
Figure I-6: PCG – Other specifications tab	I-3
Figure I-7: PCG – Performance curve generator tab	I-4
Figure I-8: PCG – performance curves	I-4

LIST OF TABLES

Table 2-1: Kloppers (2003) and current Improved Merkel method comparison	2-7
Table 2-2: Improved Merkel method and Kröger (1998 and 2004) comparison	2-7
Table 3-1: Summary of fill performance test uncertainty components	3-14
Table 5-1: Sensitivity indexes for NDWCT	5-1
Table 5-2: Sensitivity indexes for NDWCT using Equation (5.9)	5-4
Table 5-3: Test codes allowable calibration uncertainty limits	5-5
Table 5-4: Zero order uncertainties according to NDWCT performance test standards	5-5
Table 5-5: N th order uncertainties according to NDWCT performance test standards	5-6
Table 5-6: Fill performance uncertainties	5-7
Table B-1: Interpretation of finite statistics	B-3
Table D-1: Sensitivity indexes for fill test facility	D-2
Table D-2: Data logger specifications, all units in volts (DC)	D-3
Table D-3: Spatial uncertainties of thermocouples.	D-4
Table D-4: Summary of zeroth order analysis	D-4
Table D-5: First order uncertainty due to variation in parameters	D-6
Table D-6: Summary of first order analysis	D-6
Table F-1: Calibration data of pressure transducers	F-1
Table F-2: Air pressure drop over each nozzle, Pa	F-5
Table F-3: Comparison of Equation (F.2) and (F.3)	F-5
Table G-1: Legend for Figure G-1 and G-2	G-1
Table G-1: Water trough and spray zone performance test data	G-6
Table H-1: Legend for Figures H-1 and H-2	H-1
Table H-2: Fill performance test data	H-5
Table I-1: Files included in the PCG package	I-5

LIST OF SYMBOLS

A	Area, m ²
a	Surface area per unit volume, m ⁻¹
B	Systematic uncertainty
C	Confidence level
c	Coefficient or constant
c _p	Specific heat at constant pressure, J/kgK
c _v	Specific heat at constant volume, J/kgK
D	Diameter, m, or dimension
d	Diameter, m
F	Force, N
G	Mass velocity, kg/sm ²
g	Gravitational acceleration, m/s ²
H	Height, m
h	Heat transfer coefficient, W/m ² K
i	Enthalpy, J/kg
i _{fg}	Latent heat, J/kg
K	Loss coefficient, or constant
k	Thermal conductivity, W/mK
L	Length, m
M	Molecular weight, kg/mole, or Merkel, or number of locations, or number of instruments
m	Mass flow rate, kg/s
N	Number of measurements
n	Number of independent parameters
P	Poppe, or random uncertainty
PC	Performance curve
p	Pressure, Pa
Q	Heat transfer rate, W
R	Gas constant, J/kgK, or result
Ry	Characteristic flow parameter, m ⁻¹
r	Radius, m
S	Standard deviation
T	Temperature, °C or K
t	Thickness, m
U	Uncertainty
u	Uncertainty as defined by Equation (D.4)
v	Velocity, m/s
w	Humidity ratio, kg water vapour/kg dry air
X	Mole fraction, or specific variable
x	General variable
y	Experimental value

z Elevation, m

GREEK SYMBOLS

α Relaxation factor
 α_e Kinetic energy coefficient
 α_m Momentum velocity distribution correction factor defined by Equation (E.4)
 β Diameter ratio, or systematic error
 γ c_p/c_v
 Δ Differential
 δ Total error, or small amount
 ϵ Threshold for residual of an iterative solution, or random error
 θ Sensitivity index
 μ Dynamic viscosity, kg/ms
 ξ Temperature lapse rate, K/m
 ρ Density, kg/m³
 σ Area ratio, or surface tension, N/m
 ϕ Humidity ratio

DIMENSIONLESS GROUPS

Fr_D Desimetric Froude number, $\rho v^2/(\Delta\rho dg)$
 Le_f Lewis factor, $h/(c_p h_d)$
 Re Reynolds number, $\rho v L/\mu$ for a plate, or $\rho v d/\mu$ for a tube

SUBSCRIPTS

a Air
abs Absolute
amb Ambient
atm Atmosphere
av Mixture of dry air and water vapour
c Cold, or curve
cor Correlated
ct Cooling tower
ctc Cooling tower contraction
cte Cooling tower expansion
D Design
d Diameter
de Drift eliminator
dp Data point
evap Evaporation
fd Friction and drag
fi Fill
fr Frontal or face

fs	Fill support
H	Height
h	Hot
i	Inlet
K	Loss coefficient
M	Merkel
m	Mean, or momentum, or model, or mass transfer, or mixture
max	Maximum
n	Nozzle
o	Outlet
or	Orifice plate
P	Poppe, or predicted
rz	Rain zone
s	Saturation, or shell
sp	Spray
th	Throat
tot	Total
tr	Troughs
ts	Tower supports
tus	Upstream cross-section
w	Water
wb	Wet bulb
wd	Water distribution system

ACRONYMS

DALR	Dry adiabatic lapse rate, K/m
EPC	Engineering procurement and construction
IPP	Independent power producer
TC	Tower capability
WP	Work point
RSS	Root sum square

CHAPTER 1. INTRODUCTION

1.1. General overview

Figure 1-1 shows a schematic of a simple Rankine cycle used to generate electricity. Sub-cooled liquid water is pumped (Pump 1) to the boiler where heat is transferred to the water. Water enters the boiler as a compressed liquid and exits as superheated steam. The superheated steam expands in the turbine, producing shaft work to drive an electric generator. The temperature and pressure of the steam drops during expansion and usually enters the condenser as a saturated liquid-vapour mixture which rejects heat to cooling water. The hot cooling water is pumped (Pump 2) to the cooling tower where it is re-cooled by rejecting heat to the atmosphere.

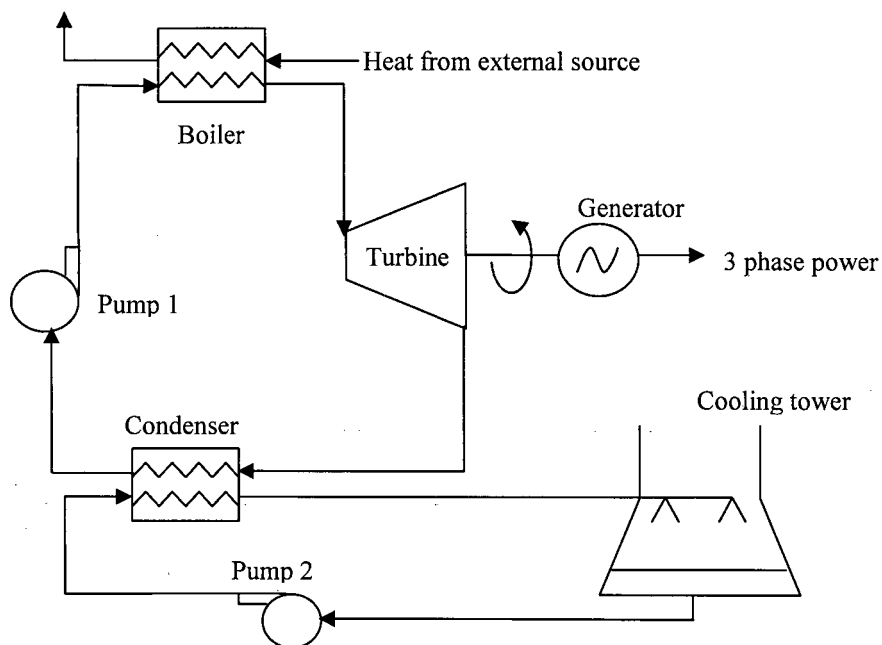


Figure 1-1: Schematic of a simplified vapour power cycle

Cooling towers are mainly classified according to the type of draught. Draught in natural draught towers is established by the difference in density between the colder, heavier atmospheric air and the warmer, moist air-vapour mixture inside the tower. For mechanical draught towers the draught is either induced or forced by a fan or blower. In a mechanical forced draught tower, the fan or blower is situated at the air inlet to the tower and for induced towers the fan is situated at the air outlet. Another classification is whether the water comes in direct contact with the air, known as wet-cooling, or not, known as dry-cooling. In wet-cooling towers, energy is removed from the water by means of heat and mass transfer. The heat transfer is due to the difference in water and air stream temperatures (Newton's law of cooling, also called convection heat transfer); whereas the driving force for the mass transfer is the difference in water vapour concentration in the air at the water surface and the free air stream (Fick's law of diffusion). In dry-cooling towers water is pumped through finned tubes where energy is removed via convection heat transfer. The working of wet-cooling towers is discussed in the next section. Hybrid towers make use of both wet- and dry-cooling and are suited for regions with relatively scarce water supplies. In this thesis the focus is on natural draught wet-cooling towers (NDWCT) shown in Figure 1-2 on the next page (to illustrate parts clearer the figure has not been drawn according to scale).

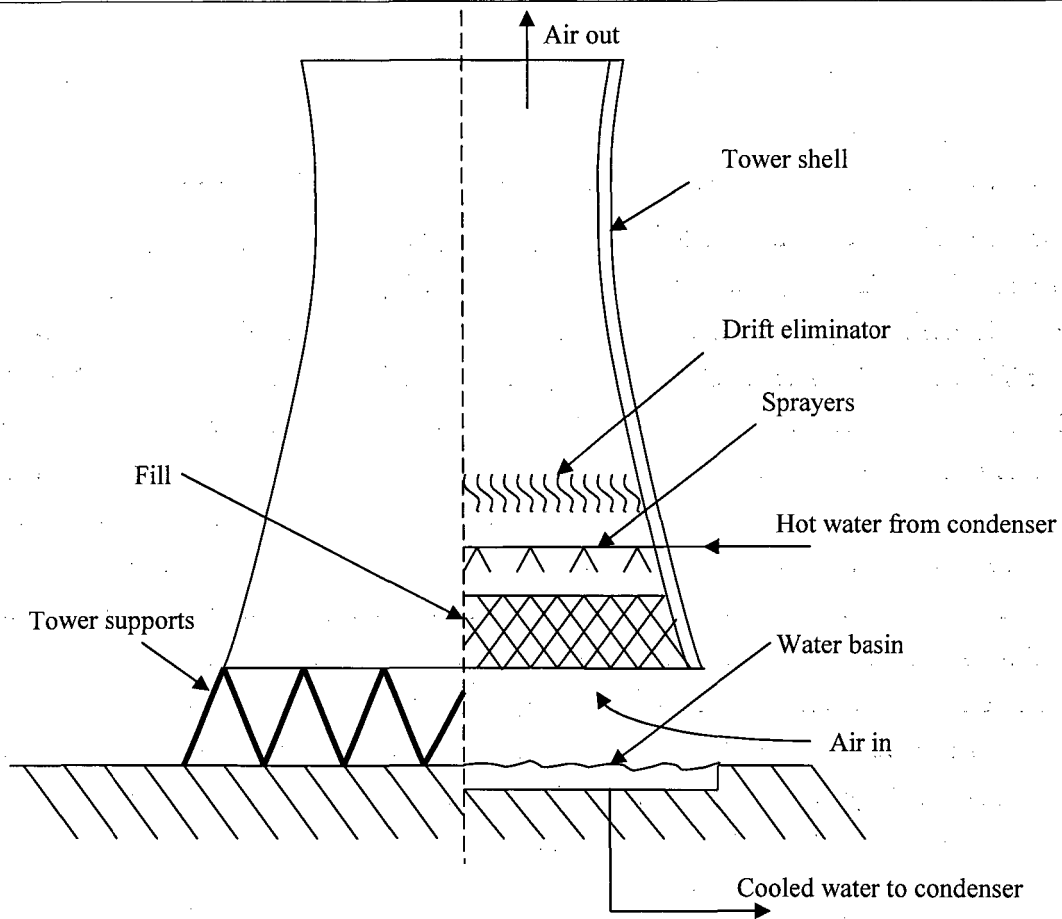


Figure 1-2: Schematic of a NDWCT

Hot water is pumped from the condenser (Pump 2, Figure 1-1) to the sprayers from where it falls onto a layer of fill material. Different types of fill include film fill, splash type and trickle pack. The purpose of the fill is to increase the heat transfer area of the water with minimum air stream pressure drop. The water trickles through the fill and then falls into the rain zone where further cooling of the water takes place. Water accumulates in the water basin from where it is pumped (Pump 2) back to the condenser. Make-up water is used to compensate for the loss in water due to evaporation. In addition a portion of the circulating water must be systematically removed as blowdown. This is to prevent the build up of dissolved solids in the circulating water. A small portion of the water is also lost due to drift. This happens when small droplets are entrained in the air stream moving through the tower. The air enters at the bottom of the tower and due to the heat and mass transfer processes becomes humid and warm, decreasing its density as it moves upward. The draught will stabilise once enough heat is absorbed by the air to induce a draught that can overcome all the pressure losses. The drift eliminators are used to capture droplets that are entrained in the air stream.

Performance of a cooling tower refers to a combination of criteria, such as plume compliance, noise level, water loss due to drift, water quality, etc. In this thesis, performance will refer to the temperature of the water in the basin of the cooling tower.

1.2. Motivation

Power generation is a multi-billion Rand industry. In the current South African environment this industry is experiencing unprecedented growth. In this year (2006), South Africa's electricity utility Eskom, announced an R97 billion capital expansion program over the next five years, (Gcabashe (2006)), of which half will be spent on expanding generation capacity, (O'Connor (2006)). A brief review of this programme is given by O'Connor (2006) who states that South Africa will need to expand generation capacity at a rate of more than 1500 MW a year. This is based on a 4.2 % annual growth in electrical demand. According to Kenny (2006) the electricity growth between 1956 and 1995 was twice the economic growth. Kenny (2006) predicts an increase in demand of 2100 MW per year. This conservative estimate is based on a 6 % annual growth in electrical demand, equal to the economic growth envisaged by the South African government. Expansion of generation capacity is thus inevitable. Eskom is building, returning to operation or doing feasibility and pre-feasibility studies on the following, (O'Connor (2006)):

- 25000 MW of potential coal-fired generation
- 6900 MW of potential gas-fired power generation
- 4800 MW of potential hydro generation

An interesting initiative investigated by Eskom is supercritical steam-cycle technology for coal-fired generation plants. This technology can provide efficiencies of 39 % for a dry-cooled plant and up to 43 % for a wet-cooled plant, (O'Connor (2006)). Van der Linde (2006) estimates the cost of a new electricity plant (coal or gas) between R5bn and R7bn per 1000 MW which translates to more or less R10bn per year invested in the expansion of generation capacity.

Many factors influence the financial risk in a project, one of them is the uncertainty in performance (see Appendix B for a discussion on the subject of uncertainty). The commercial value of a cooling tower is directly related to its performance. Contractual performance guarantees are therefore subject to high penalties, which are based on the projected life cycle production loss value associated with performance deficits. Therefore any performance uncertainties pose a financial risk, which is generally covered by including design or commercial safety margins. What is the performance uncertainty? What is an acceptable safety margin? How can performance uncertainty be reduced? What is the lowest uncertainty possible? etc. Not knowing the answers to these questions is the origin of risk or then financial risk for companies. To see where this fits into the bigger picture consider Figure 1-3 on the next page which gives a simplified layout of the developing process for a power plant.

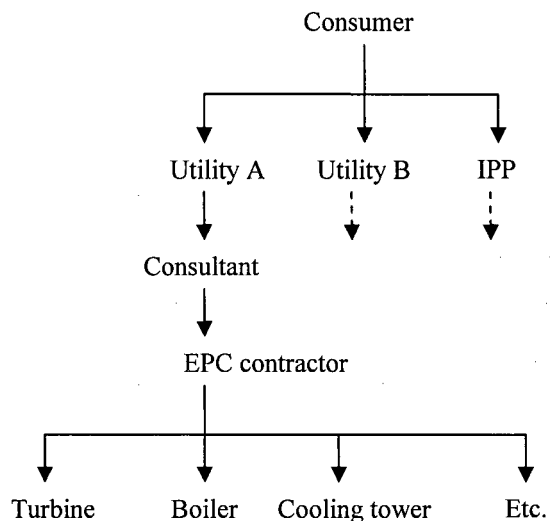


Figure 1-3: Layout of power plant developing process

First there are consumers who need a supply of electricity - in the South African context this would be the government or industry. This need is satisfied by a utility such as ESKOM or an independent power producer (IPP). The main difference between a utility and an IPP is that a utility is government owned, while an IPP is a privately owned enterprise. When a new power plant is developed, depending on the in-house know-how available, IPP's and utilities make use of consultants. The role of the consultant is to: establish the consumer's requirements, investigate local resources, obtain the necessary design information, conduct feasibility and optimisation studies, advise which technologies are best suited, develop financial models and write the design specifications, facilitate the tender process, evaluate tenders, negotiate tenders, write the purchase contract and manage the purchase contract. The engineering procurement and construction (EPC) contractor receives the order to supply the plant and execute the contract. The EPC contractor places purchase orders with sub-contractors for the supply of sub-systems, such as the turbine, boiler, cooling tower, etc. and manages these contracts. Remember that an IPP or utility is paying for a plant with a specific output. Therefore, an IPP or utility would want to make sure that they get what they are paying for. Penalties are therefore imposed on any performance deficits.

Within a specified time frame after the power plant is commissioned the performance of the power plant must be tested. If the power plant meets the guaranteed performance then no more testing will be done and the project is considered successful. If the power plant does not meet the guaranteed performance, then the EPC contractor must pay penalties to the consumer. This event will set forth performance testing of each component of the power plant by the EPC contractor. If a specific component does not meet its specifications then that supplier will pay penalties to the EPC contractor. This penalty will be related to the penalty that the EPC contractor has to pay to the consumer. In general, the trade-off is thus to reduce financial risk by reducing the uncertainty in performance, however, if the guaranteed uncertainty in performance is too stringent, the supplier's financial risk increases since the chances of exceeding the guaranteed uncertainty in performance increases. From this point of view and the fact that Eskom is planning a 25000 MW expansion of potential coal-fired generation – which inevitably will lead to expansion of cooling towers or cooling equipment – the motivation of this thesis can be stated as follows:

The motivation for this thesis is to investigate the uncertainties in a NDWCT performance test in order to equip both the supplier and owner with knowledge on the nature of the total uncertainty incurred. This knowledge will reduce the financial risk of such a project for both the supplier and owner and will make the project more competitive.

1.3. Objectives

Performance test codes like the CTI acceptance code (2000), VDMA (1991), ASME PTC (2003) and the BS 4485 (1988) have been developed to describe the instruments, test procedure and analysis methodology of test data to be used in determining the performance of cooling tower and evaporative cooling equipment. These codes stipulate *inter alia* the allowable uncertainties in measurements, as well as the method of propagating these uncertainties into the result of a performance test. A cooling tower's performance test is then deemed acceptable if the total uncertainty in the result is within certain limits. What these codes do not discuss is the nature of the uncertainty. Nature of the uncertainty refers to questions like:

- For which parameter is the result the most sensitive?
- Given the current equipment and setup, what is the smallest uncertainty that can be achieved?
- What contributes the most to the total uncertainty?
- How can the uncertainty be reduced?
- Is it necessary to use more accurate expensive instrumentation or measuring techniques?
- Which instruments need accurate calibration?
- Should we design for uncertainty?

The last question is of particular importance. In short, with a proper uncertainty analysis one can determine that certain parameters need better measuring techniques and can thus be incorporated in the design beforehand. Altering the design afterwards to accommodate for measuring equipment can become a significant financial burden for a company, (ASME PTC (2003)). In light of the above questions, the objectives of this thesis can be stated as:

- *Develop a model to predict NDWCT performance*
- *Use model to conduct a sensitivity analyses of a NDWCT*
- *Perform an uncertainty analysis of a typical NDWCT performance test*
- *Investigate test facility used to determine fill performance characteristics*
- *Use experimental data to conduct a sensitivity analysis of fill performance characteristics*
- *Perform an uncertainty analysis of a typical fill performance test*
- *Develop a model to generate performance test curves*
- *Generate a fill performance standard test procedure*
- *Evaluate performance test codes*

The NDWCT model is used in the sensitivity analysis and the generation of the performance curves. A sensitivity analysis gives one an indication of how sensitive a result is to change in its input parameters. This process, as well as the propagation of uncertainty into a result, is discussed in detail in Appendix B and D.

Modelling a NDWCT inevitably requires the use of experimental data in the form of empirical equations, for instance the performance of the fill. It will be seen in subsequent chapters that the fill plays a major

part in the performance of a NDWCT. With this in mind it was decided to investigate the measuring techniques, data reduction methods and test procedure of a typical fill performance test. The outcome of this investigation is to determine what the typical uncertainties are in fill performance characteristics.

Performance tests are rarely done at the specified designed operating conditions. Performance test curves are then used to adjust the off-design test results in order to determine whether the guarantee is met or not. The method used to generate and use performance test curves are discussed in performance test codes. Generating these curves can become quite involved. Because performance curves are such an important contractual component and used in the evaluation of NDWCT performance test data, an attempt was made to try and improve existing performance curve generating techniques and to quantify uncertainties by using the curve method as opposed to the computer model to project off-design performance. Finally, all the uncertainties must be combined in order to determine the total uncertainty found in a NDWCT performance test.

No standard or formal test procedure exists for the fill test facility used. It will be seen later on that a typical fill performance test includes a large number of variables, settings, instrumentation, time and costs. The absence of a formal test procedure and data reduction methods could lead to poor repeatability and uncertainty of test results. It was therefore decided to create a fill performance standard test procedure.

With all the necessary tools available a simplified comparison of NDWCT performance test codes was made. This is done to justify the techniques used in this thesis and to give the reader an idea of how the interpretation of test results could differ depending on the NDWCT performance test code used. However, the main objective of this exercise is to evaluate whether or not the allowable uncertainty in the result of the performance test is achievable or not. It also answers some of the questions pertaining to the nature of NDWCT performance uncertainty.

1.4. Approach and layout of thesis

This section describes the approach and layout of the thesis. Each chapter heading starts off with the objective at which the chapter is aimed.

CHAPTER 1. INTRODUCTION

Chapter 1 gives a brief description of cooling towers and basic operation. It highlights the motivation for the thesis accompanied by the objectives and layout.

CHAPTER 2. MODELLING OF NDWCT PERFORMANCE

- *Develop a model to predict NDWCT performance*

This chapter discusses the theory and method used to model a NDWCT. The model is based on the Merkel method with an improved energy equation. The improved energy equation is used to determine the heat rejection rate of the NDWCT and includes the loss in water mass flow rate due to evaporation. A numerical comparison is given between the Merkel method with and without the inclusion of evaporation.

Lastly, a qualitative comparison is given between the Merkel method with an improved energy equation and the Poppe method.

CHAPTER 3. FILL PERFORMANCE TEST FACILITY

- *Investigate test facility used to determine fill performance characteristics*
- *Use experimental data to conduct a sensitivity analysis of fill performance characteristics*
- *Perform an uncertainty analysis of a typical fill performance test*

The fill test facility is used to determine fill performance characteristics. The objectives of the experiment were (a) to investigate the test facility and test procedure and (b) use results of a typical fill performance test to conduct a sensitivity and uncertainty analysis. The uncertainty in the fill performance was then propagated into the performance of a NDWCT as can be seen in Chapter 5. In Chapter 3 the following topics were discussed:

- Presenting fill performance characteristics
- Experimental setup
- Experimental procedure
- Evaluation of experimental setup and test procedure with regard to:
 - Blockage effect of water troughs
 - Water mass flow rate
 - Air mass flow rate
 - Water outlet temperature
- Results of the combined water trough and spray zone performance test
- Results of fill performance test
- Uncertainty analysis

The experimental procedure discussed in this chapter gives the reader an overview of how the experiment was conducted. Warm-up, preparation of equipment and shut-down details are discussed in Chapter 4. A sample calculation showing the processing or reduction of experimental data is given in Appendix C.

CHAPTER 4. FILL PERFORMANCE STANDARD TEST PROCEDURE

- *Generate a fill performance standard test procedure*

As was stated in the objectives for this thesis, the absence of a standard fill test procedure and data reduction method could lead to poor repeatability and uncertainty of test results. It will be seen that a typical fill performance test comprises a considerable amount of variables, settings, instrumentation, time and costs. With this in mind, the sole objective of this chapter was to formulate a fill performance standard test procedure. The data reduction and calibration techniques used in this thesis automatically forms part of the test procedure. The procedure is presented in the form of a check list. The procedure addresses the following topics:

- Pipe and instrument diagram
- Check list
 - Heating of the water in the reservoir
 - Tunnel preparation
 - Start-up
 - Performance testing
 - Shut-down

- Test conditions
- Recommendations
- Time frame

CHAPTER 5. NDWCT PERFORMANCE EVALUATION

- *Use model to conduct a sensitivity analyses of a NDWCT*
- *Perform an uncertainty analysis of a typical NDWCT performance test*
- *Develop a model to generate performance test curves*
- *Evaluate performance test codes*

The first objective of this chapter is to determine whether or not the prescribed uncertainties in the result of NDWCT performance test are achievable or not. The second objective is to investigate what the effect of typical fill performance characteristic uncertainties is on tower performance. The chapter starts off with the sensitivity indexes of a typical NDWCT, followed by a comparison of the different performance test standards used. The comparative section discusses the following: performance parameter, validity of test, measurement uncertainties and uncertainty analysis. The results obtained from the fill performance test discussed in Appendix D and Chapter 3 is also incorporated in the comparative study.

CHAPTER 6. CONCLUSION AND RECOMMENDATIONS

This chapter gives an overview of the main conclusions drawn from the thesis. Most of the conclusions are repeated from the conclusions made in each chapter. The chapter also gives recommendations for future work.

NOTE

The reader is advised to first read the section on uncertainty analysis, Appendix B. This section discusses the terminology and the uncertainty analysis procedure used in this thesis. The procedure and terms are not discussed again in the main chapters and the author assumes that reader is familiar with this section. In some numerical examples answers are given to many decimal places. This should not be interpreted as a degree of accuracy as these values were taken from computer program outputs.

CHAPTER 2. MODELLING OF NDWCT PERFORMANCE

2.1. Introduction

The NDWCT model is used to evaluate the sensitivity indexes, i.e. partial differentials, of Equation (B.17). It is also used to generate the performance curves as described in Appendix I. The Merkel (1926) and Poppe (1991) methods are the two most popular methods used to model the heat and mass transfer of the evaporative process in a NDWCT. The e-NTU method developed by Jaber and Webb (1989) makes use of the same simplifying assumptions as the Merkel method. Due to its simplifying assumptions the Merkel method is not as accurate as the more complicated Poppe method. Kloppers and Kröger (2005a) recommends modelling a NDWCT using the Merkel method with an improved energy equation. The improved energy equation is used for calculating the heat rejection rate of the tower and includes the energy associated with water evaporation. In this chapter the Merkel method with an improved energy equation is discussed. A numerical comparison is given between the Merkel method with and without the inclusion of evaporation. Lastly, a qualitative comparison is given between the Merkel method with an improved energy equation and Poppe method

2.2. Merkel method with an improved energy equation

CONSERVATION OF ENERGY AND MASS

The one dimensional governing equations for heat and mass transfer in a counter flow evaporative process, e.g. fill region, according to the Merkel method are

$$\frac{di_{ma}}{dz} = \frac{h_d a_{fr} A_{fr}}{m_a} (i_{masw} - i_{ma}) \quad (2.1)$$

and

$$\frac{dT_w}{dz} = \frac{m_a}{m_w} \frac{1}{c_{pw}} \frac{di_{ma}}{dz} \quad (2.2)$$

where

h_d = mass transfer coefficient, $\text{kg/m}^2\text{s}$

a_{fr} = area density of the fill, i.e. the wetted area divided by the corresponding volume of fill, m^{-1}

A_{fr} = frontal area of the fill, m^2

m_w = inlet water mass flow rate, kg/s

i_{masw} = enthalpy of saturated air at air-water interface which is at T_w , J/kg

i_{ma} = enthalpy of main air stream, J/kg

T_w = bulk water temperature, K

m_a = dry air mass flow rate, kg/s

c_{pw} = specific heat of water at constant pressure, J/kgK

dz = incremental height, m

Combining Equations (2.1) and (2.2) and integrating yields

$$\begin{aligned}
 Me_{fiM} &= \frac{h_d A}{m_w} = \frac{h_d a_{fi} A_{fr} L_{fi}}{m_w} = \int_{T_{wo}}^{T_{wi}} \frac{c_{pw} dT_w}{(i_{masw} - i_{ma})} \\
 &\approx \frac{c_{pwm} (T_{wi} - T_{wo})}{4} \left(\frac{1}{\Delta i_{(1)}} + \frac{1}{\Delta i_{(2)}} + \frac{1}{\Delta i_{(3)}} + \frac{1}{\Delta i_{(4)}} \right)
 \end{aligned} \tag{2.3}$$

where

L_{fi} = height of fill, m

T_{wo} = temperature of water exiting the fill, K

T_{wi} = temperature of water entering the fill, K

The enthalpy differentials are dependent on the following intermediate temperatures:

$$T_{w(1)} = T_{wo} + 0.1(313.15 - T_{wo})$$

$$T_{w(2)} = T_{wo} + 0.4(313.15 - T_{wo})$$

$$T_{w(3)} = T_{wo} + 0.6(313.15 - T_{wo})$$

$$T_{w(4)} = T_{wo} + 0.9(313.15 - T_{wo})$$

Equation (2.3) is the fill Merkel number according to the Merkel method. The state of air exiting the fill can not be calculated from Equation (2.1) and (2.2), since to achieve this one needs at least two properties. The first of Merkel's critical assumptions is that the state of air exiting the fill region is saturated. In the derivation of Equations (2.1) and (2.2) Merkel makes two more critical assumptions:

- The Lewis factor is equal to 1
- The reduction of water flow rate due to evaporation is neglected.

The integral of Equation (2.3) must be solved numerically. Many techniques have been used as discussed by Kloppers and Kröger (2005b). They found that the Chebyshev technique (right hand side of Equation (2.3)) is generally very accurate when compared to the composite Simpson rule with 100 intervals which has an error of the fourth order, (Gerald and Wheatley (1999)). The c_{pw} values can be calculated from Equation (A.19). The enthalpy of saturated air at the air water interface, i_{masw} , can be calculated from Equation (A.17). The enthalpy of the main air stream, i_{ma} , can be calculated by employing Equation (2.2).

$$\begin{aligned}
 m_a di_{ma} &= m_w c_{pwm} dT_w \\
 di_{ma} &= \frac{m_w c_{pwm} dT_w}{m_a}
 \end{aligned} \tag{2.4}$$

The energy associated with the evaporation is ignored for a second time in Equation (2.4). When modelling a NDWCT this assumption has no effect on the water outlet temperature (at most a small effect due to its influence on the draught), if applied consistently. This is explained with the aid of Figure 2.1 on the next page. The flow chart on the left hand side of Figure 2-1 depicts a simplified process followed when determining the fill Merkel number experimentally. See Chapter 3 for more details on this process. In short, the water and air inlet and outlet temperatures, as well as mass flow rates are measured and are then converted to a Merkel number using Equations (2.3) and (2.4). A curve is then fitted through the data that correlates Merkel number in terms of parameters such as water inlet temperatures and air and water mass velocities.

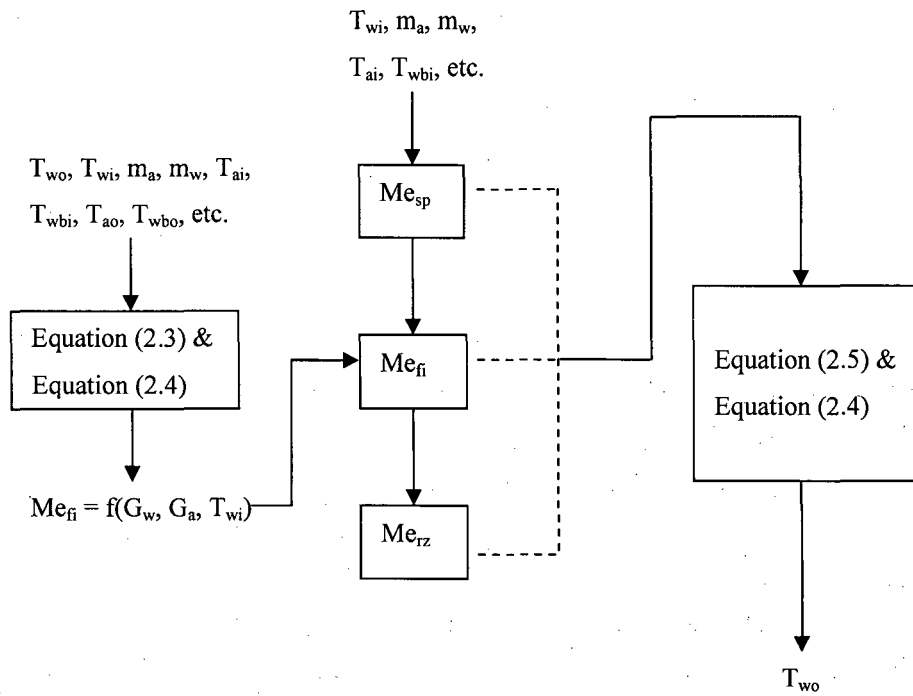


Figure 2-1: Application of Merkel numbers in NDWCT modelling

The flow chart in the middle and right hand side of Figure 2-1 shows the process followed when modelling a NDWCT. Given the same G_w , G_a and T_{wi} values as measured in the experimental setup, the correlations used in the NDWCT model should give a fill Merkel number that is equal to the experimentally determined value. This Merkel number can then be used in conjunction with Equation (2.5) and (2.4) to solve for the water outlet temperature. The Merkel numbers for the spray and rain zone are determined and used in a similar manner. Equation (2.5) shows the mathematical relationship for the middle and right hand flow charts of Figure 2-1.

$$\begin{aligned}
 Me_{sp} + Me_{fi} + Me_{rz} &= \frac{h_{sp} a_{sp} A_{sp} L_{sp}}{m_w} + \frac{h_d a_{fi} A_{fi} L_{fi}}{m_w} + \frac{h_{drz} a_{rz} A_{fi} L_{rz}}{m_w} \\
 &= \int_{T_{wo}}^{T_{wi}} \frac{c_{pw} dT_w}{(i_{masw} - i_{ma})}
 \end{aligned}
 \tag{2.5}$$

where

rz = rain zone, region below fill

sp = spray zone, region between sprayers and air outlet of fill

T_{wi} = temperature of water entering the cooling tower, K

T_{wo} = temperature of water in basin of cooling tower, K

Equation (2.5) must be solved iteratively, following the reverse process used to determine the Merkel number from experimental data. This iterative solution will again incorporate an energy balance. Since Equation (2.4) was used in the experimental setup, the same method must be used again to solve Equation (2.5). If evaporation had been included in Equation (2.4) the value of the fill Merkel number would have been different, but the water outlet temperature would still be the same since the physical process has not changed. With the water outlet temperature known we can now proceed to calculate the actual rate of heat rejected by the cooling tower. For this, the energy associated with evaporation has to be included. The improved energy equation as given by Kloppers and Kröger (2005a) is then

$$m_w c_{pwm} dT_w + m_{w(evap)} c_{pwm} T_{wo} = m_a di_{ma} \quad (2.6)$$

$$m_w c_{pwm} (T_{wi} - T_{wo}) + m_a (w_5 - w_1) c_{pwm} (T_{wo} - 273.15) = m_a (i_{ma5} - i_{ma1})$$

where

m_w = inlet water mass flow rate, kg/s

$m_{w(evap)}$ = mass of water evaporated, kg/s

w_5 = humidity ratio above the drift eliminators, kg/kg dry air

w_1 = humidity ratio at tower inlet, kg /kg

c_{pwm} = specific heat of the water evaluated at $(T_{wi} + T_{wo})/2$, J/kgK

T_{wo} = water outlet temperature, K

The subscripted numbers indicate the various locations on the tower and can be viewed in Figure I-5. Technically, the c_{pwm} value in the second term on the left hand side of Equation (2.6) should be evaluated at the water outlet temperature. However, the maximum change in c_{pw} values in the region of 330 K to 290 K is less than 0.3 %. With this in mind, and the fact that the $m_{w(evap)}$ is considerably smaller than the m_w value, it can be concluded that the c_{pw} value can be evaluated at the arithmetic mean of the inlet and outlet water temperatures. From the Merkel number, the convective heat and mass transfer coefficients can be determined with the aid of the Lewis factor, Le_f , defined as

$$\frac{h}{c_{pma} h_d} = Le_f \quad (2.7)$$

The Lewis factor indicates the relative rates of heat and mass transfer in an evaporative process. From Equation (2.3) one can thus see that an increase in Merkel number will result in an increase in the mass transfer coefficient. Since Merkel assumed Le_f equal to unity one can see from Equation (2.7) that the convective heat transfer coefficient, h , will increase proportionally with h_d . It can thus be concluded that an increase in Merkel number will result in an increase in both heat and mass transfer coefficients which will result in lower water outlet temperatures.

CONSERVATION OF MOMENTUM

The momentum equation is satisfied when the pressure differential at the mean fill height between the outside and inside of the tower is equal to the sum of the pressure drops across all the flow resistances. This equation is also known as the draught equation and is given by Kröger (1998 and 2004) for a NDWCT as

$$(p_{a1} - p_{a7}) - (p_{a1} - p_{a34}) - (p_{a34} - p_{a6}) - (p_{a6} - p_{a7}) =$$

$$\left(K_{tsfi} + K_{ctfi} + K_{rzfi} + K_{fsfi} + K_{ctefi} + K_{ffi} + K_{ctefi} + K_{spfi} + K_{wdfi} + K_{defi} \right) \times$$

$$\frac{\left(\frac{m_{av15}}{A_{fr}} \right)^2}{2\rho_{av15}} + \alpha_{e6} \frac{\left(\frac{m_{av6}}{A_{fr}} \right)^2}{2\rho_{av6}} \quad (2.8)$$

The pressure drops on the left hand side of the Equation (2.8) are given by Kröger (1998 and 2004) as

$$(p_{a1} - p_{a7}) = p_{a1} \left[1 - \left(1 - 0.00975 \frac{H_6}{T_{a1}} \right)^{3.5(1+w_1)} \left(1 - \frac{w_1}{w_1+0.62198} \right) \right] \quad (2.9)$$

$$(p_{a1} - p_{a34}) = p_{a1} \left[1 - \left(1 - 0.00975 \frac{H_3 + L_{fi}/2}{T_{a1}} \right)^{3.5(1+w_1)} \left(1 - \frac{w_1}{w_1+0.62198} \right) \right] \quad (2.10)$$

$$(p_{a34} - p_{a6}) = p_{a5} \left[1 - \left(1 + \xi_{T_{a5}} \frac{H_6 - H_3 - 0.5L_{fi}}{T_{a5}} \right)^{\xi_{T_{a5}}(w_5+0.62198)} \right] \quad (2.11)$$

$$(p_{a6} - p_{a7}) = \left(0.02 Fr_D^{-1.5} - \frac{0.14}{Fr_D} \right) \frac{\left(\frac{m_{av5}}{A_6} \right)^2}{\rho_{av6}} \quad (2.12)$$

SOLUTION ALGORITHM

The inputs to the solution algorithm as well as tower configurations are given in Appendix J. The nature of the problem renders itself to an iterative solution with the following iteration variables:

- Mean air-vapour mass flow rate though the fill, m_{av15}
- Static pressure after the drift eliminators, p_{a5}
- Air temperature after the drift eliminators, T_{a5}
- Water outlet temperature, T_{wo}
- Static pressure at tower outlet, p_{a6}

The solution converges when $\max_{res} \leq \varepsilon$, where \max_{res} is equal to the maximum absolute value of the following residuals

$$\text{Draught}_{res} = LH_{draught} - RH_{draught} \leq \varepsilon \quad (2.13)$$

$$p_{a5 res} = p_{a5 new} - p_{a5 old} \leq \varepsilon \quad (2.14)$$

$$Q_{res} = Q_w - Q_a \leq \varepsilon \quad (2.15)$$

$$Me_{res} = Me_{int} - Me_{tot} \leq \varepsilon \quad (2.16)$$

$$p_{a6 res} = p_{a6 new} - p_{a6 old} \leq \varepsilon \quad (2.17)$$

where

ε = allowable threshold of \max_{res}

$LH_{draught}, RH_{draught}$ = left hand and right hand side of Equation (2.8), Pa

$$p_{a5} = p_{a1} \left[1 - \left(1 - 0.00975 \frac{H_3 + L_{fi}/2}{T_{a1}} \right)^{3.5(1+w_1)} \left(1 - \frac{w_1}{w_1+0.62198} \right) \right]$$

$$- \left(K_{tsfi} + K_{ctfi} + K_{t_zfi} + K_{fsfi} + K_{ctcffi} + K_{ffi} + K_{ctcffi} + K_{spfi} + K_{wdfi} + K_{defi} \right) \times \frac{\left(\frac{m_{av15}}{A_{fi}} \right)^2}{2\rho_{av15}}$$

Q_w = heat rejected by water given by left hand side of Equation (2.6), W

Q_a = heat absorbed by air given by right hand side of Equation (2.6), W

Me_{int} = Merkel number given by Equation (2.5)

Me_{tot} = sum of Merkel numbers given by performance correlations

$$p_{a6} = p_{a7} + \left[0.02Fr_D^{-1.5} - \frac{0.14}{Fr_D} \right] \left(\frac{m_{av5}}{A_6} \right)^2 / \rho_{av6}$$

The variables were adjusted using the following algorithm

$$m_{av15new} = m_{av15old} + \alpha_{mav15}(Draught_{res}) \quad (2.18)$$

$$p_{a5new} = p_{a5old} + \alpha_{pa5}(p_{a5res}) \quad (2.19)$$

$$T_{a5new} = T_{a5old} + \alpha_{Ta5}(Q_{res}/Q_a) \quad (2.20)$$

$$T_{wonew} = T_{woold} + \alpha_{Two}(Me_{res}/Me_{tot}) \quad (2.21)$$

$$p_{a6new} = p_{a6old} + \alpha_{pa6}(p_{a6res}) \quad (2.22)$$

The α values indicate the corresponding relaxation factors. The variables were initialised using the technique described in Kloppers (2003). It was found that the following relaxation factors gave a converged solution ($\varepsilon = 0.001$) over the widest range of operating conditions: $\alpha_{mav15} = 1$, $\alpha_{pa5} = 0.1$, $\alpha_{Ta5} = 0.2$, $\alpha_{pa6} = 0.1$ and $\alpha_{Two} = 0.1$. A sample calculation for modelling NDWCT employing the Merkel method is given by Kröger (1998 and 2004). The Kröger (2004) method was adopted in this thesis. However, Equation (2.6) was used to determine the heat rejected by the cooling tower instead of the one given in Kröger (1998 and 2004). The following new correlations were not in the model of Kröger (1998) but were incorporated in Kröger (2004):

- Tower inlet loss coefficient, De Villiers and Kröger (1999)
- Temperature lapse rate inside the tower, Kloppers (2003)

A NDWCT sample calculation for modelling a NDWCT employing the Merkel method with an improved energy equation was done in MATHCAD 12 and can be viewed on the CD attached to this thesis.

2.3. NDWCT modelling with and without inclusion of evaporation

In this section a comparison is given for NDWCT modelling using the Merkel method with and without the inclusion of evaporation in the energy equation. The energy equation is used to determine the tower heat rejection rate. A sample calculation of NDWCT modelling employing the Merkel method without evaporation is given by Kröger (1998 and 2004). In the rest of the thesis the phrase “Improved Merkel method” will refer to the modelling of a NDWCT using the Merkel method with an improved energy equation as given by Equation (2.6). First the Improved Merkel method of Kloppers (2003) is compared with the Improved Merkel method used in this thesis, see Table 2-1. The column labelled 2006 in both Table 2-1 and 2-2 refers to the Improved Merkel method used in this thesis. The parameters that determine the performance for a given NDWCT are the air dry and wet bulb temperature at ground level, T_{a1} and T_{wb1} , atmospheric pressure, p_{a1} , ambient temperature gradient, dT_a/dz , inlet water mass flow rate, m_w , and water inlet temperature, T_{wi} . These parameters are collectively called the Work Point (WP) (see Appendix K for discussion of dT_a/dz as independent input parameter). Table 2-1 shows the results of a NDWCT with the following WP: $T_{a1} = 16.85$ °C (290 K), $T_{wb1} = 11.47$ °C (284.62 K), $p_{a1} = 84100$ Pa, $dT_a/dz = -0.00975$ K/m from ground level, $m_w = 12500$ kg/s and $T_{wi} = 40$ °C (313.15 K). The configuration of the tower is similar to the one in Kloppers (2003) and is available in Appendix J.

Table 2-1: Kloppers (2003) and current Improved Merkel method comparison

Description	Symbols	2006	Kloppers (2003)
Heat rejected by cooling tower, MW	Q	983.3	980
Water outlet temperature, K	T_{wo}	294.9	294.8
Air temperature at fill air outlet, K	T_{as}	300.3	300.4
Mean air-vapour mass flow rate through fill, kg/s	m_{av15}	16304	16300
Mass of water evaporated, kg/s	$m_{w(evap)}$	319	320

Note that the values of Kloppers (2003) had to be read from a graph. With this in mind one can conclude from Table 2-1 that the Improved Merkel method used in this thesis is consistent with the one used in Kloppers (2003). One can now proceed to compare the Improved Merkel method with the Merkel method as given by Kröger (1998 and 2004). Table 2-2 shows the results of a NDWCT with the following WP: $T_{a1} = 15.45$ °C (288.6 K), $T_{wb1} = 11.05$ °C (284.2 K), $p_{a1} = 84100$ Pa, $dT_a/dz = -0.00975$ K/m from ground level, $m_w = 12500$ kg/s and $T_{wi} = 40$ °C (313.15 K). The configuration of the tower is similar to the one in Kröger (1998 and 2004) and is available in Appendix J. Only relevant parameters are shown. The column labelled % Dev 1998 refers to the deviation between the Kröger (1998) model and the model used in this thesis, similar for % Dev 2004 and the Kröger (2004) model. Note that the Kröger (2004) model and its 2006 equivalent have a different tower configuration to that of the Kröger (1998) model and its 2006 equivalent. See Appendix J.

Table 2-2: Improved Merkel method and Kröger (1998 and 2004) comparison

Description	Symbol	2006	Kröger (1998)	% Dev 1998	2006	Kröger (2004)	% Dev 2004
Heat rejected by cooling tower, MW	Q	997.977	972.714	2.56	1003.1648	972.06	3.15
<u>Loss coefficients</u>							
Tower inlet	K_{ctfi}	6.9041	4.9472	33.02	5.68721	5.686	0.02
Rain zone	K_{rzfi}	6.52932	7.203276	-9.82	6.39427	6.474	-1.24
Fill	K_{fi}	3.94982	3.90828	1.06	3.88397	3.91657	-0.84
Spray zone	K_{spfi}	0.68211	0.67957	0.37	0.6792	0.679934	-0.11
Drift eliminator	K_{defi}	5.48667	5.47101	0.29	5.47129	5.472924	-0.03
Sum of loss coefficients	K_{sum}	25.79671	24.456	5.34	24.3615	24.476184	-0.47
<u>Merkel number</u>							
Rain zone	Me_{rz}	0.41381	0.414556	-0.18	0.41512	0.414391	0.18
Fill	Me_{fi}	0.92859	0.934026	-0.58	0.93779	0.93287	0.53
Spray zone	Me_{sp}	0.11453	0.115088	-0.49	0.11547	0.11497	0.43
Sum of Merkel numbers	Me_{tot}	1.45693	1.463671	-0.46	1.468387	1.46223	0.42
<u>Other</u>							
Cooling range ($T_{wi} - T_{wo}$), K	z	18.565	18.624	-0.32	18.664	18.6115	0.28
Mass of water evaporated, kg/s	$m_{w(evap)}$	316.40993	308.5173	2.53	318.0854	308.304	3.12
Dry air mass flow rate, kg/s	m_a	16397.01	16556.58	-0.97	16667.6	16522.464	0.87
Humidity ratio at fill air outlet, kg/kg	w_s	0.02743	0.02676	2.47	0.027212	0.02679	1.56
Enthalpy at fill air outlet, J/kg dry air	i_{mas}	96981.46	94865.621	2.21	96304.62	94947.398	1.42

From Table 2-2 one can see that loss coefficients of the tower inlet and rain zone of the 2006 model do not compare well at all with those of the Kröger (1998) model. As was stated on the previous page a new

tower inlet loss coefficient correlation was used in the current Improved Merkel method. Also, the rain zone loss coefficient of Kröger (1998) was never referred to the mean air conditions through the fill. The combined effect is that due to the higher flow resistance, the current Improved Merkel method will predict lower air mass flow rates as can be seen at the bottom part of Table 2-2. Although the Improved Merkel method predicts lower air mass flow rates, it still predicts higher heat rejection rates due to the extra energy removed as a result of evaporation. The 2006 model shows good correlation with the Kröger (2004) model. This is due to inclusion of the new correlations for the tower inlet loss coefficient and lapse rate inside the tower in the Kröger (2004) model, as well as the fact that the rain zone loss coefficient was referred in Kröger (2004) to the mean air conditions through the fill. One should remember that the nature of the problem renders itself to an iterative solution and that small deviations in the results are inevitable.

2.4. Poppe method

The Poppe method has two different sets of heat and mass transfer governing equations to accommodate for air exiting the fill that is saturated and unsaturated. Unlike Merkel's method, the Poppe method thus does not assume saturated air conditions at fill air outlet. It also includes the water loss due to evaporation in Equation (2.4). Instead of assuming a Lewis factor of 1, Poppe employs the empirical relation of Bosnjakovic (1965) to determine its value. The governing equations for heat and mass transfer according to the Poppe method can be found in Kloppers and Kröger (2005b). A discussion on the Lewis factor and its influence in cooling tower performance is found in Kloppers and Kröger (2005c).

2.5. Comparison of the Improved Merkel and Poppe method

Kloppers (2003) gives a detailed comparison of the Improved Merkel and Poppe methods of analysis. He shows that overall these two models are very close to each other. The temperature of the water in the basin of cooling tower and heat rejection rates are almost identical. The most notable deviation is the temperature of air exiting the fill and the mean air-vapour mass flow rate at hot dry ambient conditions, as well as the water evaporation rate during colder moist conditions. These deviations are now discussed.

TEMPERATURE OF AIR EXITING THE FILL AND MEAN AIR-VAPOUR MASS FLOW

The mean air-vapour mass flow rate is strongly dependent on the temperature of air exiting the fill. This is because the density of the air inside the tower is inversely proportional to the air temperature. In turn, the draught through the tower is directly proportional to the difference in density inside and outside the tower. As the density difference between the inside and outside of the tower increases, so does the pressure differential that induces the draught. The draught, or air-vapour mass flow rate, will increase until the pressure losses through the tower equal the pressure differential. The deviation in air outlet temperature, and hence the mean air-vapour mass flow rate, can be explained with the concepts of a simplified psychrometric chart shown in Figure 2-2 on the next page.

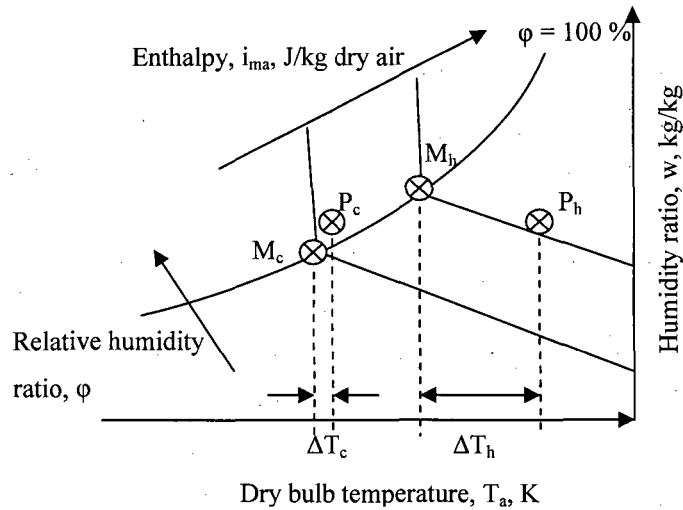


Figure 2-2: Simplified psychrometric chart showing properties of air exiting the fill

Figure 2-2 shows the properties of air exiting the fill using the Poppe and Improved Merkel method. The subscripts c refers to when cold moist ambient air is considered and h to when hot dry ambient air is considered. The symbols P and M indicate the Poppe and Improved Merkel method respectively. The figure is only illustrative and should not be interpreted as exact values. First consider the case for cold moist ambient air. The Improved Merkel method assumes that the fill air outlet conditions will be saturated, while the Poppe method predicts super-saturated air outlet conditions. The two methods predict similar enthalpies for the outlet air. In the super-saturated region of a psychrometric chart, $\phi > 100\%$, the lines of constant enthalpy are close to each other (weakly dependent on the dry bulb temperature) hence the two methods will predict similar outlet dry bulb temperatures for colder moist air, i.e. ΔT_c will be small. For hot and dry ambient air, $\phi < 100\%$, the Improved Merkel method still assumes air outlet conditions that are saturated, while the Poppe method predicts outlet air that is unsaturated. The two methods might predict similar enthalpies for the outlet air, but in the unsaturated region enthalpy is strongly dependent on outlet temperature, hence the difference in fill air outlet air temperatures at hotter, dry ambient temperatures, i.e. $\Delta T_h > \Delta T_c$. In general the Poppe method will predict a higher air outlet temperature which will result in a lower density inside the tower and hence a higher mean air-vapour mass flow rate due to the increase in driving potential. The Poppe method also predicts a slightly higher heat rejection rate and thus a lower water outlet temperature. From the figures presented by Kloppers (2003) this difference in water outlet temperatures is less than 0.1 K.

WATER EVAPORATION RATE

For colder moist ambient conditions the Improved Merkel method predicts water evaporation rates that are lower than the Poppe method. This is again due to the fact that the Merkel method assumes saturated air conditions at the fill air outlet. Air that moves from unsaturated to saturated conditions due to evaporation will acquire less water vapour than air that moves from unsaturated to super-saturated conditions.

2.6. Conclusion

With the ever growing computing capacity of modern computers, it is now possible to model the performance of complex systems such as a NDWCT using computational fluid dynamics (CFD).

However, Kröger (1998) points out that even the most sophisticated models make use of empirical or experimental data e.g. fill performance characteristics, and simplifying assumptions to avoid excessive complexity. These models are thus not necessarily better than a one dimensional model, but are essential when non-uniform flow fields in the tower are considered. This is confirmed by Mohiuddin and Kant (1991) who compared eight models predicting mechanical draught wet cooling tower performance. Mohiuddin and Kant (1991) discusses the governing equations as well as assumptions of each model. They show that the deviation from experimental data for both the one and two dimensional models is generally in good agreement. Since the objective of this thesis is not to develop a robust multi-dimensional model for a NDWCT, it was decided to use the one dimensional Improved Merkel method. This method predicts NDWCT performance that is almost identical to that of the more complicated Poppe method. This is especially the case for water outlet temperatures and heat rejection rates. Discrepancies are mainly due to Merkel's assumption of saturated air outlet conditions at the fill air outlet, which affects the following:

- Fill air outlet air temperature at hot dry ambient conditions
- Mean air-vapour mass flow rate at hot dry ambient conditions
- Water evaporation rate at colder moist conditions

The same method used to determine fill performance characteristics experimentally, must be used to model fill performance in a NDWCT, (Kloppers and Kröger (2005a)). In order to determine the Poppe number for fill in an experimental setup, the fill air outlet conditions must be measured accurately. This has been found to be almost impossible, since water droplets are usually entrained in the air stream and complicates the measurement of dry and wet bulb measurements. The Merkel method however, does not have this disadvantage and is thus an attractive method to model fill behaviour.

It was decided to model the NDWCT using the Improved Merkel method, due to its simplicity and relative accuracy compared to the more rigorous Poppe method.

CHAPTER 3. FILL PERFORMANCE TEST FACILITY

3.1. Introduction

The “Natklos” test facility at Stellenbosch University was used to determine fill performance characteristics. The objectives of the experiment were (a) to investigate the measuring techniques, data reduction methods and test procedure of the test facility and (b) use results of a typical fill performance test to conduct an uncertainty analysis. The uncertainty in the fill performance will then be propagated into the performance of a NDWCT as discussed in Chapter 5.

Cooling tower fills or packs are used to increase the heat transfer area between the water and air stream. This is done by breaking the water into smaller drops (Splash and Trickle pack) or by creating a film of water that runs down the packing (Film). Figure 3-1 shows three types of fills commonly used in cooling towers.

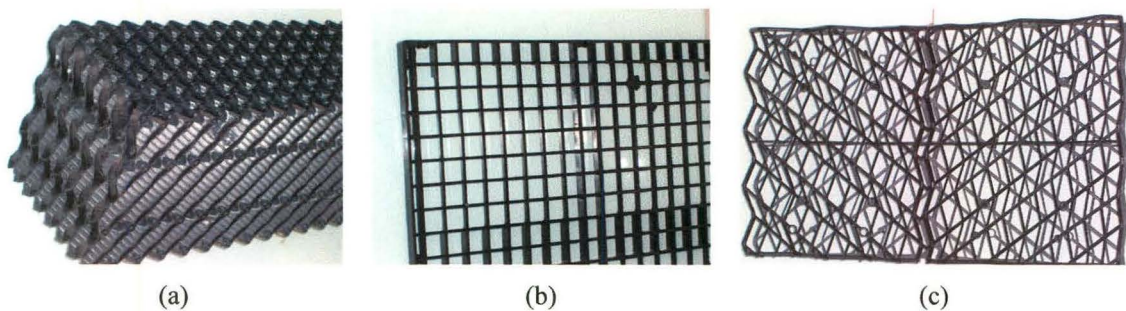


Figure 3-1: Fill types, (a) Film , (b) Splash, (c) Trickle pack

The air pressure drop created by the fill will decrease the draught through the tower and hence the heat transfer from the water to the air. Mohiuddin and Kant (1996) states the factors influencing the choice of fill are its heat transfer capability, air pressure drop, packing cost and durability. In this chapter the following topics are discussed:

- Presenting fill performance characteristics
- Experimental setup
- Experimental procedure
- Evaluation of experimental setup and test procedure with regard to:
 - Blockage effect of water troughs
 - Water mass flow rate
 - Air mass flow rate
 - Water outlet temperature
- Results of the combined water trough and spray zone performance test
- Results of fill performance test
- Uncertainty analysis

The experimental procedure discussed in this chapter gives the reader an overview of how the experiment was conducted. Warm-up, preparation of equipment and shut-down details are discussed in Chapter 4. A sample calculation showing the reduction of experimental data is given in Appendix C.

3.2. Presenting fill performance characteristics

The transfer performance is described by the fill's Merkel number or transfer coefficient correlation. The air pressure drop over the fill is described in terms of an air pressure loss coefficient correlation

3.2.1. Air pressure loss coefficient

The fill air pressure loss coefficient is determined by measuring the static air pressure drop across the fill, (Δp_{fi}), as shown in Figure E-2. The static air pressure drop across the fill measured in the counter flow test section is derived in Appendix E and is given by Equation (E.10) as

$$\Delta p_{fi} = \Delta p_{fd} + (\rho_o v_{mo}^2 - \rho_i v_{mi}^2) - (\rho_{amb} - \rho_m) L_{fi} g \quad (3.1)$$

This equation assumes uniform, incompressible, one dimensional steady state flow. The assumption of uniform, one dimensional flow is proven to be acceptable later on in this chapter. However, care should be taken when testing low resistance fill, as the blockage effect of the water troughs will cause the flow to be non-uniform at the edges of the test section. The fill static air pressure drop is due to frictional and drag effects, as well as momentum changes in the air stream due to heating and mass transfer. The third term on the right hand side of Equation (3-1) is the buoyancy force due to the density differences of the hot air inside the test section and that of the colder air inside the pressure transducer tube external to the test facility. The density of the ambient air is essentially equal to the density of the air entering the test section, i.e. ρ_{avi} . Equation (3.1) can thus be rewritten in terms of air-vapour flow rates and properties as

$$\Delta p_{fi} = \Delta p_{fd} + (\rho_{avo} v_{avo}^2 - \rho_{avi} v_{avi}^2) - (\rho_{avi} - \rho_{avm}) L_{fi} g$$

By making Δp_{fd} the subject of the above equation, an air pressure loss coefficient which is determined by frictional and drag effects only, can be defined as

$$K_{fd} = \frac{2\Delta p_{fd}}{\rho v^2} = \frac{2 \left[\Delta p_{fi} - (\rho_{avo} v_{avo}^2 - \rho_{avi} v_{avi}^2) + (\rho_{avi} - \rho_{avm}) g L_{fi} \right]}{\rho v^2} \quad (3.2)$$

In this thesis the reference conditions for the denominator was chosen to be the mean air-vapour mass flow rate, thus

$$K_{fdm} = \frac{2 \left[\Delta p_{fi} - (\rho_{avo} v_{avo}^2 - \rho_{avi} v_{avi}^2) + (\rho_{avi} - \rho_{avm}) g L_{fi} \right] \rho_{avm} A_{fr}^2}{m_{avm}^2} \quad (3.3)$$

Equation (3.3) is sometimes also given per unit length of fill, i.e. $K_{fdm1} = K_{fdm} / L_{fi}$. The air pressure drop is determined for different air and water mass flow rates. The results are then correlated using empirical equations. Kloppers and Kröger (2003) gives a summary of correlations used in the past. They also proposed a new general empirical correlation based on the ideas of the Ergun equation (1952) for air pressure drop through packed beds. The new correlation accounts for the form drag and viscous drag effects as well as the effects that are dependent on the water mass flow rate and the configuration of the fill i.e.

$$\frac{K_{fdm}}{L_{fi}} = c_1 G_w^{c_2} G_a^{c_3} + c_4 G_w^{c_5} G_a^{c_6} \quad (3.4)$$

where

L_{fi} = length of fill, m

G_w = water mass velocity, kg/sm²

G_a = air mass velocity, kg/sm^2

The coefficients c_1 to c_6 are determined from experimental data. Tests conducted at the “Natklos” test facility in September 2004, showed that the height of the fill, L_{fi} , also had a small effect. Equation (3.4) can thus be adapted to give

$$\frac{K_{fdm}}{L_{fi}} = (c_1 G_w^{c_2} G_a^{c_3} + c_4 G_w^{c_5} G_a^{c_6}) L_{fi}^{c_7} \tag{3.5}$$

3.2.2. Transfer coefficient

The Merkel number of the fill is determined from Equation (2.3). The September 2004 tests showed that the following equation correlated well with experimental data

$$\frac{Me}{L_{fi}} = c_1 G_w^{c_2} G_a^{c_3} L_{fi}^{c_4} T_{wi}^{c_5} \tag{3.6}$$

3.3. Experimental setup and test procedure

A schematic layout and picture of the fill test facility is shown in Figure 3-2 and 3-3, followed by a pipe and instrument diagram.

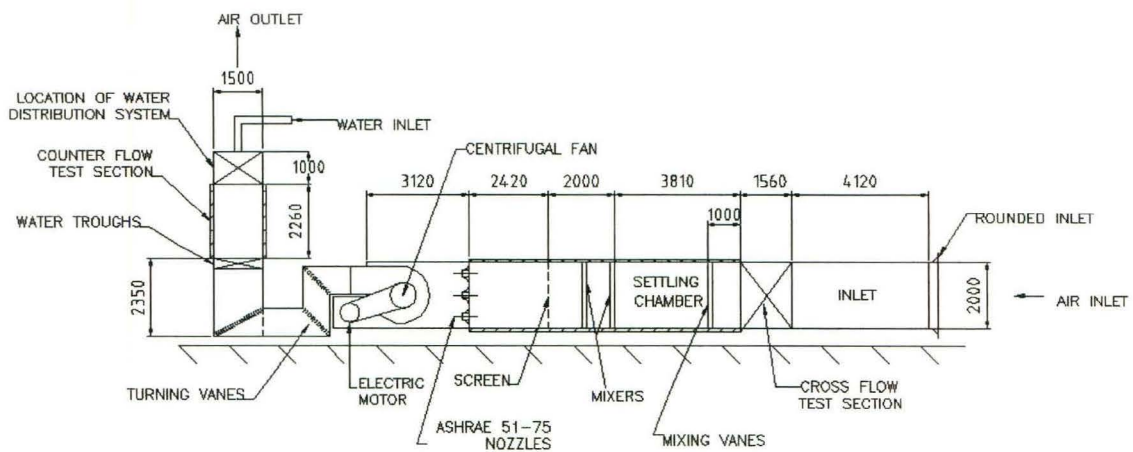


Figure 3-2: Layout of fill test facility, all dimensions in mm

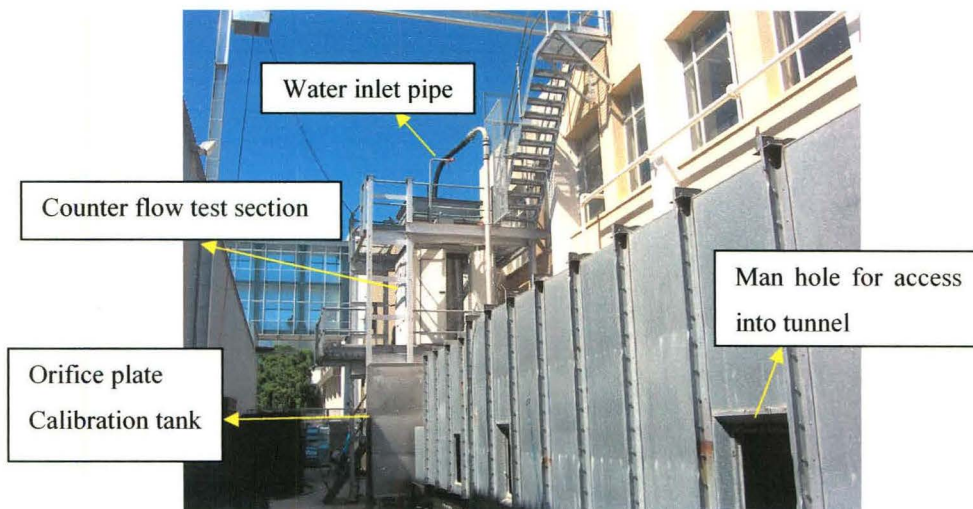


Figure 3-3: Picture of fill test facility

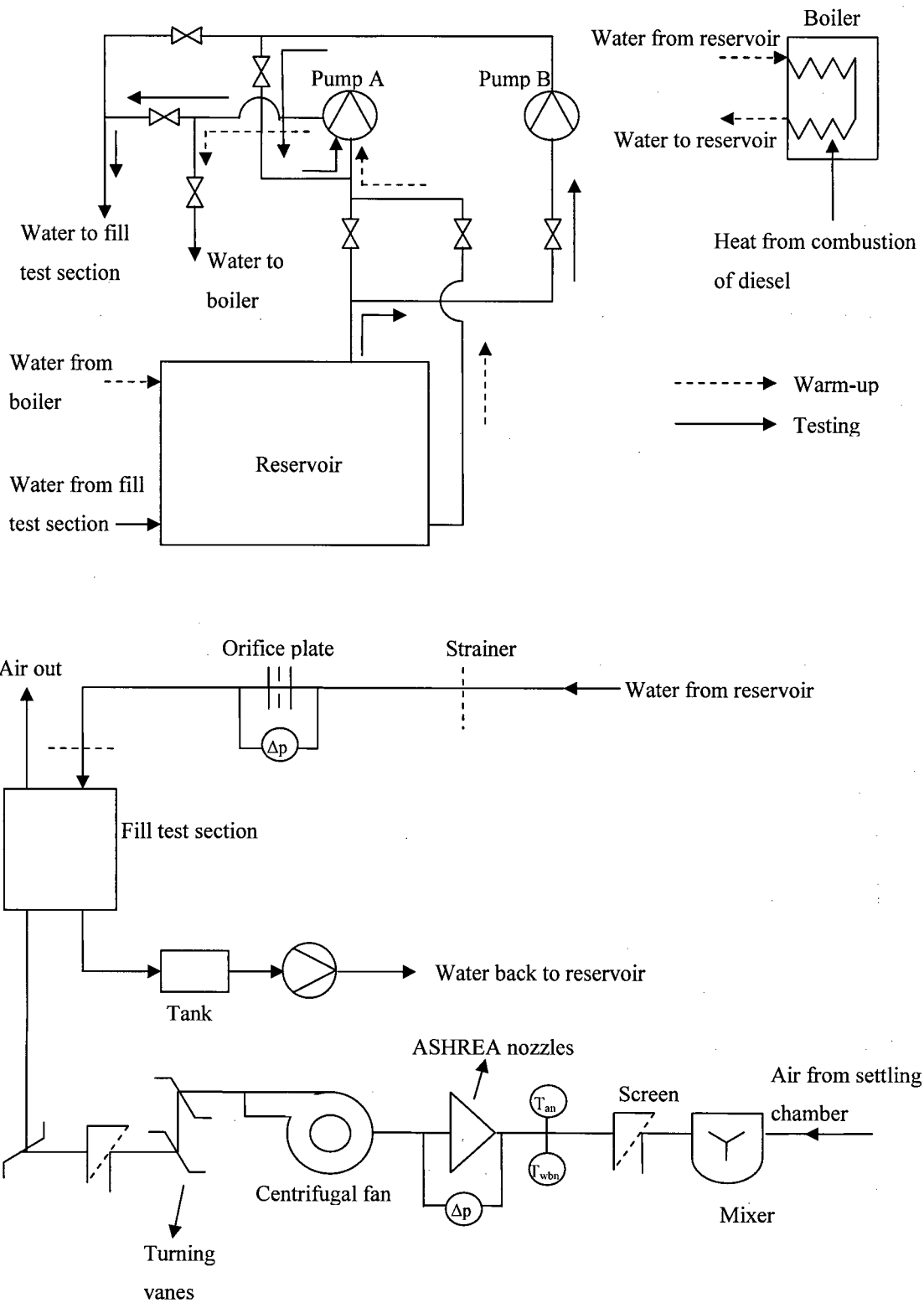


Figure 3-4: Pipe and instrument diagram of fill test facility

Hot water is pumped from an underground reservoir to the top of the test section. The reservoir has a capacity of 45 m³. The water is heated by recycling it through a 150 kW diesel-fired boiler. During a test, the heated water is pumped from the top of the reservoir to the test section where it is cooled. The cooled water is then fed back to the bottom of the reservoir. This ensures that stratification occurs in the reservoir and that the water temperature entering the fill test section will remain almost constant for short test runs. The water flow rate is determined from the water pressure drop across an orifice plate installed in the

water supply line according to British Standard 1042 (1981). Air is drawn through the tunnel by a 50 kW centrifugal fan with variable speed control. The mass flow rate of the air is determined by measuring the air pressure drop across one or more of the five ASHRAE 51-75 elliptical flow nozzles mounted in the horizontal section of the wind tunnel as shown in Figure 3-5. For the current test only the top three nozzles were used.

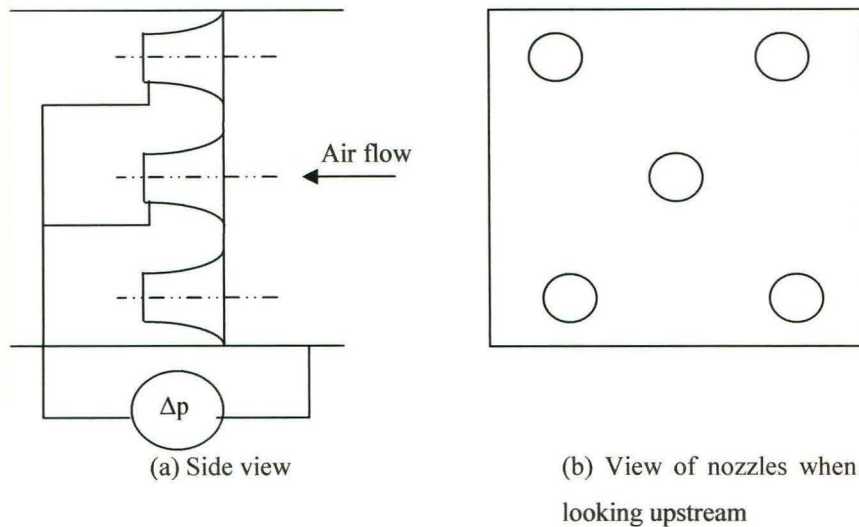


Figure 3-5: Nozzle air pressure drop measurement used to determine air-vapour mass flow rate

The air pressure drop through the nozzles is measured using a calibrated electronic pressure transducer. The temperatures are measured using copper–constantan thermocouples. The air temperature is measured upstream of the nozzles to accurately predict the density of the air through the nozzles. The pressure before the nozzles is assumed to be atmospheric. Four thermocouples are available to measure the dry bulb temperatures and another four to measure the wet bulb temperatures, see Figure 3-6. In the background of the figure are the mixers and screen.

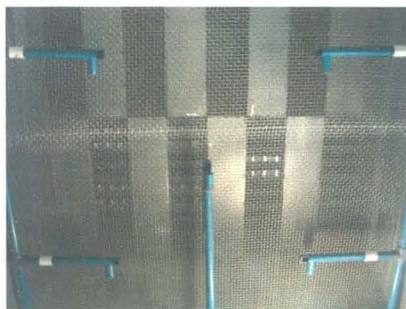


Figure 3-6: Layout of thermocouples upstream of nozzles

One dry and wet bulb thermocouple is situated inside the blue PVC pipes and a fan is used to aspirate air over the thermocouples. The middle temperature station was not used in the experiment. Figure 3-7 on the next page shows a pipe and instrument diagram of the counter flow fill test section.

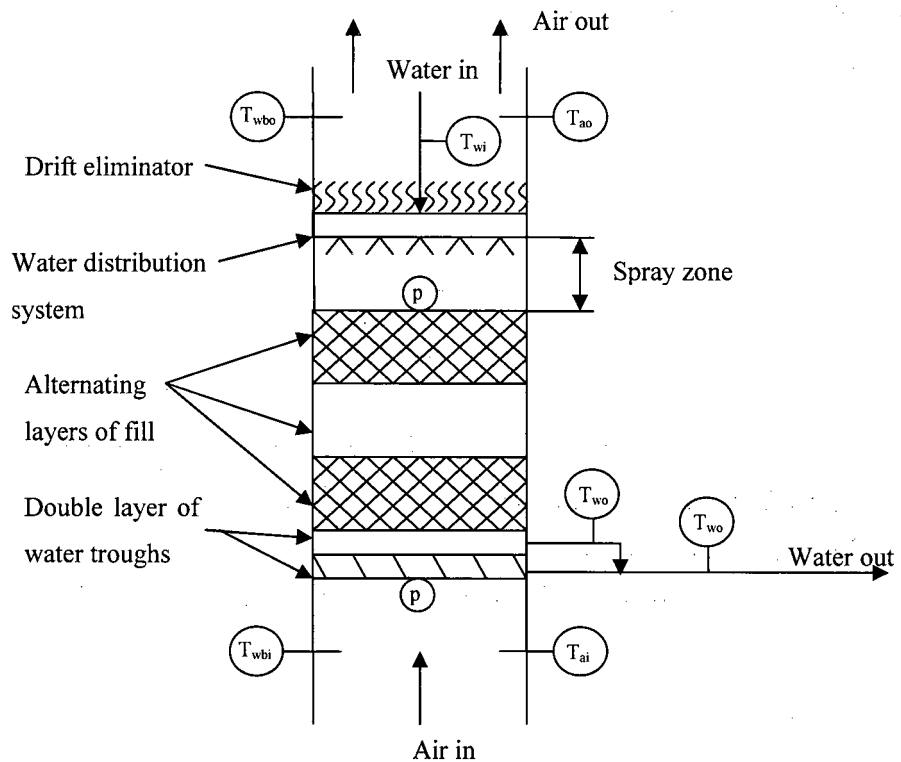


Figure 3-7: Pipe and instrument diagram of counter flow fill test section

The air dry bulb and wet bulb temperatures are again measured below the water troughs. These temperatures differ from the temperatures measured upstream of the nozzles due to influence of the fan. The average temperatures of the air below the troughs will be used to evaluate the inlet properties to the test section. The temperature measurement stations are similar to the one shown in Figure 3-6. The air pressure drop across the fill and troughs is measured by six static pressure probes. Two are installed below the troughs and four are installed above the fill. The air pressure drop across the water troughs is subtracted from the total air pressure drop to obtain the air pressure drop across the fill. It is assumed that the air pressure drop of the 200 mm spray zone is negligible in comparison with the air pressure drop over the water troughs.

The water inlet temperature is measured in the supply line at the top of the water distribution system with three thermocouples placed at 120° angles. The water outlet temperature is measured in PVC pipes that drain the water from the extraction troughs. The water outlet temperature of the upper and lower water trough sections is measured separately. The combined Merkel number of the water troughs and spray zone is subtracted from the total Merkel number to get the Merkel number of the fill.

In the past, the dry and wet bulb temperature of the outlet air was measured using four thermocouples situated in a horizontal plane, similar to the setup in Figure 3-6. It was also measured using a cyclone method. Air was sucked from the air outlet section and then drawn into a cyclone where centrifugal forces displace water drops to the peripheral walls of the device. This would ensure that no water impingement occurs on the thermocouples, thereby distorting the dry bulb temperature measurements. These air outlet temperatures were then used in calculating the air pressure loss coefficient of the fill and an energy

profile over the area and multiplying it by the inlet density of the test section. The mass flow rate deviation is the difference between the integrated velocity profile method and the mass flow rate as calculated in Appendix C. The correction coefficient and air-vapour mass flow rate deviation are also shown.

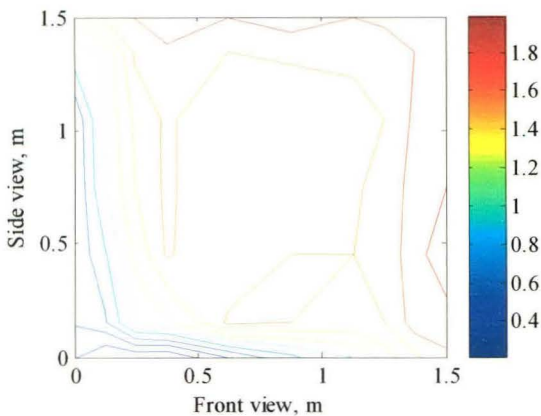
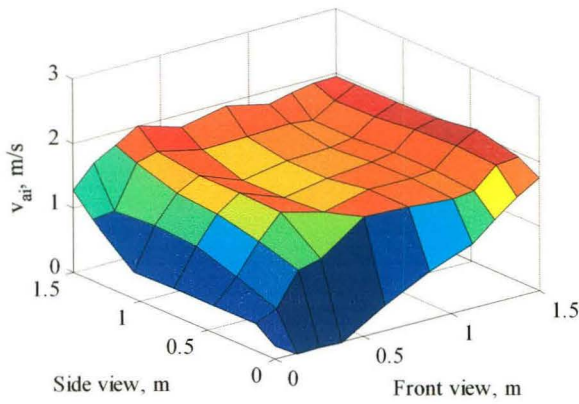


Figure 3-9: Inlet velocity profile, $v_{avi} = 1.822$ m/s,

$$\alpha_{mi} = 1.076 \%, m_{avi dev} = -4.028 \%$$

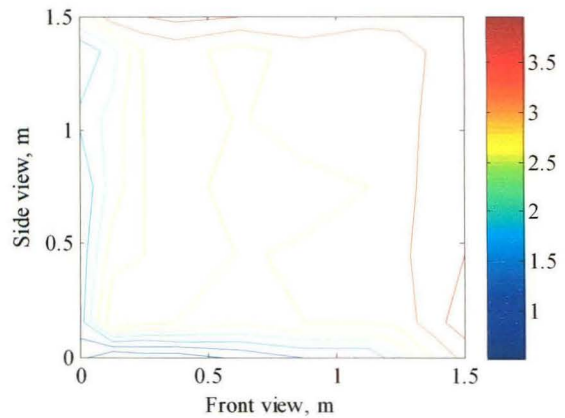
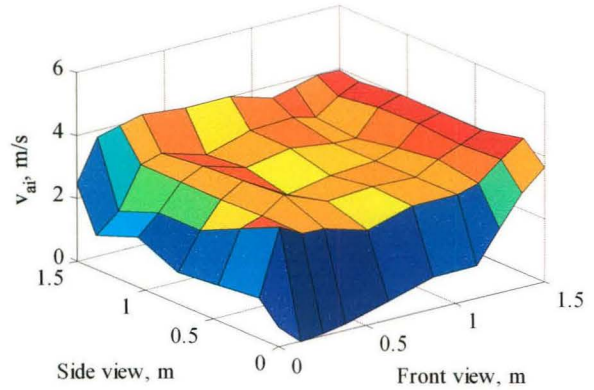


Figure 3-10: Inlet velocity profile, $v_{avi} = 3.658$ m/s,

$$\alpha_{mi} = 1.065 \%, m_{avi dev} = -4.358 \%$$

From the above set of figures one can see that the momentum velocity correction factor decreases for increasing air flow rate. The magnitude of α_{mi} will be very close to unity in the presence of high resistance fill. However, when low resistance fill is tested, care should be taken to include the α_{mi} values in Equation (3.1). From Equation (3.3) one can see that if α_{mi} is 7 % greater than unity, then the air pressure loss coefficient will be 7 % higher had it not been included (one can assume that $\alpha_{mo} \approx 1$). From Figure 3-8 one can also see that the inlet velocity vectors are not truly one dimensional. Tests were done on high resistance fill to see what the velocity vectors looked like after 150 mm of fill. For high resistance fill the air outlet velocity vectors were uni-directional and the assumption of one dimensional is adequate, however this will not necessarily be the case for low resistance fill.

3.4.2. Water mass flow rate

From the sensitivity indexes of Table D-1 one can see that Δp_{or} and hence the water mass flow rate plays an important part in calculating fill performance characteristics. It was thus decided to compare the water mass flow rate predicted by British Standard 1042 (1981) to that of a calibration test. See Appendix F for details. In this test the orifice plate was calibrated by diverting the water into a calibration tank and taking the time needed to fill the tank with a certain mass of water. Figure F-3 compares the results from the BS

method and the calibration tank. From Figure F-3 one can see that the BS method correlates well with the calibration tank data. Discrepancies are mainly at lower mass flow rates. On page 18, section 7.3.1 of British Standard 1042 (1981) the limits of use for the standard are given. For the type of orifice plate used the lower limit on the Reynolds number, Re_D , is given as $1260 \times \beta^2 \times D = 1260 \times 0.4769^2 \times 130 = 37254$, where $\beta = d/D$. See British Standard 1042 (1981) for more detail. The Re_D at the lowest mass flow rate was calculated to be 37262. One can thus see that the lower mass flow rate is very close to the lower limit of the acceptable range and could thus be the reason for the higher discrepancy.

3.4.3. Air mass flow rate

From Table D-1 one can see that Δp_{nth} and hence the air mass flow rate also plays a big role in determining fill performance characteristics. Following along the same line as the previous section, the accuracy of the method used to determine the air mass flow was evaluated. See Appendix F for details. In short, the air mass flow rate given by Kröger (2004) was compared to that given by the Bernoulli equation. It was found that the discrepancies between these two equations were negligible. Due to its simplicity and comparative accuracy, it was thus decided to use the Bernoulli equation to determine the air mass flow rate.

3.4.4. Water outlet temperature

From Table D-1 one can see the Merkel number is very sensitive to water outlet temperatures. This required further investigation into the method of determining water outlet temperatures. In the current setup the water temperature in the upper and lower water trough sections is measured separately. This requires the use of a mass weighted average to determine the water outlet temperature. A test was conducted to determine what percentage of the total inlet water mass flow rate is collected by the lower water troughs. See Appendix F for details. From Figure F-6 to F-7 one can make the following conclusions:

- An increase in air mass flow rate tends to increase the percentage water mass flow rate in the lower water troughs.
- The percentage water mass flow rate in the lower water troughs tends to be higher for the fill test (Figure F-7) than for the water troughs and spray zone performance test (Figure F-6).
- The percentage water mass flow rate in the lower water troughs stays more or less constant over the entire range of water inlet mass flow rates, for both the fill and combined water trough and spray zone test.

From the data presented in Figure F-6 and F-7, it was decided to calculate the water outlet temperature as

$$T_{wo} = 0.1T_{wob} + 0.9T_{wot} \quad (3.7)$$

where

T_{wob} = water temperature in the lower water trough section, K

T_{wot} = water temperature in the upper water trough section, K

3.5. Combined water trough and spray zone performance test

To determine the performance characteristics of the fill, the performance characteristics of the spray zone and water troughs must be subtracted from the total (spray zone, water troughs and fill) performance

characteristics obtained from the counter flow fill test. Before the fill performance test could proceed it was necessary to first determine the combined water trough and spray zone performance characteristics. In this section the setup and test procedure of the experiment is explained, followed by a discussion of the results. Sections 3.2 to 3.4 are applicable to this experiment as well.

3.5.1. Setup and test procedure

The combined performance characteristics of the water troughs and spray zone are determined by lowering the water distribution system to a height of 200 mm (height of the spray zone in Figure 3-7) above the upper section of water troughs. The same procedure is then followed as with the fill performance test. A pipe and instrument diagram of the experimental setup is shown in Figure 3-11. Strings of wool were used to visualise the velocity vectors at the air outlet of the upper water trough section. The pressure probes were then placed so that the velocity vectors are adjacent to the probes.

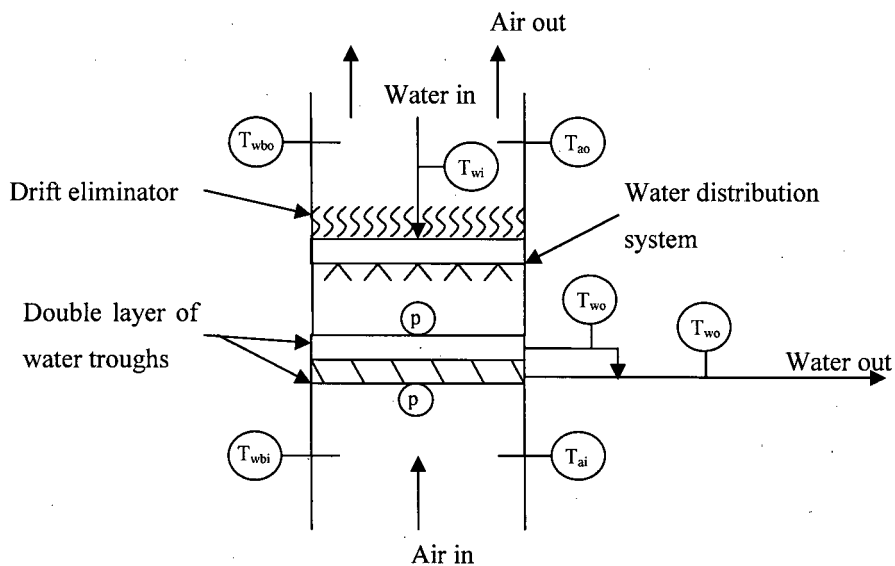


Figure 3-11: Pipe and instrument diagram of water troughs and spray zone performance test

3.5.2. Discussion of water troughs and spray zone performance test results

The results of the water troughs and spray zone performance test are presented in Appendix G. Similar tests were done in September 2004. According to these tests, the Merkel number of the water troughs and spray zone is given by

$$Me_{tr} = 0.134G_w^{0.080}G_a^{0.514} \quad (3.8)$$

and the air pressure drop across the water troughs is given by

$$\Delta p_{tr} = 0.6954G_w^{0.2471}G_a^{2.3365} + 0.00526G_w^{3.9812}G_a^{0.3947} \quad (3.9)$$

The air pressure drop across the water troughs in the absence of water is given as

$$\Delta p_{tr} = 1.63G_a^{1.57} \quad (3.10)$$

The following sections discuss the comparison of the above and new correlations with experimental data. The limits of the new correlations given in this section and Section 3.6.1 should be viewed as

“guidelines” rather than exact constraints. It should be interpreted as “for lower and higher water mass flow rates”. The data and figures for the water troughs and spray zone performance test are given in Appendix G.

MERKEL NUMBER

Figure G-1 (a), (c), (e), (g) and (i) show that the experimental results in general do not correlate well with Equation (3.8). The experimental results for the Merkel number are much higher than predicted by Equation (3.8). The results also indicate the water inlet temperature has a negative effect on the Merkel number, meaning that as the water inlet temperature increases for a given G_a and G_w value, the Merkel number decreases. This effect is not present in Equation (3.8). It also seems that the water mass flow rate has a larger effect than predicted by Equation (3.8). By fitting a new curve through the data points of Figure G-1 (a), (c), (e), (g) and (i), better correlation was obtained, see Figure G-2 (a), (c), (e), (g) and (i). The new correlations are

$$Me_{tr} = 0.7822G_w^{-0.0772}G_a^{0.3984}T_{wi}^{-0.4159} \quad (3.11)$$

for $1.350 \text{ kg/sm}^2 < G_w < 2.752 \text{ kg/sm}^2$ and

$$Me_{tr} = 0.6589G_w^{0.2214}G_a^{0.3814}T_{wi}^{-0.4187} \quad (3.12)$$

for $4.118 \text{ kg/sm}^2 < G_w < 5.561 \text{ kg/sm}^2$, where T_{wi} is in °C for both equations.

From the exponents of the T_{wi} and G_w terms one can see that the water inlet temperature has a significant negative effect on the Merkel number and that the water mass flow rate has a larger positive effect on Merkel number only at higher water mass flow rates. Figure G-3 illustrates the effect of using different equations to calculate the water outlet temperature: Figure G-3 (a), (c), (e), (g) and (i) - water outlet temperature is taken as the mean of the temperature in the lower and upper water trough sections, Figure G-3 (b), (d), (f), (h) and (j) - water outlet temperature is taken to be the temperature in the upper water trough section. In the case of Figure G-3 (a), (c), (e), (g) and (i) the Merkel number is much higher than what is predicted when using Equation (3.7). This is due to the fact that the colder water in the lower water trough section now has the same averaging weight as the temperature in the upper section and hence decreases the total water outlet temperature considerably. This lower water outlet temperature will increase the Merkel number, since it can only be achieved if the cooling capability of the water trough and spray zone, and hence the Merkel number, increases. The opposite happens when considering Figure G-3 (b), (d), (f), (h) and (j). In this case the water outlet temperature is too high. This effect is smaller than with Figure G-3 (a), (c), (e), (g) and (i) since the temperature of the water in the lower trough section only contributes to 10 % of the total water outlet temperature.

AIR PRESSURE DROP

From Figure G-4 and G-5, one can see that the current experimental results of the dry test correlate well with Equation (3.10). However, Figure G-1 (b), (d), (f), (h) and (j) shows that experimental results for the wet test in general do not correlate well with Equation (3.9). The measured air pressure drop is much lower than what is predicted by Equation (3.9). As with Equation (3.9) the effect of water inlet temperature is very small. The experimental results show that water mass flow rate has a smaller effect than what is predicted by Equation (3.9). It can be seen that Equation (3.9) predicts much higher air pressure drops at higher air mass flow rates relative to the experimental data. One has to keep in mind that

measuring pressures in the region of 1 to 15 Pa in a spray zone will always be problematic. For instance, if a 1 mm drop is to clog the pressure tappings, then a deviation of approximately 10 Pa ($\rho_w g h \approx 1000 \times 10 \times 0.001 = 10$ Pa) can be incurred. Still, an attempt was made to fit a new curve through the data points of Figure G-1 (b), (d), (f), (h) and (j). From Figure G-2 (b), (d), (f), (h) and (j), one can see that the new curves show better correlation with the experimental data. The new correlations are

$$\Delta p_{tr} = \left(0.6621 G_w^{0.0232} G_a^{1.6138} + 0.6621 G_w^{0.0232} G_a^{1.6138} \right) T_{wi}^{0.0303} \quad (3.13)$$

for $1.350 \text{ kg/sm}^2 < G_w < 2.752 \text{ kg/sm}^2$ and

$$\Delta p_{tr} = \left(0.7609 G_w^{0.6419} G_a^{1.1371} + 0.7609 G_w^{0.6419} G_a^{1.1371} \right) T_{wi}^{-0.0803} \quad (3.14)$$

for $4.118 \text{ kg/sm}^2 < G_w < 5.561 \text{ kg/sm}^2$, where T_{wi} is in °C for both equations.

From the exponent of T_{wi} , one can see that the water inlet temperature does have a small effect on the air pressure drop. It can also be seen that the water mass flow rate has a lesser effect than what is predicted by Equation (3.9).

3.6. Fill performance test

With the performance characteristics of the water troughs and spray zone determined, it is now possible to determine the fill performance characteristics. Equation (3.11) to (3.14) were used to determine the combined performance characteristics of the water troughs and spray zone in the following experiments.

3.6.1. Discussion of fill performance test results

The results of the fill performance test are presented in Appendix H. Similar tests were done in September 2004. According to these tests, the Merkel number applicable to a given depth of fill is given by

$$\frac{Me_{fi}}{L_{fi}} = 6.453 G_w^{-0.918} G_a^{0.680} T_{wi}^{-0.329} \quad (3.15)$$

where T_{wi} is in °C, and the air pressure loss coefficient due to friction and drag effects only is given by

$$\frac{K_{fdm}}{L_{fi}} = 9.427 G_w^{0.081} G_a^{-0.669} + 6.326 G_w^{0.058} G_a^{0.061} \quad (3.16)$$

The air pressure drop over the fill under dry conditions is given as

$$\Delta p_{fi} = 9.619 G_a^{1.781} \quad (3.17)$$

MERKEL NUMBER

Before any conclusion can be made regarding the results presented in Figure H-1, the uncertainty analysis of Appendix D, as well as the water troughs and spray zone performance correlations has to be considered. If the uncertainty due to curve fit errors is ignored from Equation (D.9) then the total uncertainty of the Merkel number is given as

$$U_{M,tot} = \sqrt{(0.2100)^2 + (0.1933)^2 - (0.1834)^2} = 0.2187 \text{ m}^{-1} \quad (3.18)$$

This is the uncertainty in the data points of Figure H-1 (a), (c) and (e). When compared to Equation (3.8), Equation (3.11) to (3.14) predict combined water trough and spray zone Merkel numbers that are roughly 0.15 higher. The total Merkel number (fill plus water troughs and spray zone) is given by

$$\frac{Me_{fi}}{L_{fi}} = \frac{Me_{fiTOT} - Me_{tr}}{L_{fi}} \quad (3.19)$$

From Equation (3.19) one can see that a 0.15 higher combined water trough and spray zone Merkel number will result in an experimental Me_{fi}/L_{fi} value that is $0.15/1.524 = 0.1 \text{ m}^{-1}$ lower than what would be predicted by Equation (3.15). From Figure H-1 (a), (c) and (e), one can see that in general, the experimental results are indeed lower than the prediction of Equation (3.15). To confirm this, the fill performance test data was analysed using the water troughs and spray zone correlations of Equation (3.8) and (3.9). The results did show better correlation with Equation (3.15) only at higher water mass flow rates. Considering the 0.2187 m^{-1} uncertainty and the lower 0.1 m^{-1} value, one can thus conclude that the experimental data is acceptable. At lower water mass flow rates the discrepancy is higher. It will also be seen that not all of the data is presented in Figure H-1 (a), (c) and (e). At lower water mass flow rates, it was found that the voltage signal produced by the pressure transducer measuring the water pressure drop over the orifice plate was unstable. The reason for this is still not clear. A possible explanation is that the signal to noise ratio at lower mass flow rates, and hence lower voltage, is not high enough to generate an acceptable output. These data points were not included in any analysis presented in this thesis. The discrepancies at lower water mass flow rates should however not be discarded, since this is the typical operating range of a NDWCT (a water mass flow rate of 3 kg/s in the test facility translates to a G_w value of $3/2.25 = 1.333 \text{ kg/sm}^2$). An attempt was made to fit a new curve through the data points of Figure H-1 (a), (c) and (e), incorporating the results at lower water mass flow rates, see Figure H-2 (a), (c) and (e).

The new correlations are

$$\frac{Me_{fi}}{L_{fi}} = 2.2038 G_w^{-0.8904} G_a^{0.7694} T_{wi}^{-0.1202} \quad (3.20)$$

for $1.346 \text{ kg/sm}^2 < G_w < 2.766 \text{ kg/sm}^2$ and

$$\frac{Me_{fi}}{L_{fi}} = 1.2411 G_w^{-1.1303} G_a^{1.0966} T_{wi}^{0.0819} \quad (3.21)$$

for $4.134 \text{ kg/sm}^2 < G_w < 5.557 \text{ kg/sm}^2$, where T_{wi} is in $^{\circ}\text{C}$ for both equations.

The effect of using different equations to calculate the water outlet temperature is shown in Figure H-3. The same arguments as for the water troughs and spray zone performance tests are applicable to these results.

AIR PRESSURE LOSS COEFFICIENT

From Figure H-4 one can see that the current experimental results of the dry test correlate well with Equation (3.17). For the wet test, Figure H-1 (b), (d) and (f) shows that discrepancies are mainly at lower air and water mass flow rates. For $G_a < 2 \text{ kg/sm}^2$ and $G_w < 2.7 \text{ kg/sm}^2$ the air pressure drop over the water troughs are in the region of $1 - 3 \text{ Pa}$ and $13 - 30 \text{ Pa}$ for the fill only. Again one can see that a 1 mm drop could have a large effect on the air pressure drop over the fill and hence the K_{fdm}/L_{fi} value. It can thus be concluded that the experimental results are acceptable. Note that some of the experimental results at lower water and air mass flow rates have been omitted. This is due to the fact that measuring these low air pressure drops is almost impossible and hence the results have been excluded in the analysis. To improve the correlation of Equation (3.16) a new curve was fitted through the data points of Figure H-1 (b), (d) and (f), see Figure H-2 (b), (d) and (f). The new correlations are

$$\frac{K_{fdm}}{L_{fi}} = \left(8.8714 G_w^{0.0837} G_a^{-0.2203} + 8.8714 G_w^{0.0837} G_a^{-0.2203} \right) T_{wi}^{-0.0626} \quad (3.22)$$

for $1.346 \text{ kg/sm}^2 < G_w < 2.766 \text{ kg/sm}^2$ and

$$\frac{K_{fdm}}{L_{fi}} = \left(6.5903G_w^{0.1980}G_a^{-0.2522} + 6.5903G_w^{0.1980}G_a^{-0.2522} \right) T_{wi}^{-0.0300} \quad (3.23)$$

for $4.134 \text{ kg/sm}^2 < G_w < 5.557 \text{ kg/sm}^2$, where T_{wi} is in °C for both equations.

3.7. Uncertainty analysis

The fill performance uncertainty analysis is presented in Appendix D. The total uncertainty can be considered smaller than what it really is, since the uncertainty of the water troughs and spray zone performance as well as orifice plate has not been incorporated. The total uncertainty in the fill Merkel number is 0.2854 m^{-1} and 0.4699 m^{-1} for the air pressure loss coefficient. The reference tower used in Chapter 5 to evaluate NDWCT uncertainties has a total Merkel number of $1.47/2.504 = 0.587 \text{ m}^{-1}$. This means that the uncertainty on the tower Merkel number due to fill performance uncertainty is $0.2854/0.587 \times 100 = 48.6\%$. From Chapter 5 it will be seen that these uncertainties, especially the Merkel number then, can lead to enormous overall tower performance uncertainty. Table 3-1 gives a summary of the fill performance test uncertainty components, followed by a discussion of how to decrease this uncertainty. The first column indicates the parameter measured. The headings of the next columns are explained below:

- $B_{0,1,1}$ = systematic uncertainty due to calibration curve fit errors
- $B_{0,2,3}$ = systematic uncertainty due to data logging system
- $B_{0,2,4}$ = spatial uncertainty
- B_0 = combined zeroth order systematic uncertainty
- $P_{1,2,5}$ = random uncertainty due to variation of parameter being measured
- P_1 = combined first order uncertainty
- θ = sensitivity indexes
- $u_{0,K}$ = uncertainty in K_{fdm1} due to B_0 uncertainty of specific parameter
- $u_{0,M}$ = uncertainty in Me_{fi1} due to B_0 uncertainty of specific parameter
- $u_{1,K}$ = uncertainty in K_{fdm1} due to P_1 uncertainty of specific parameter
- $u_{1,M}$ = uncertainty in Me_{fi1} due to P_1 uncertainty of specific parameter

Table 3-1: Summary of fill performance test uncertainty components

Parameter, x_i	$(B_{0,1,1})_{x_i}$	$(B_{0,2,3})_{x_i}$	$(B_{0,2,4})_{x_i}$	$(B_0)_{x_i}$	$(P_{1,2,5})_{x_i}$ $= (P_1)_{x_i}$	$(\theta_K)_{x_i}$	$(\theta_M)_{x_i}$	$(u_{K,0})_{x_i}$	$(u_{M,0})_{x_i}$	$(u_{K,1})_{x_i}$	$(u_{M,1})_{x_i}$
p_{atm} , Pa	0	20	0	20	0	0.0001	0	0.0025	0.0005	0	0
T_{ai} , K	0	0.5187	0.3158	0.6073	0.0028	-0.0260	-0.0010	0.0158	0.0006	0.0001	0
T_{wbi} , K	0	0.5187	0.4848	0.7100	0.0029	-0.0330	0.1581	0.0235	0.1122	0.0001	0.0005
p_{ai} , V	0.0003	0.0023	0	0.0023	0.0004	0.0576	0.0036	0.0001	0.0000	0	0
Δp_{fTRO} , V	0.0004	0.0023	0	0.0023	0.0003	206.7915	0	0.4738	0.0000	0.0558	0
T_{wis} , K	0	0.5187	0.3019	0.6001	0.0090	-0.0236	0.0417	0.0142	0.0250	0.0002	0.0004
T_{vos} , K	0	0.5187	0.1050	0.5292	0.0147	0.0241	-0.3388	0.0128	0.1793	0.0004	0.0050
Δp_{or} , V	0.0101	0.0023	0	0.0103	0.0244	-0.8988	2.4911	0.0093	0.0258	0.0219	0.0607
T_{wbi} , K	0	0.5187	0.0659	0.5229	0.0037	0.0325	0.0019	0.0170	0.0010	0.0001	0
T_{an} , K	0	0.5187	0.2480	0.5749	0.0073	0.0330	0.0019	0.0190	0.0011	0.0002	0
Δp_{nub} , V	0.0043	0.0023	0	0.0049	0.0018	-34.0509	-1.9590	0.1653	0.0095	0.0605	0.0035

3.7.1. Zeroth order

The minimum uncertainty that can be attained using the current test setup and procedure is reflected in the zeroth order uncertainties. The zeroth order uncertainty for the Merkel number and air pressure loss coefficient is calculated in Appendix D to be 0.2100 m^{-1} and 0.4248 m^{-1} respectively. This can only be reduced by improving test equipment or measuring techniques and will now be discussed for the Merkel number and air pressure loss coefficient respectively.

MERKEL NUMBER

The $u_{M,0}$ entries in Table 3-1 shows that T_{wbi} has the biggest contribution to the zeroth order uncertainty in Me_{fi} , relative to the other air temperatures. This is due to its relatively high sensitivity index. Its uncertainty can be reduced by (a) using a better data logger and (b) having more measurement locations. Option (a) will have the effect of decreasing the $B_{0,2,3}$ value, see Table D-2 and discussion thereof. Option (b) will decrease the spatial uncertainty as described on page D-3.

T_{wo} is the temperature measurement that has the highest sensitivity index and hence the biggest zeroth order uncertainty contribution. Its uncertainty can be reduced similar as to T_{wbi} . In addition, extra care should be taken when determining the weighted averages of the lower and upper water trough section temperatures as discussed in Section 3.4.4.

The uncertainty in the T_{wi} measurement is also of concern. Due to its relative low sensitivity index relative to T_{wbi} and T_{wo} , its effect on Me_{fi} is slightly dampened. Its uncertainty can however be reduced similar as to T_{wbi} .

Although the uncertainties in both the Δp_{or} and Δp_{nth} measurements are relatively low (Δp_{or} typical varies from 1.25 V to 5.60 V and Δp_{nth} from 1.15 V to 2.54 V), it is greatly amplified by their respective sensitivity index. Better equipment might improve the measurement uncertainty but will have a lesser effect on the zeroth order uncertainty in Me_{fi} .

AIR PRESSURE LOSS COEFFICIENT

All the temperature measurements have comparative sensitivity indexes and contribute more or less equally to the zeroth order uncertainty in K_{fdm1} . The uncertainty in the temperature measurements can be reduced similar as to T_{wbi} for the Merkel number case.

The same arguments regarding Δp_{or} and Δp_{nth} for the Merkel number cases are applicable to Δp_{FITOT} and Δp_{nth} (Δp_{FITOT} typically varies from 1.03 V to 1.26 V) for the air pressure loss coefficient.

3.7.2. First order

This order of uncertainty reflects the variability in the parameter being measured. The first order uncertainty for the Merkel number and air pressure loss coefficient is calculated in Appendix D to be 0.1933 m^{-1} and 0.1836 m^{-1} respectively. These values also include the uncertainty of the performance correlations due to curve fit errors. These uncertainties are not shown in Table D-3 but are calculated to be 0.1834 m^{-1} for the Merkel number and 0.1818 m^{-1} for the air pressure loss coefficient. One can thus see that the biggest contribution to the first order uncertainty for both the Merkel number and air pressure loss coefficient is due to performance correlation curve fit errors. An attempt was made to reduce these

uncertainties by generating performance correlations that are only applicable in certain regions, see Equations (3.20) to (3.23), and is recommended for future work.

From the last two columns of Table 3-1 one can see that only the pressure measurements have considerable contributions to the first order uncertainties in Me_{f1} and K_{fdm1} . The uncertainties in the pressure measurements can only be improved by taking more measurements.

3.8. Conclusion

In this chapter the different ways of presenting fill performance characteristics were discussed. The setup used to determine fill performance characteristics, as well as test procedure was discussed. Aspects that need careful attention are the water trough blockage effect, water and air mass flows and the water outlet temperature.

The British Standard 1042 (1981) was used to determine the water mass flow rate through the orifice plate installed in the supply line. It should be noted that at lower water mass velocities the orifice plate is operating near the limit of its lower acceptable range. This could lead to poor experimental results and the experimenter should keep this in mind when planning the experiment.

The Bernoulli equation was used to determine the air mass flow rate through the ASHREA 51-75 nozzles (see Equation (F.2)). This equation showed good correlation when compared the more complex equation given by Equation (F.1). Either equation can be used.

The water trough blockage effect can cause the inlet velocity profile to be non-uniform which means that the air pressure drop given by Equation (3.1) for $\alpha_{mi} = 1.0$ is invalid. The magnitude of α_{mi} will be very close to unity in the presence of high resistance fill. However, this will not necessarily be the case for low resistance fill.

The water outlet temperature is measured separately in the lower and upper water trough sections. This requires the use of a mass weighted average to determine the water outlet temperature. From experiments it was found that the water outlet temperature should be calculated according to Equation (3.7).

In order to determine the fill performance characteristics, the combined water trough and spray zone performance characteristics had to be determined first. Experimental data did not show good correlation with previous work. The experimental results for the Merkel number were much higher than those predicted by Equation (3.8). The results also indicated that the water inlet temperature had a negative effect on the Merkel number. This effect is not present in Equation (3.8). It was also found the water mass flow rate had a larger effect than what was predicted by Equation (3.8). Experimental results for the air pressure drop over the water troughs for dry air only showed good correlation with previous work, i.e. Equation (3.10). However, experimental results for the wet test in general did not correlate well with Equation (3.9). The measured air pressure drop was much lower than what was predicted by Equation (3.9). As with Equation (3.9) the effect of water inlet temperature was very small. The experimental results showed that water mass flow rate had a smaller effect than what was predicted by Equation (3.9). It was found that Equation (3.9) predicted much higher air pressure drops at higher air mass flow rates

relative to the experimental data. It should be noted that measuring pressures in the region of 1 to 15 Pa in a spray zone will always be problematic (1 mm water \approx 10 Pa). New correlations for the combined performance characteristics of the water troughs and spray zone were derived. These correlations were used in determining the fill performance characteristics.

It was found that the new combined performance characteristics of the water troughs and spray zone predicted Merkel numbers that are roughly 0.15 higher than Equation (3.8). This would result in an experimental Me_{fi}/L_{fi} value that is $0.15/1.524 = 0.1 \text{ m}^{-1}$ lower than what would have been predicted by Equation (3.15). It was found that in general, the experimental results were indeed lower than the prediction of Equation (3.15). To confirm this, the fill performance test data was analysed using the water trough and spray zone correlations of Equation (3.8) and (3.9). The results did show better correlation with Equation (3.15) at higher water mass flow rates. Considering the 0.1293 m^{-1} uncertainty in the data points and the 0.1 m^{-1} lower value, it was concluded that the experimental data was acceptable. At lower water mass flow rates, typically in the region of 3 kg/s, the discrepancy was higher. At these water mass flow rates it was found that the voltage signal produced by the pressure transducer measuring the air pressure drop over the orifice plate was unstable. A possible explanation is that the signal to noise ratio at lower mass flow rates, and hence lower voltage, was not high enough to generate an acceptable output. These data points were not included in any analysis. The discrepancies at lower water mass flow rates should however not be discarded, since this is the typical operating range of a NDWCT (a water mass flow rate of 3 kg/s in the test facility translates to a G_w value of $3/2.25 = 1.333 \text{ kg/sm}^2$). For the air pressure drop over the fill it, was found that the results of the dry test correlated well with Equation (3.17). For the wet test, discrepancies in the air pressure loss coefficient were mainly at lower air and water mass flow rates. New correlations for the fill performance characteristics were derived and are given by Equation (3.20) to (3.23).

The uncertainty analysis showed that the total uncertainty in the fill Merkel number is 0.2854 m^{-1} and 0.4699 m^{-1} for the air pressure loss coefficient. The zeroth order uncertainty for the Merkel number and air pressure loss coefficient was calculated to be 0.2100 m^{-1} and 0.4248 m^{-1} respectively, while the first order uncertainty for the Merkel number and air pressure loss coefficient was calculated to be 0.1933 m^{-1} and 0.2008 m^{-1} respectively. Using a better data logger, more measurement locations and better curve fit methods, it is possible to reduce the total uncertainty in the fill performance characteristics.

CHAPTER 4. FILL PERFORMANCE STANDARD TEST PROCEDURE

4.1. Introduction

As was stated in the objectives for this thesis, the absence of a formal fill test procedure and data reduction method could lead to poor repeatability and uncertainty of test results. From Chapter 3 and Equation (D.1) and (D.2) one can see that such a test includes a large number of variables, settings, calibrations and instrumentation. With this in mind, the sole objective of this chapter is to formulate a fill performance standard test procedure. The data reduction and calibration techniques used in this thesis automatically forms part of the test procedure. The ranges of water inlet temperatures, water mass flow rates and air mass flow rates for a fill performance test are approximately $50\text{ }^{\circ}\text{C} - 20\text{ }^{\circ}\text{C}$, $3\text{ kg/s} - 12.5\text{ kg/s}$ and $3\text{ kg/s} - 8.5\text{ kg/s}$ respectively. Higher air mass flow rates are possible if more of the five ASHRAE 51 – 75 nozzles are unblocked. The procedure is presented in the form of a check list containing all the necessary activities. The activities do not necessarily have to be completed chronologically. Figure 4-3, which follows the check list, presents photographs of all the equipment.

The procedure addresses the following topics:

- Pipe and instrument diagram
- Check list
 - Heating of the water in the reservoir
 - Tunnel preparation
 - Start-up
 - Performance testing
 - Shut-down
 - Test conditions
 - Recommendations
 - Time frame
- Photographs of equipment

The procedure also discusses the methodology followed to measure air outlet temperatures. Although these temperature were not used in this thesis, they might be used in future work hence the inclusion in the test procedure. The term approach is defined as the difference between the water outlet temperatures at the fill test section minus the air wet bulb temperature at the inlet to the water troughs.

4.2. Pipe and instrument diagram

The diagram is presented on the next page. The top diagram shows a pipe and instrument diagram of the fill test facility, followed by a pipe and instrument diagram of the counter flow fill test section.

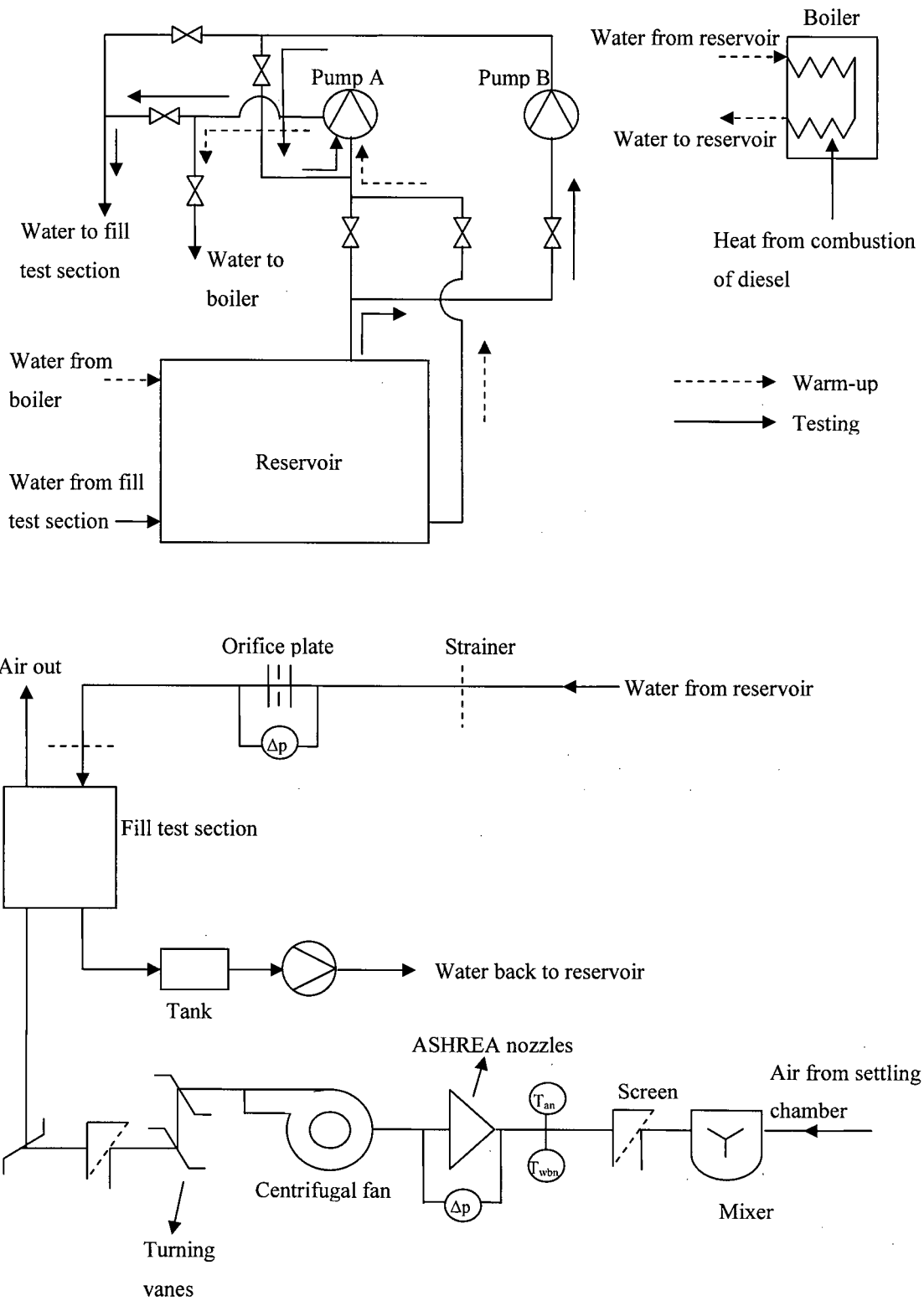


Figure 4-1: Pipe and instrument diagram of fill test facility

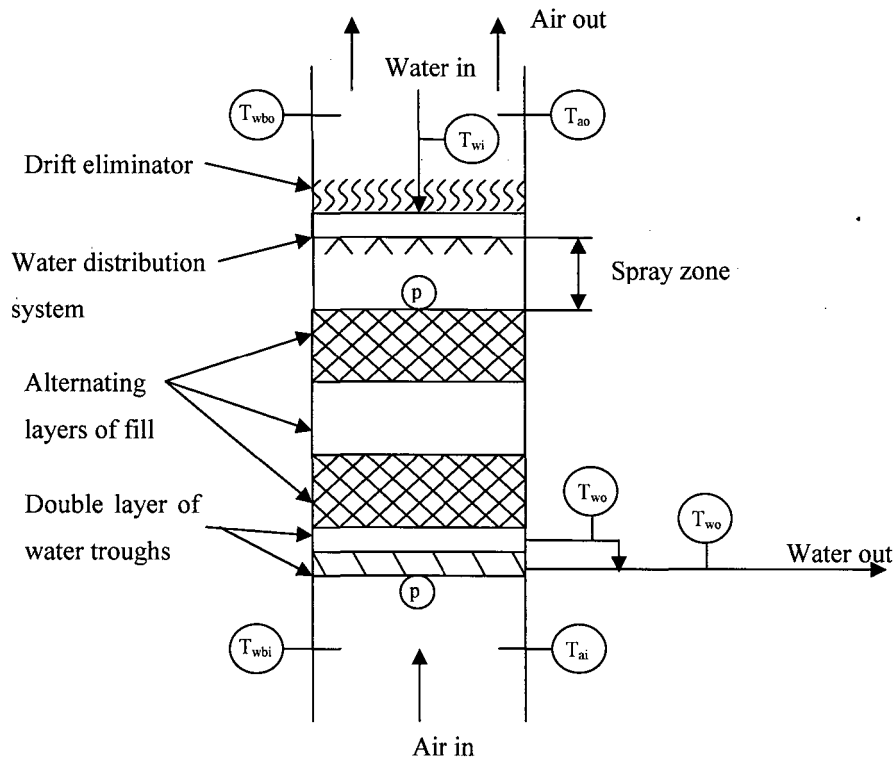


Figure 4-2: Pipe and instrument diagram of counter flow fill test section

4.3. Check list

The check list is given below. The first column indicates the activity reference number, followed by a description of the activity, a picture reference number and a tick box. The picture reference number refers to the pictures in Figure 4-3, unless otherwise stated. Figure 4-3 is presented after the check list. The activities do not necessarily have to be completed chronologically.

HEATING OF THE WATER IN THE RESERVOIR

1	Ensure that reservoir is filled with water	(a)	
2	Ensure that 500 litre diesel tank is full	(b)	
	Configure valves at water reservoir:	(4-1)	-
3	• Pump A sucks water from bottom of tank through smaller diameter pipe		
4	• Pump B remains switched off		
5	• Water is heated in boiler and discharged back into top of tank	(c)	
6	Ensure that water is circulating through boiler by switching on Pump A	(z), (aa)	
7	Open valve at bottom of diesel tank – diesel supply for boiler	(d)	
8	Switch on boiler	(e)	
9	Measure water temperature at top of reservoir with thermocouple or thermometer	(a)	
10	Reheat water to 2-4 °C (measured as deep as possible) above the desired water temperature		
	When temperature is reached:		-
11	• Switch off boiler	(e)	

12	• Close valve in diesel supply line	(d)	
13	• Let water recalculate through boiler for 10-15 minutes before switching off pump A		
14	Wait 6-8 hours before proceeding to fill tests	(z), (aa)	

TUNNEL PREPARATION - AFTER COMPLETION OF ACTIVITY 14

	Switch on Δp_{or} power supply:	(f)	-
15	• Input between 12 and 24 volts		
16	• Ensure maximum ampere input		
	Calibrate all pressure transducers		-
17	• Δp_{fiTOT}	(g)	
18	• p_{ai}	(g)	
19	• Δp_{nth}	(h)	
20	• Δp_{or}	(i)	
	Air side		-
21	Remove and wash all the wicks of the wet bulb temperature sensors	(j)	
22	Place wet bulb wicks back over thermocouples	(j)	
23	Unblock holes in pipes of water distribution system	(k)	
24	Place fill in test section	(l)	
25	Wet wicks of wet bulb thermocouples at tower outlet	(m)	
26	Drain water from cyclone system	(n)	
27	Connect vacuum cleaner to cyclone system	(o)	
28	Wet wicks of wet bulb thermocouples at water trough inlet	(p)	
29	Wet wicks of wet bulb thermocouples at nozzle inlet	(q)	
	Ensure that all pressure pipes and tappings are securely connected:		-
30	• Δp_{fiTOT}		
31	• p_{ai}		
32	• Δp_{nth}		
	Check that all pressure pipes are air tight:		-
33	• Δp_{fiTOT}		
34	• p_{ai}		
35	• Δp_{nth}		
	Check that no condensate is present in pressure pipes:		-
36	• Δp_{fiTOT}		
37	• p_{ai}		
38	• Δp_{nth}		
39	Close all manholes	(r), (s)	
40	Close all test section doors tightly	(l)	
			-
	Water side		-

CHAPTER 4. FILL PERFORMANCE TEST PROCEDURE

41	Clean strainer in water inlet pipe at the water distribution system	(m)	
42	Clean strainer in water supply line, upstream of orifice	(t)	
	Configure valves at water reservoir:	(4-1)	-
43	• Pump B sucks water from top of tank through the one way foot valve of the large diameter pipe		
44	• Pump A is connected in series with pump B		
45	• Cooled water is pumped back into bottom of tank		
46	Open gate valve situated at the counterflow test section	(u)	
47	Zero Δp_{or}		
48	Bleed Δp_{or}		
49	Ensure that valves of Δp_{or} are configured correctly	(v), (w)	

START-UP

	Take zero readings:		-
50	• p_{abs}	(ad)	
51	• Δp_{TOT}		
52	• p_{ai}		
53	• Δp_{nth}		
54	Engage main switch	(x)	
55	Switch on 50 kW centrifugal fan and two wet bulb aspirator fans	(y)	
56	Switch on pump B and pump C	(aa), (ac)	
57	At higher water flow rates switch on pump A as well	(aa)	
58	Switch on vacuum cleaner	(o)	
	Increase air mass flow rate to any set value and wait until following stabilises:	(g)	-
59	• Water inlet temperature		
60	• Wet bulb temperatures at water trough inlet		
61	• Wet bulb temperatures at nozzle inlet		
62	Check that all instrumentation gives acceptable outputs		

PERFORMANCE TESTING

	At each setting wait until the following stabilises		-
63	• Air pressure drop over nozzles		
64	• Water pressure drop over orifice plate		
65	• Water inlet temperature		
66	• Wet bulb temperatures at water trough inlet		
67	• Wet bulb temperatures at nozzle inlet		
68	Time to stabilise is approximately 2 minutes		
69	Log data every 2 seconds over a 40 second period		
70	Check that no condensate is present in pressure pipes		
71	Water mass flow rates should be such that reserve pump power is available if strainer clogs up		

SHUT-DOWN

72	Switch off pump A, B and C	(aa), (ac)	
73	Switch off 50 kW centrifugal fan and two wet bulb fans	(y)	
	Take zero readings:		-
74	• p_{abs}		
75	• Δp_{TOT}		
76	• p_{ai}		
77	• Δp_{nth}		
78	Switch off Δp_{or} power supply	(f)	

TEST CONDITIONS

79	Testing must be conducted when it is dark or when radiation effects from the sun is negligible, for instance overcast conditions.		
80	A minimum approach of 10 °C is required.		
81	Tests should be done, if possible, in dry cold ambient air rather than hot or cold humid air.		

RECOMMENDATIONS

82	Heat water during day and switch off at night. Allow settling time as per activity 14.		
83	Start testing early morning before sunrise. Early morning ambient conditions are more stable and radiation effects are also negligible.		
84	Prepare tunnel while water is heated.		
85	Keep bucket of water and syringe close by to wet wicks of wet bulb thermocouples during test.		
86	A test requires at least two persons.		
87	First conduct a dry test and analyse data. This serves as both an overall check and reference for further testing.		

TIME FRAME

88	A test consisting of 4 water mass flow rates and 5 air mass flow rates per water mass flow rate takes about 4 hours.		
89	The water in the reservoir can be heated at approximately 2 °C per hour.		
90	Preparation of the tunnel takes approximately 2 days.		

4.4. Photographs of equipment



(a)



(b)



(c)



(d)



(e)



(f)



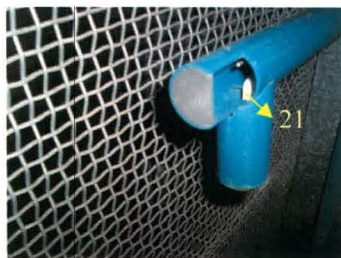
(g)



(h)



(i)



(j)

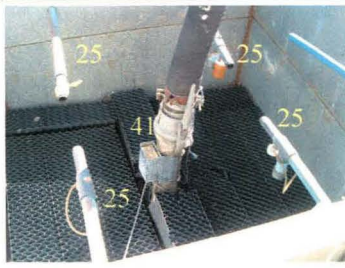


(k)



(l)

Figure 4-3: Photographs of equipment



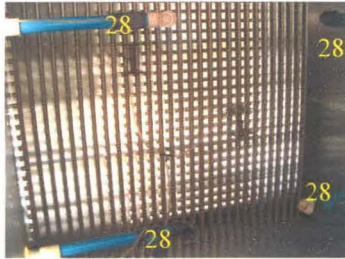
(m)



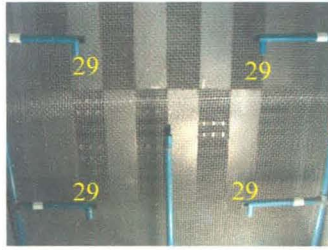
(n)



(o)



(p)



(q)



(r)



(s)



(t)



(u)



(v)



(w)



(x)



(y)



(z)



(aa)

Figure 4-3: (continued) Photographs of equipment

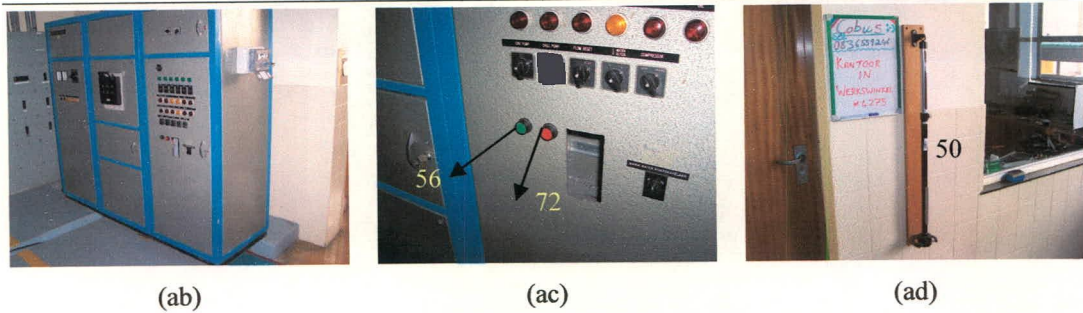


Figure 4-3: (continued) Photographs of equipment

4.5. Conclusion

This chapter presented a fill performance test standard. The standard is presented in the form of check list.

The standard discusses the following topics:

- Pipe and instrument diagram
- Check list
 - Heating of the water in the reservoir
 - Tunnel preparation
 - Start-up
 - Performance testing
 - Shut-down
 - Test conditions
 - Recommendations
 - Time frame
- Photographs of equipment

CHAPTER 5. NDWCT PERFORMANCE EVALUATION

5.1. Introduction

Performance test codes are primarily developed to determine whether or not a NDWCT test is acceptable. Deviations from guarantees must be agreed upon before hand and are not covered in performance test standards. Most standards stipulate a maximum allowable uncertainty in the result. This uncertainty is due to for example inaccurate instrumentation, unsteadiness of parameter being measured and calibration errors (referred to collectively as measurement errors or measurement uncertainties in this chapter). If the final uncertainty in the result is within the allowable prescribed uncertainty then the test is deemed acceptable. It is this prescribed uncertainty that will be investigated in this chapter. The first objective is to determine whether or not this uncertainty is achievable or not. The second objective is to investigate what effect typical fill performance characteristic uncertainties have on tower performance. The chapter starts off with the sensitivity indexes of a typical NDWCT, followed by a comparison of the different performance test standards used. The comparative section discusses the following: performance parameter, validity of test, measurement uncertainties and uncertainty analysis. The results obtained from the fill performance test discussed in Appendix D and Chapter 3 are also incorporated in the comparative study.

5.2. NDWCT sensitivity indexes

The same cooling tower and WP used in the Kröger (1998) model are used here to calculate the sensitivity indexes. The sensitivity indexes are calculated according to Equation (B.17) and are given in Table 5-1. The relationship between the water temperature in the basin of the tower, T_{wo} , and the input parameters are given below.

$$R_T = T_{wo} = f_T(T_{a1}, T_{wb1}, p_{a1}, T_{wi}, m_w) = f_T(x_1, x_2, x_3, x_4, x_5) \quad (5.1)$$

Note that dT_a/dz is not an input parameter in Equation (5.1). This is explained in Appendix K. The T_{wo} value of Equation (5.1) were evaluated with the Improved Merkel method as discussed in Section 2.2. The last column of Table 5-1 has units of K per SI unit of input parameter, e.g. the units of $(\theta_T)_{p_{a1}}$ is K/Pa.

Table 5-1: Sensitivity indexes for NDWCT

Parameter, x_i	WP	δ_{x_i}	$\frac{\delta_{x_i}}{x_i} \times 100\%$	$T_{wo} _{WP-\delta_{x_i}}$	$T_{wo} _{WP+\delta_{x_i}}$	$(\theta_T)_{x_i}$
T_{a1} , K	288.6	2	1	294.2604	294.9314	0.1677
T_{wb1} , K	284.2	2	1	293.8850	295.3396	0.3637
p_{a1} , Pa	84100	500	1	294.5711	294.5975	2.635E-05
m_w , kg/s	12500	500	4	294.4944	294.6752	1.808E-04
T_{wi} , K	313.15	2	1	294.3792	294.7562	0.09424
Me_{fi}	0.92859	0.09286	10	295.0696	294.1357	-5.0285
K_{fdm}	3.86010	0.38601	10	294.5603	294.6086	0.06264

From the sensitivity indexes in the last column of Table 5-1, one can see that NDWCT tower performance is most sensitive for Me_{fi} , followed by T_{wb1} and T_{a1} .

5.3. Performance test code comparative study

The three performance test codes studied in this section are ASME PTC (2003), CTI (2000) and British Standard 4485 (1998).

5.3.1. Performance parameter for NDWCT

ASME relates the performance of a NDWCT to tower capability. Tower capability (TC) is expressed as the ratio of the measured test water flow rate to the predicted test water flow rate.

$$TC(\%) = \frac{\text{Measured test water flow rate}}{\text{Predicted test water flow rate}} 100 \quad (5.2)$$

Performance curves are used in conjunction with measured test conditions to determine what the predicted water flow rate is.

BS uses the ratio of water mass velocity to air mass velocity, i.e. L/G or G_w/G_a . TC is defined as the ratio of the predicted L/G value to the design L/G value

$$TC(\%) = \frac{\left(\frac{L}{G}\right)_P}{\left(\frac{L}{G}\right)_D} 100 \quad (5.3)$$

The first step is to determine the as-tested (L/G) value. This value is then used in conjunction with a characteristic curve to determine the $(L/G)_P$ value. A characteristic curve is similar to a performance curve and includes a plot of the total Merkel number of the tower versus L/G . Other parameters include for instance design wet bulb temperature and cooling range.

CTI uses the same method as ASME.

5.3.2. Performance curves

All codes make use of performance curves. The basic objective of performance curves is to adjust results at test conditions to design conditions in order to determine whether or not guarantees are met. All three standards make use of cumbersome and unnecessary complex performance curves. An attempt was made to improve the current performance curve methods. The result is a software package, Performance Curve Generator (PCG), presented in Appendix I. PCG allows the user to quickly and easily adjust results at test conditions to design conditions. PCG also shows good comparison with the one dimensional Improved Merkel method, see Figure I-4. This is due to the fact that method used to generate the performance curves are based on the one dimensional model data. The software comprises of a user interface written in Microsoft Visual Basic 6.0 and a solver written in FOTRAN 77.

5.3.3. Validity of test

A performance test is deemed ASME approved if the calculated overall uncertainty in the tower capability is less than $\pm 6.0\%$. This uncertainty is only due to measurement errors. The code does not cover deviations from guarantees. ASME stipulates that deviations from guarantees should be agreed upon before hand.

CTI gives no requirements to whether or not a test is deemed CTI approved. It only states that if an uncertainty analysis is required, it should be agreed upon by both parties prior to testing

BS states that a tower should be deemed acceptable if the evaluated result from the test equals or exceeds 95 % of the design capability. Unlike the other codes, this standard then does state whether or not a guarantee is met. In other words if a performance test is deemed BS approved, it implies that the cooling tower has passed it performance test and that it is ready for operation. It mentions that measurement uncertainties should be considered, but gives no further information.

5.3.4. Model modifications

In order to determine what the effect of measurement uncertainties will be on the final result of a NDWCT performance test, some modifications to the model [Equation (5.1)] used to determine the sensitivity indexes of Table 5-1 are necessary. Since ASME is the only standard that gives a clear definition as to whether or not a test is deemed acceptable, it was decided to use their performance parameters to conduct further investigation.

The performance parameter for an ASME approved test is given as

$$R_m = TC = \frac{m_{wM}}{m_{wP}} = f_m(T_{al}, T_{wbl}, P_{al}, T_{wi}, T_{wo}) = f_m(x_1, x_2, x_3, x_4, x_5) \quad (5.4)$$

where the subscript M referrer to the as-measured water mass flow rate and the subscript P to the as-predicted water mass flow rate. The subscript m indicates that the result of interest is the water mass flow rate. The uncertainty in the result can be written as

$$\begin{aligned} U_{TC} &= \sqrt{\left(\frac{\partial TC}{\partial m_w} U_{mM}\right)^2 + \left(\frac{\partial TC}{\partial m_w} U_{mP}\right)^2} \\ &= \sqrt{\left(\frac{1}{m_{wP}} U_{mM}\right)^2 + \left(-\frac{m_{wM}}{m_{wP}^2} U_{mP}\right)^2} \end{aligned} \quad (5.5)$$

To prevent the analysis from becoming too complex, correlated systematic uncertainties have been ignored. First consider the U_{mP} term. This is the uncertainty in the predicted value of the water mass flow rate. The model used [Equation (5.1)] does not predict m_w but T_{wo} as given by

$$R_T = T_{wo} = f_T(T_{al}, T_{wbl}, P_{al}, T_{wi}, m_w) \quad (5.6)$$

where the subscript T indicates that the result of interest is the water temperature in basin of cooling tower. If it were used to predict m_w , the functional relationship would be according to Equation (5.4)

$$R_m = m_{wP} = f_m(T_{al}, T_{wbl}, P_{al}, T_{wi}, T_{wo}) \quad (5.7)$$

The total uncertainty in m_{wP} would then be

$$U_{mP} = \sqrt{\left(\frac{\partial m_{wP}}{\partial T_{a1}} U_{T_{a1}}\right)^2 + \left(\frac{\partial m_{wP}}{\partial T_{wbl}} U_{T_{wbl}}\right)^2 + \left(\frac{\partial m_{wP}}{\partial p_{a1}} U_{p_{a1}}\right)^2 + \left(\frac{\partial m_{wP}}{\partial T_{wi}} U_{T_{wi}}\right)^2 + \left(\frac{\partial m_{wP}}{\partial T_{wo}} U_{T_{wo}}\right)^2} \quad (5.8)$$

The uncertainties under the square root in Equation (5.5) and (5.8) indicate the combined value of the zeroth and first order uncertainties of the particular parameter. The sensitivity indexes can be expanded by using the chain rule of differentiation to give

$$\frac{\partial m_w}{\partial T_{a1}} = \frac{\partial m_w}{\partial T_{wo}} \frac{\partial T_{wo}}{\partial T_{a1}} = \left(\frac{\partial T_{wo}}{\partial m_w}\right)^{-1} \frac{\partial T_{wo}}{\partial T_{a1}} \quad (5.9)$$

Note that since sensitivity indexes indicate the relationship between an independent and dependent variable, the subscript P can be omitted from the m_w terms in Equation (5.9). The other five sensitivity indexes can be expanded in a similar manner. Equation (5.9) indicates that the θ values from Table 5-1 can be used to evaluate the sensitivity indexes of Equation (5.8). This is because both terms on the right hand side of Equation (5.9) are known values from Table 5-1. The new sensitivity indexes are listed below. The last column has units of kg/s per SI unit of input parameter, e.g. the units of $(\theta_{mP})_{T_{a1}}$ is kg/sK.

Table 5-2: Sensitivity indexes for NDWCT using Equation (5.9)

Parameter, x_i	$(\theta_{mP})_{x_i}$
T_{a1} , K	928.012
T_{wbl} , K	2011.801
p_{a1} , Pa	0.1458
T_{wo} , K	5532.2
T_{wi} , K	521.368
Me_{fi}	-27819.0
K_{fdm}	346.555

It is now possible to determine the total uncertainty in the result of Equation (5.8) by using the sensitivity indexes of Table 5-2. The only unknowns in Equation (5.8) are the uncertainties of the input parameters. The values of these uncertainties are the topic of discussion in next section. Equation (5.8) can be now be substituted into Equation (5.5) in order to calculate U_{TC} . The last unknowns in Equation (5.5) are the m_{wP} and m_{wM} values. The sample calculation given in Appendix F of ASME PTC (2003) for a NDWCT was used to estimate these values. According to this sample calculation m_{wP} was 3.3 % lower than m_{wM} . If m_{wM} is taken to be equal to the m_w value used to estimate the θ values of Table 5-1, then m_{wP} can be taken as $12500 \times 96.7\% = 12087.5$ kg/s.

5.3.5. Measurement uncertainties and uncertainty analysis

MEASUREMENT UNCERTAINTIES

All three codes stipulate that instrumentation or measuring devices should be calibrated against specific standards to within certain limits. If these uncertainties are propagated into the result then total uncertainty in the result would be considered a zeroth order uncertainty since this is the lowest possible

uncertainty that can be achieved. Table 5-3 on the next page shows the allowable calibration uncertainty limits in each parameter for the three different standards, as well as corresponding values determined for the fill performance test experiment, Table D-4.

Table 5-3: Test codes allowable calibration uncertainty limits

Parameter	ASME	BS	CTI	Table D-4
T_{al} , °C	0.05	0.05	0.05	0.6073
T_{wbl} , °C	0.05	0.05	0.05	0.7100
p_{al} , Pa	-	-	-	20
T_{wo} , °C	0.05	0.05	0.05	0.5292
T_{wi} , °C	0.05	0.05	0.05	0.6001
m_w , kg/s (% of m_w value)	1%	0.6%	1%	-

The 0.6 % BS value for water mass flow rate is the typical uncertainty found in the discharge coefficient according to British Standard 1042 (1981). The temperature values in the right hand column indicate the combined uncertainty due to the data logging system, see Table D-2 and discussion thereof, and due to spatial variation, see Table D-3. The 20 Pa value is due to resolution error. When comparing the allowable temperature calibration uncertainties of the performance test standards (column 2 to 4 of Table 5-3) with those of the uncertainties calculated once the instrumentation is installed (last column of Table 5-3) one can conclude that even if it is possible to calibrate thermocouples in ideal, clinical, total stable laboratory conditions to the required uncertainty level, these efforts will be rendered useless once the instrumentation is installed. However, it was still decided to propagate these values into the result, using Equation (5.8). The results are shown in Table 5-4. The right hand column indicates the uncertainty in the predicted water mass flow rate due to the uncertainty in the corresponding parameter and is calculated for a specific parameter as

$$(u_{mP,0})_{x_i} = \sqrt{(\theta_{mP} B_0)_{x_i}^2} \quad (5.10)$$

Table 5-4: Zero order uncertainties according to NDWCT performance test standards

Parameter, x_i	θ_{mP,x_i}	B_{0,x_i}	$(u_{mP,0})_{x_i}$
T_{al} , K	928.012	0.05	46.401
T_{wbl} , K	2011.801	0.05	100.590
p_{al} , Pa	0.1458	20	2.915
T_{wo} , K	5532.2	0.05	276.61
T_{wi} , K	521.368	0.05	26.068

The 20 Pa value was used due to lack of a better value. The total zero order uncertainty in the water mass flow rate is calculated as

$$U_{mP} = \sqrt{\sum_{i=1}^5 (\theta_{mP} B_0)_{x_i}^2} = \sqrt{\sum_{i=1}^5 (u_{mP,0})_{x_i}^2} = 299.122 \text{ kg/s} \quad (5.11)$$

From Equation (5.5) the total zero order uncertainty in TC is calculated as

$$\begin{aligned}
 U_{TC} &= \sqrt{\left(\frac{1}{m_{wP}} U_{mM}\right)^2 + \left(-\frac{m_{wM}}{m_{wP}^2} U_{mP}\right)^2} \\
 &= \sqrt{\left(\frac{1}{12087.5} 125\right)^2 + \left(-\frac{12500}{12087.5^2} 299.122\right)^2} \\
 &= 0.02760
 \end{aligned} \tag{5.12}$$

The percentage uncertainty in TC is thus $0.02760 / (12500/12087.5) \times 100 = 2.669\%$. As was stated earlier, ASME allows only a 6 % uncertainty on the TC value. Hence if only calibration uncertainties are considered then the uncertainty in TC is already 24 % of the allowable value. This analysis was repeated for an N'th order analysis. Typical values given in Appendix D of ASME were used. Table 5-5 shows the results.

Table 5-5: N'th order uncertainties according to NDWCT performance test standards

Parameter, x_i	$(\theta_{mP})_{x_i}$	$U_{x_i,tot}$	$(u_{mP,tot})_{x_i}$
T_{a1} , K	928.012	0.2278	211.381
T_{wb1} , K	2011.801	0.2278	458.244
p_{a1} , Pa	0.1458	337.880	49.250
T_{w0} , K	5532.2	0.0889	491.75
T_{wi} , K	521.368	0.0889	46.344

Following along the same lines as the previous analysis, the percentage uncertainty in TC was calculated to be 6.435 %. This means that the tower has failed the performance test. From the experience gained in conducting the fill performance tests the author feels that the $U_{x_i,tot}$ values in Table 5-5 are too low. From Table 3-1 one can see that the first order uncertainties of the temperature measurements for the fill performance tests are much lower than the zero order uncertainties. With this in mind it was thus decided to propagate these zero order uncertainties, as indicated in Table 5-3, into the result to see what the minimum uncertainties in the TC parameter would be. The result showed that the uncertainty in TC is 27.479 %. This includes a 0.6 % uncertainty in m_w according to British Standard 1042 (1981).

The uncertainty in TC due to modelling uncertainties, e.g. fill performance characteristics, are not covered by performance test codes. The objective of the following section is to evaluate the effect of uncertainty in fill performance on TC. This effect obviously depends on the type of fill and work point of the tower. For the reference tower, expanded metal fill was used which has a relative low loss coefficient compared to, for instance, film type fill. In the following analysis, only fill loss coefficient and fill Merkel number uncertainties were considered. It was found that the effect of uncertainty in the loss coefficient is negligibly small compared to the effect of uncertainty in the fill Merkel number. The fill performance uncertainties derived in Appendix D were used to propagate into TC. The total uncertainty in the fill Merkel number was taken as $0.2854 \times 2.504 = 0.7146$ and the uncertainty in K_{fdm} was taken as $0.4699 \times 2.504 = 1.1766$. Only these two uncertainties were considered and not any measurement uncertainties. The results are shown in Table 5-6 on the next page.

Table 5-6: Fill performance uncertainties

Parameter, x_i	$(\theta_{mP})_{x_i}$	$U_{x_i,tot}$	$(u_{mP,tot})_{x_i}$
T_{a1} , K	928.012	0	0
T_{wb1} , K	2011.801	0	0
p_{a1} , Pa	0.1458	0	0
T_{wo} , K	5532.2	0	0
T_{wi} , K	521.368	0	0
Me_{fi}	-27819.0	0.7146	-19879.6
K_{fdm}	346.555	1.1766	407.771

The uncertainty in TC is calculated to be an enormous 164 %. This is understandable if one considers that the total Merkel number of the specific cooling tower is 1.47, indicating that the uncertainty in the total Merkel number is $0.7146 / 1.47 \times 100 = 48.6$ %. One can also see that the fill Merkel number has a much more dominant effect than the loss coefficient. From this result one can conclude that the cooling tower performance is extremely sensitive to fill performance Merkel number and that adequate modelling of its performance is paramount. Another investigation was conducted to determine what the minimum uncertainty in the fill Merkel number must be in order to establish a 6 % uncertainty on TC. It was found that the uncertainty in the fill Merkel number per unit length, i.e. Me_{fi} , has to be smaller than 0.0104 m^{-1} . This uncertainty ignores any measuring uncertainties during the testing of the tower. It also does not include the uncertainty in fill loss coefficient.

UNCERTAINTY ANALYSIS

Only ASME provided a thorough method for determining the uncertainty in the final result. This method agrees with the method presented in Appendix B except for the calculation of the combined standard deviation of a group of measurements used to determine one parameter. ASME uses the following to determine this standard deviation

$$\langle S_x \rangle = \frac{\sqrt{\sum_{k=1}^M S_{xk}^2}}{M} \quad (5.13)$$

whereas both Coleman and Steele (1999) and Figliola and Beasley (2000) use Equation (B.6)

$$\langle S_x \rangle = \sqrt{\frac{\sum_{k=1}^M S_{xk}^2}{M}} \quad (5.14)$$

The difference is the M value of Equation (5.22) that is not included in the square root term. This will result in uncertainty estimates of ASME that are too low.

5.4. Conclusion

The three performance test codes studied in this Chapter are ASME PTC (2003), CTI (2000) and British Standard 4485 (1998). These standards relate tower performance to Tower Capability (TC). ASME and CTI use the same definition of TC, i.e. ratio of measured water mass flow rate to predicted water mass flow rate. BS expresses TC as the ratio of the as-tested (L/G) value to the predicted (L/G) value. The ASME standard was used for further investigation since it is the only standard that gives a clear definition as to whether or not a test is deemed acceptable. In order to validate whether or not the allowable uncertainties in TC stipulated by ASME are achievable, some modifications to the model described by Equation (5.1) were necessary. These modifications mainly included the use of the chain rule of differentiation in order to determine the new sensitivity indexes as given by Equation (5.9).

All three standards make use of cumbersome and unnecessary complex performance curves. PCG is a computer program developed for this thesis, which allows the user to quickly and easily adjust results at test conditions to design conditions. PCG shows good comparison with the one dimensional Improved Merkel method.

Typical uncertainties found in tower input variables were propagated into the TC value. This was done to evaluate the adequacy of the 6 % allowable uncertainty in the TC value according to ASME. Propagating the calibration uncertainties prescribed by ASME, the uncertainty in TC was found to be 2.669 %. This resembles the minimum possible uncertainty that can be attained. Propagating typical Nth order uncertainties as given in Appendix D of ASME, the uncertainty in TC was found to be 6.435 %. The zero order uncertainties determined in Appendix D for similar variables were also propagated into the TC value. The result showed that the uncertainty in TC was 27.479 %. From these results it can be concluded that a 6 % uncertainty limit on TC is unrealistic and too stringent.

When considering only fill performance uncertainties the total uncertainty in TC was found to be 164 %. This is understandable if one considers that the total Merkel number of the specific cooling tower is 1.47, indicating that the uncertainty in the total Merkel number is $0.7146 / 1.47 \times 100 = 48.6$ %. If only the Merkel number of the fill is considered then an uncertainty of 0.0104 m^{-1} in the Me_{fil} value will already generate a 6 % uncertainty in TC. These numbers will obviously vary depending on the type of fill used and the work point of the cooling tower. It is stressed again that the effect of fill performance characteristics are not covered by performance test codes. This analysis then serves to sensitise the reader that accuracy in fill performance characteristics is paramount.

CHAPTER 6. CONCLUSION AND RECOMMENDATIONS

This chapter gives an overview of the main conclusions drawn from the thesis. Most of the conclusions are repeated from the conclusions made in each chapter. It also gives recommendations for future work.

6.1. Conclusion

CHAPTER 2

Kloppers and Kröger (2005a) recommends modelling a NDWCT using the Merkel method with an improved energy equation. The improved energy equation is used for calculating the heat rejection rate of the tower and includes the energy associated with water evaporation. This method is referred to as the Improved Merkel method.

The same method used to determine fill characteristics when modelling a cooling tower must be used when determining fill characteristics in an experimental setup (Kloppers and Kröger (2005a)). In order to determine the Poppe number for fill in an experimental setup, the fill air outlet conditions must be measured accurately. This has been found to be almost impossible, since water drops are usually entrained in the air stream which complicates the measurement of dry and wet bulb measurements. The Merkel method however, does not require fill air outlet temperature measurements and is thus an attractive method to model fill behaviour.

It was decided to model the NDWCT using the Improved Merkel method, due to its simplicity and acceptable accuracy compared to the more robust Poppe method.

CHAPTER 3

In this chapter the different ways of presenting fill performance characteristics are discussed. The experimental setup used to determine fill performance characteristics, as well as test procedure is discussed. Aspects that need careful attention are the blockage effect of the water troughs, water and air mass flows and the fill water outlet temperature.

The blockage effect can cause the inlet velocity profile to be non-uniform which means that the air pressure drop given by Equation (3.1) for $\alpha_{mi} = 1.0$ is invalid. The magnitude of α_{mi} will be very close to unity in the presence of high resistance fill. However, this will not necessarily be the case for low resistance fill.

The fill water outlet temperature is measured separately in the lower and upper water trough sections. The results show that the use of a mass weighted average is required to determine the mean fill outlet water temperature, according to Equation (3.7).

In order to determine the fill performance characteristics the combined spray zone and water trough performance characteristics had to be determined first. Experimental data did not show good correlation with previous data. New correlations for the spray zone and water trough performance characteristics are

given by Equation (3.11) to (3.14). These correlations were used in determining the fill performance characteristics.

It was concluded that the fill performance experimental data was acceptable. New correlations for the fill performance characteristics (Me_{fi} and $K_{f,dm}$) are given by Equation (3.20) to (3.23). The uncertainty analysis showed that the total uncertainty in the fill Merkel number is 0.2854 m^{-1} and 0.4699 m^{-1} for the loss coefficient. The zeroth order uncertainty for the Merkel number and loss coefficient was calculated to be 0.2100 m^{-1} and 0.4248 m^{-1} , respectively. While the first order uncertainty for the Merkel number and loss coefficient was calculated to be 0.1933 m^{-1} and 0.2008 m^{-1} , respectively. By using a better data logger, more measurement locations and better curve fit methods, it is possible to reduce the total uncertainty in the fill performance characteristics.

CHAPTER 4

As was stated in the objectives for this thesis, the absence of a formal fill test procedure and data reduction method could lead to poor repeatability and uncertainty of test results. The objective of this chapter was to formulate a fill performance standard test procedure. The data reduction and calibration techniques used in this thesis automatically forms part of the test procedure. The procedure is presented in the form of a check list and addresses the following topics:

- Pipe and instrument diagram
- Check list
 - Heating of the water in the reservoir
 - Tunnel preparation
 - Start-up
 - Performance testing
 - Shut-down
 - Test conditions
 - Recommendations
 - Time frame
- Photographs of equipment

CHAPTER 5

Typical uncertainties found in tower input variables were propagated into the TC value. This was done to evaluate the adequacy of the 6 % allowable uncertainty in the TC value according to ASME. Propagating the calibration uncertainties prescribed by ASME, the uncertainty in TC was found to be 2.669 %. This resembles the minimum possible uncertainty that can be attained. Propagating typical Nth order uncertainties as given in Appendix D of ASME, the uncertainty in TC was found to be 6.435 %. The zero order uncertainties determined in Appendix D for similar variables were also propagated into the TC value. The result showed that the uncertainty in TC was 27.479 %. From these results it can be concluded that a 6 % uncertainty limit on TC is unrealistic and too stringent.

When considering only fill performance uncertainties the total uncertainty in TC was found to be 164 %. This is understandable if one considers that the total Merkel number of the specific cooling tower is 1.47,

indicating that the uncertainty in the total Merkel number is $0.7146 / 1.47 \times 100 = 48.6\%$. If only the Merkel number of the fill is considered then an uncertainty of 0.0104 m^{-1} in the Me_{fill} value will already generate a 6 % uncertainty in TC. These numbers will obviously vary depending on the type of fill used and the work point of the cooling tower. It is stressed again that the effect of fill performance characteristics are not covered by performance test codes. This analysis then serves to sensitise the reader that accuracy in fill performance characteristics is paramount.

6.2. Recommendations

CHAPTER 2

The draught equation used in the Improved Merkel method can be improved as discussed in Appendix K.

CHAPTER 3

As was stated in Appendix D, the uncertainty in the fill performance characteristics can be considered smaller than what it really is, since it does not include the uncertainties due to the spray zone and water trough performance characteristics and the orifice plate itself. The next step would be to quantify these uncertainties and then to include them in the total uncertainty of the fill performance. Bette curve fit methods also need to be addressed. It is recommended that curve fitting should be done though the data region where the tower is most likely to operate, instead of over the entire range of operating conditions. The uncertainty due to curve fit errors should also be based on the region where the tower is most likely to operate. This will generate a curve fit uncertainty that is more representative of typical tower operating conditions.

CHAPTER 4

As modifications to the test tunnel are made the test procedure presented in this chapter should be updated.

CHAPTER 5

This thesis focussed on fill performance since the fill plays such a large roll in NDWCT performance. The analysis presented can be repeated for other regions of the tower as well, e.g. rain zone, drift eliminators, spray zone, etc., or even other types of fill.

TEST FACILITY

The uncertainty in the fill performance characteristics can be reduced as discussed in Chapter 3. Modifications to the test facility should include accurate measurement of fill air outlet temperatures and an auxiliary orifice plate to check water mass flow rates. With these two modifications an energy balance can be conducted which will add more credibility to the test results. The strainer and water distribution system also needs attention. The strainer is too fine and gets clogged easily. The water pressure drop induced by the strainer and water distribution system is also very high. The water pressure drop over the strainer can be reduced by inserting an expansion chamber before the strainer. This will reduce the velocity and hence water pressure drop over the strainer. It was found that a relatively large amount of water is lost due to drift. This is because the water jets exiting the holes of the water distribution system have a high speed. On impingement with the horizontal plates of the water distribution system, the water

drops are broken up into smaller drops that get entrained into the main air stream. The lower water inlet velocity generated by the expansion chamber before the strainer could reduce this water lost. It was also found that the water distribution is quite sparse. This has little effect on cross fluted fill, since the water can be transferred outward or inward quite easily. However, for straight through fill, it can happen that sections of the fill will stay totally dry.

PCG

The PCG package includes an open source code. Modifications to the program can thus be easily made. The software should be modified to allow the user to define the performance characteristics of other regions of the tower, e.g. rain zone, spray zone, drift eliminators, water distribution system, etc. It will be seen that the graphical display of the performance curves is sometimes inadequate. This is due to scaling problems and needs further attention. It is recommended that the solver and user interface is generated using the same software. The single main advantage of this is the elimination of communication problems between different software.

Regarding the commerce of cooling towers, it is suggested that a disk should be supplied together with a cooling tower with which the client can obtain results similar as to those of the PCG package. The disc should replace the performance curves typically found in test standards as these curve methods are too cumbersome and unnecessary complex.

CHAPTER 7. REFERENCES

ASME, 2003, Atmospheric water cooling equipment, Performance test codes, ASME PTC 23-2003, New York.

Bosnjakovic, F., 1965, *Technische Thermodynamik*, Theodor Steinkopf, Dresden.

BSI, 1981, Methods of measurement of fluid flow in closed conduits, BS 1042: Section 1.1: 1981.

BSI, 1988, Water cooling towers, Methods of performance testing, BS 4485: Part 2: 1988.

Coleman, H.W. and Steele, W.G., 1991, *Experimentation and Uncertainty analysis for Engineers*, John Wiley and Sons, Inc., New York.

CTI, 2000, Acceptance Test Code for Water Cooling Towers, ACT-105, Houston.

De Villiers, E. and Kröger, D.G., 1999, Inlet Losses in Counterflow Wet-Cooling Towers, Joint Power Generation Conference, Vol. 2, PWR-Vol. 34, ASME.

Figliola, S.F. and Beasley, D.E., *Theory and Design for Mechanical Measurements*, John Wiley and Sons, Inc., New York.

Gcabashe, T.S., 2006, Chief executive's report, Eskom Holdings Limited Annual Report, p. 33.

Gerald, C.F. and Wheatley P.O., 1999, *Applied Numerical Analysis*, 6th Edition, Addison-Wesley, U.S.A.

Jaber, H. and Webb, R.L., November 1989, Design of Cooling Towers by the Effectiveness-NTU Method, Journal of Heat Transfer, Vol. 111, pp. 837-843.

Kenny, A., 2006, Heads should roll, FINWEEK, March 23, p. 13.

Kline, S.J. and McClintock, F.A., January 1953, Describing Uncertainties in Single-Sample Experiments, Mechanical Engineering, Vol. 75, pp. 3-8.

Kloppers, J.C. and Kröger D.G., 2003, Loss coefficient correlation for wet-cooling tower fills, Applied Thermal Engineering, Vol. 23, pp. 2201-2211.

Kloppers, J.C. and Kröger D.G., 2005b, A critical investigation into the heat and mass transfer analysis of wet-cooling towers, International Journal of Heat and Mass Transfer, Vol. 48, pp. 765-777.

- Kloppers, J.C. and Kröger D.G., 2005c, The Lewis factor and its influence on the performance prediction of counterflow wet-cooling towers, *International Journal of Heat and Mass Transfer*, Vol. 44, pp. 879-884.
- Kloppers, J.C. and Kröger D.G., 2005d, Influence of temperature inversions on wet-cooling tower performance, *Applied Thermal Engineering*, Vol. 25, pp. 1325-1336.
- Kloppers, J.C. and Kröger D.G., January 2005a, Cooling Tower Performance Evaluation: Merkel, Poppe, and e-NTU Methods of Analysis, *Journal of Engineering for Gas Turbines and Power*, Vol. 127, pp. 1-7.
- Kloppers, J.C., December 2003, *A critical evaluation and refinement of the performance prediction of wet-cooling towers*, Ph.D. Thesis, University of Stellenbosch, South Africa.
- Kröger, D.G., 1998, *Air-cooled Heat Exchangers and Cooling Towers, Thermal-flow Performance Evaluation and Design*, Begell House, Inc., New York.
- Kröger, D.G., 2004, *Air-cooled Heat Exchangers and Cooling Towers, Thermal-flow Performance Evaluation and Design*, PennWell Corp., Tulsa, Oklahoma.
- Merkel, F., January 1926, Verdunstungskühlung, *VDI Zeitschrift*, Vol. 70 Jan-Jun 1926, pp. 123-128.
- Mohiuddin, A.K.M. and Kant, K., 1991, Analysis of mechanical draft wet cooling towers, *Journal of energy, heat and mass transfer*, Vol. 13, pp. 165-187.
- Mohiuddin, A.K.M. and Kant, K., 1996, Knowledge base for the systematic design of wet cooling towers. Part 2: Fill and other design parameters, *International Journal of Refrigeration*, Vol. 19, No. 1, pp. 52-60.
- NIST ITS-90, 1990, available at http://srdata.nist.gov/its90/useofdatabase/use_of_database.html
- O'Connor, P., 2006, Eskom's generation capacity expansion plans, *ESI – The Power Journal of Africa*, I, pp. 40-43.
- Poppe, M. and Rögener, H., 1991, Berechnung von Rückkühlwerken, *VDI-Wärmeatlas*, Mi 1 – Mi 15.
- S. Ergun, 1952, Fluid flow through packed columns, *Chemical Engineering Process*, Vol. 48, pp. 89-94.
- Schlumberger Technologies, 1990, 3595 Series Isolated Measurement Pods, Installation Guide.
- Solartron, 1996, 359574A IMPVIEW, Operator Manual.
- Van der Linde, B., 2006, Heads should roll, *FINWEEK*, March 23, pp. 12-14.

VDMA, 1991, Wärmetechnische Abnahmemessungen an zwangsbelüfteten, standardisierten Naßkühltürmen.

APPENDIX A. THERMOPHYSICAL PROPERTIES

A.1. Introduction

This appendix shows the equations used to determine the properties of fluids as summarised by Kröger (1998 and 2004)

THERMOPHYSICAL PROPERTIES OF DRY AIR FROM 220 K TO 380 K AT STANDARD ATMOSPHERIC PRESSURE (101325 Pa)

Density

$$\rho_a = p_a / (287.08T), \text{ kg/m}^3 \quad (\text{A.1})$$

Specific heat

$$c_{pa} = 1.045356 \times 10^3 - 3.161783 \times 10^{-1}T + 7.083814 \times 10^{-4}T^2 - 2.705209 \times 10^{-7}T^3, \text{ J/kgK} \quad (\text{A.2})$$

Dynamic viscosity

$$\mu_a = 2.287973 \times 10^{-6} + 6.259793 \times 10^{-8}T - 3.131956 \times 10^{-11}T^2 + 8.15038 \times 10^{-15}T^3, \text{ kg/sm} \quad (\text{A.3})$$

Thermal conductivity

$$k_a = -4.937787 \times 10^{-4} + 1.018087 \times 10^{-4}T - 4.627937 \times 10^{-8}T^2 + 1.250603 \times 10^{-11}T^3, \text{ W/mK} \quad (\text{A.4})$$

THERMOPHYSICAL PROPERTIES OF SATURATED WATER VAPOUR FROM 273.15 K TO 380 K

Vapour pressure

$$p_v = 10^z, \text{ Pa} \\ z = 10.79586(1 - 273.16/T) + 5.02808 \log_{10}(273.16/T) + 1.50474 \times 10^{-4} [1 - 10^{-8.29692((T/273.16)-1)}] + 4.2873 \times 10^{-4} [10^{4.76955(1 - 273.16/T)} - 1] + 2.786118312 \quad (\text{A.5})$$

Specific heat

$$c_{pv} = 1.3605 \times 10^3 + 2.31334T - 2.46784 \times 10^{-10}T^5 + 5.91332 \times 10^{-13}T^6, \text{ J/kgK} \quad (\text{A.6})$$

Dynamic viscosity

$$\mu_v = 2.562435 \times 10^{-6} + 1.816683 \times 10^{-8}T + 2.579066 \times 10^{-11}T^2 - 1.067299 \times 10^{-14}T^3, \text{ kg/sm} \quad (\text{A.7})$$

Thermal conductivity

$$k_v = 1.3046 \times 10^{-2} - 3.756191 \times 10^{-5}T + 2.217964 \times 10^{-7}T^2 - 1.111562 \times 10^{-10}T^3, \text{ W/mK} \quad (\text{A.8})$$

Vapour density

$$\rho_v = -4.062329056 + 0.10277044T - 9.76300388 \times 10^{-4}T^2 + 4.475240795 \times 10^{-6}T^3 - 1.004596894 \times 10^{-8}T^4 + 8.9154895 \times 10^{-12}T^5, \text{ kg/m}^3 \quad (\text{A.9})$$

THERMOPHYSICAL PROPERTIES OF MIXTURES OF AIR AND WATER VAPOUR

Density

$$\rho_{av} = (1 + w) [1 - w/(w + 0.62198)] p_{abs}/(287.08T), \text{ kg/m}^3 \quad (\text{A.10})$$

Specific heat

$$c_{pav} = (c_{pa} + w c_{pv})/(1 + w), \text{ J/K kg air-vapour} \quad (\text{A.11})$$

or the specific heat of the air-vapour mixture per unit mass of dry air:

$$c_{pma} = (c_{pa} + w c_{pv}), \text{ J/K kg dry air} \quad (\text{A.12})$$

Dynamic viscosity

$$\mu_{av} = (X_a \mu_a M_a^{0.5} + X_v \mu_v M_v^{0.5}) / (X_a M_a^{0.5} + X_v M_v^{0.5}), \text{ kg/ms} \quad (\text{A.13})$$

where $M_a = 28.97 \text{ kg/mole}$, $M_v = 18.016 \text{ kg/mole}$, $X_a = 1/(1 + 1.608 w)$ and

$$X_v = w/(w + 0.622)$$

Thermal conductivity

$$k_{av} = (X_a k_a M_a^{0.33} + X_v k_v M_v^{0.33}) / (X_a M_a^{0.33} + X_v M_v^{0.33}), \text{ W/mK} \quad (\text{A.14})$$

Humidity ratio

$$w = \left(\frac{2501.6 - 2.3263(T_{wb} - 273.15)}{2501.6 + 1.8577(T - 273.15) - 4.184(T_{wb} - 273.15)} \right) \left(\frac{0.62509 p_{vwb}}{p_{abs} - 1.005 p_{vwb}} \right) - \left(\frac{1.00416(T - T_{wb})}{2501.6 + 1.8577(T - 273.15) - 4.184(T_{wb} - 273.15)} \right) \quad (\text{A.15})$$

Enthalpy

$$i_{av} = [c_{pa}(T - 273.15) + w\{i_{fgwo} + c_{pv}(T - 273.15)\}]/(1 + w), \text{ J/kg air-vapour} \quad (\text{A.16})$$

or the enthalpy of the air-vapour mixture per unit mass of dry air:

$$i_{ma} = c_{pa}(T - 273.15) + w[i_{fgwo} + c_{pv}(T - 273.15)], \text{ J/kg air-vapour} \quad (\text{A.17})$$

where the specific heats are evaluated at $(T + 273.15)/2$ and the latent heat i_{fgwo} , is evaluated at 273.15K according to equation (A.11) and (A.12).

THERMOPHYSICAL PROPERTIES OF SATURATED WATER LIQUID FROM 273.15 K TO 380 K

Density

$$\rho_w = (1.49343 \times 10^{-3} - 3.7164 \times 10^{-6} T + 7.09782 \times 10^{-9} T^2 - 1.90321 \times 10^{-20} T^6)^{-1}, \text{ kg/m}^3 \quad (\text{A.18})$$

Specific heat:

$$c_{pw} = 8.15599 \times 10^3 - 2.80627 \times 10 T + 5.11283 \times 10^{-2} T^2 - 2.17582 \times 10^{-13} T^6, \text{ J/kgK} \quad (\text{A.19})$$

Dynamic viscosity:

$$\mu_w = 2.414 \times 10^{-5} \times 10^{247.8/(T-140)}, \text{ kg/sm} \quad (\text{A.20})$$

Thermal conductivity:

$$k_w = -6.14255 \times 10^{-1} + 6.9962 \times 10^{-3} T - 1.01075 \times 10^{-5} T^2 + 4.74737 \times 10^{-12} T^4, \text{ W/mK} \quad (\text{A.21})$$

Latent heat of evaporation

$$i_{fgw} = 3.4831814 \times 10^6 - 5.8627703 \times 10^3 T + 12.139568 T^2 - 1.40290431 \times 10^{-2} T^3, \text{ J/K} \quad (\text{A.22})$$

Surface tension

$$\sigma_w = 5.148103 \times 10^{-2} + 3.998714 \times 10^{-4} T - 1.4721869 \times 10^{-6} T^2 + 1.21405335 \times 10^{-9} T^3, \text{ N/m} \quad (\text{A.23})$$

APPENDIX B. UNCERTAINTY ANALYSIS

B.1. Introduction

Much work has been done in the field of uncertainty analysis since the classical paper of Kline and McClintock (1953). Coleman and Steele (1999) gives detailed information and is recommended for advanced readers, while Figliola and Beasley (2000) has a more introductory approach and is recommended for newcomers in the field of uncertainty analysis. Each cooling tower performance test code has its own way of analysing uncertainty in performance test measurement data. Chapter 5 discusses these differences in more detail. In this appendix the basic concepts, definitions and methodology of propagating uncertainty into a result is presented. The procedure contains features found in performance test codes and other available literature. The method of propagating uncertainties into the results, as discussed in Section B.3, is well explained by both Figliola and Beasley (2000) and Coleman and Steele (1999). The latter however, also introduces the concept of systematic correlated uncertainties as defined by Equation (B.18) and (B.19). Theory presented in this chapter will be used to determine the uncertainty in the fill performance characteristics, see Appendix D. This uncertainty is then propagated into the performance of a NDWCT, see Chapter 5.

B.2. Basic concepts and definitions

ABSOLUTE, SYSTEMATIC AND PRECISION ERRORS

An error is the difference between the true value of a measurement and the value assigned to it by our instrumentation. When the sign of the difference is ignored the term absolute error is used. In this thesis the term “error” will be used. Two types of errors exist, namely systematic or bias and random or precision errors. Theoretically, a systematic error is the error in the measurement that stays constant with every reading. The random error manifests itself as data scatter due to the varying nature of the measured parameter. A further distinction is given later in this appendix. Consider measuring a parameter X over a period of time. The total error made for the i 'th measurement, δ_i , is equal to the sum of the systematic error, β and random error, ϵ_i .

$$\delta_i = \beta + \epsilon_i \quad (\text{B.1})$$

The relationship of Equation (B.1) for the i and $i+1$ 'th measurement is shown below.

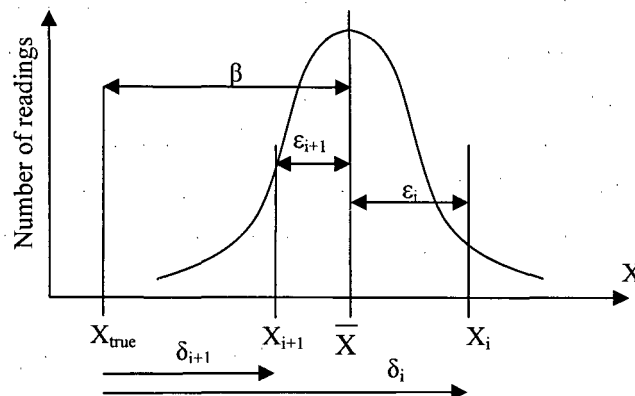


Figure B-1: Random and systematic errors

If we take an infinite number of measurements, the data will most likely follow the Gaussian or Normal distribution with population parameters, mean value μ , and standard deviation σ . It is claimed by Coleman and Steele (1999) that the Gaussian or Normal distribution describes more real cases of experimental and instrumental variability than any other distribution. Since we cannot take an infinite number of readings, our best estimate of X_{true} is

$$X_{\text{true}} = \bar{X} \pm U_X \quad C \quad (\text{B.2})$$

where

\bar{X} = our best estimate of μ , given by Equation (B.3)

U_X = the uncertainty or band width within which we estimate X_{true} to be in

C = the confidence we have in our estimate of X_{true}

In many engineering practices a confidence level of 95 % is considered sufficient. This is supported by ASME PTC (2003) and is therefore used in the rest of this thesis. The value U_X is termed the uncertainty in our estimate of X_{true} . Note that unlike an error, an uncertainty is always accompanied by a confidence level. Equation (B.11) gives more detail regarding the confidence level used.

FINITE STATISTICS

Based on the assumption of a Normal distribution, the following finite statistics are used and can be found in any statistics textbook. The general variable x will now be used instead of X .

The average value for a number of measurements made by one instrument is given as

$$\bar{x} = \frac{1}{N} \sum_{i=1}^N x_i \quad (\text{B.3})$$

where

N = is equal to the number of readings

x = the parameter investigated

For parameters calculated from the measurements of a group of instruments, the combined average of the group is given as

$$\langle \bar{x} \rangle = \frac{\sum_{k=1}^M \bar{x}_k}{M} \quad (\text{B.4})$$

where

M = number of instruments

The standard deviation for a number of measurements made by one instrument is given as

$$S_x = \sqrt{\frac{\sum_{i=1}^N (x_i - \bar{x})^2}{N-1}} \quad (\text{B.5})$$

For parameters calculated from the measurements of a group of instruments, the combined standard deviation of the group is given as

$$\langle S_x \rangle = \sqrt{\frac{\sum_{k=1}^M S_{x_k}^2}{M}} \quad (\text{B.6})$$

The standard deviation of the means based on a single set of measurements made by one instrument, is given as

$$S_x = \frac{S_x}{\sqrt{N}} \tag{B.7}$$

The standard deviation of the means based on a single set of measurements of a group of instruments, is given as

$$\langle S_x \rangle = \frac{\langle S_x \rangle}{\sqrt{MN}} \tag{B.8}$$

The standard deviation of errors made when fitting a curve through experimental data is given as

$$S_{yx} = \sqrt{\frac{\sum_{i=1}^N (y_{ci} - y_i)^2}{N - m}} \tag{B.9}$$

where

m = degrees of freedom of the curve fit

y_i = experimental value

y_{ci} = value given by the curve fit

For instance, if a linear curve is fitted through the data then $m = 2$ since only the gradient of the line and the y-intercept can be used to adjust the curve. To illustrate the concepts and definitions given above, consider the scenario depicted on the right hand side of Figure B-2 on the next page. Air is moving through a duct where four thermocouples are situated. The thermocouples are used to determine the average air inlet temperature, which in turn is used to calculate the air-vapour mass flow rate. Measurements were taken over time, yielding the hypothetical distributions shown in Figure B-2 (a) to (d). What we want is *one, true mean* temperature that is *representative of all* the temperature measured in the cross sectional plane over time. Table B-1 shows the application of the above equations and interpretation thereof. Each thermocouple took N number of readings. In Figure B-2 (e) all the data was grouped under one curve.

Table B-1: Interpretation of finite statistics

Figure	Equation	Interpretation
(a) – (d)	$S_{T_k} = \sqrt{\frac{\sum_{i=1}^N (T_{k_i} - \bar{T}_k)^2}{N - 1}}$	Standard deviation of temperature readings at location k , where $k = 1, 2, 3, 4$
(e)	$S_T = \sqrt{\frac{\sum_{i=1}^{4N} (T_i - \langle \bar{T} \rangle)^2}{4N - 1}}$	Standard deviation of the air temperature in the cross sectional area. This is the largest standard deviation, since it includes deviations due to the air properties not just at one location, but at all the measurement locations.
(f)	$\langle S_T \rangle = \sqrt{\frac{\sum_{k=1}^4 (S_{T_k})^2}{4}}$	Combined standard deviation of the group of thermocouples.
(g)	$\langle S_{\bar{T}} \rangle = \frac{\langle S_T \rangle}{\sqrt{4N}}$	Standard deviation of the true mean temperature

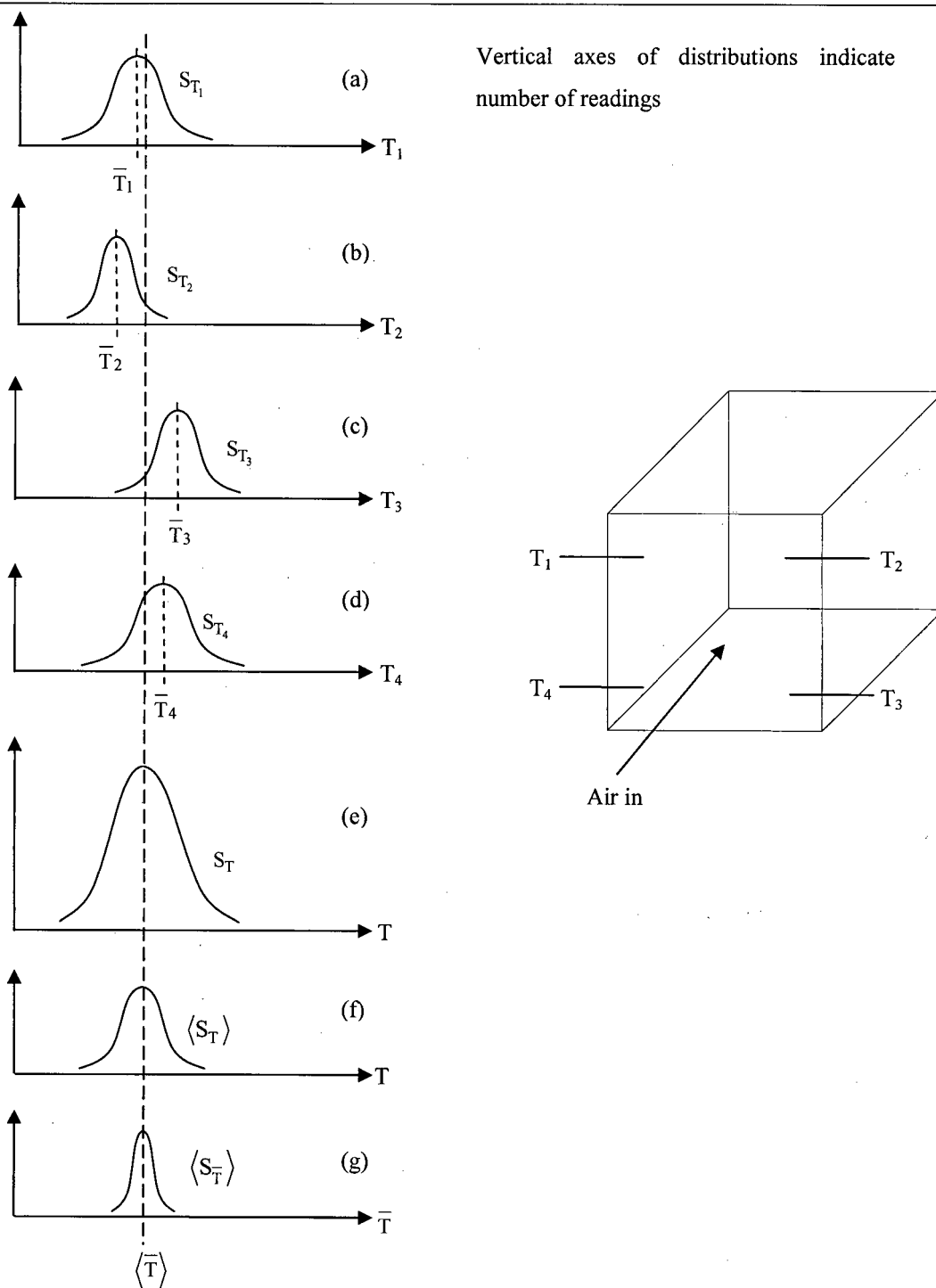


Figure B-2: Hypothetical distribution of data and experimental setup.

Since we are looking for one true mean temperature, the bottom distribution of Figure B-2 is of importance. The fact that the distribution is narrower is due to the averaging process as can be seen from Equation (B.8). This averaging process will also dampen the randomness found at each location. The last concept to address is that of errors due a spatial diverse sample. ASME PTC (2003) defines this concept as, “the difference between the true average value of a parameter and the average produced by an array of instruments ... In principle the error associated with this variation could be calculated as an integration error.” The code continues to state that normally an insufficient number of locations are available to treat

this error as an integration error and that the uncertainty associate with this error is considered to be systematic. The standard deviation due to a spatial diverse sample is given by ASME PTC (2003) as

$$S_{\text{spatial}} = \sqrt{\frac{\sum_{k=1}^M (\bar{x}_k - \langle \bar{x} \rangle)^2}{M-1}} \quad (\text{B.10})$$

UNCERTAINTY

The focus of uncertainty analysis is to determine the band width, $\pm U_x$ of Equation (B.2). The general variable x will now be used instead of X . The t-statistic is used to adjust this band width according to the confidence level we want. Coleman and Steele (1999) shows that for $N > 10$ and $C = 95\%$ one can take $t \approx 2$. This is also supported by ASME PTC (2003). Thus from Equation (B.2) we can say that

$$\begin{aligned} x_{\text{true}} &= \bar{x} \pm t S_x \\ &\approx \bar{x} \pm 2 S_x = \bar{x} \pm U_x \quad C=95\% \end{aligned} \quad (\text{B.11})$$

where

S_x = standard deviation of the general variable x

In this case the uncertainty in the parameter x had only one source of uncertainty, for example the calibration curve of a pressure transducer or the unsteadiness of the parameter x . For more than one uncertainty the combined uncertainty is calculated using the Root Sum Square (RSS) method, i.e.

$$U = \sqrt{\sum (2S_x)^2} = \sqrt{\sum (U_x)^2} \quad C = 95\% \quad (\text{B.12})$$

It will be seen that the $2 \times$ (standard deviation) product will feature throughout the uncertainty analysis. In addition to the definition given in the beginning of Section B.2, the following definitions are also used to differentiate between random and systematic uncertainties.

Random uncertainties, P

These uncertainties are due to the varying nature of the parameter being measured and are dependent on time and the number of measurements taken.

Systematic uncertainties, B

These uncertainties arise due to errors inherent in the instrumentation or method used. Systematic uncertainties are not affected by time or number or readings.

B.3. Propagation of uncertainty into the result

Consider a result R that is a function of n parameters

$$R = f_R(x_1, x_2, \dots, x_n) \quad (\text{B.13})$$

Equation (B.13) is also called the data reduction equation. Each parameter consists of a systematic and random uncertainty. The propagation of systematic and random uncertainties into the results will be considered separately. As Coleman puts it, "A bias is a fixed error that can be reduced by calibration. However, a random error is a variable error that can be reduced by the use of multiple readings. This differing behaviour of the two error components makes it desirable and necessary to consider the components separately." Propagating uncertainty into a result is explained with the aid of the road map shown in Figure B-3 on the next page.

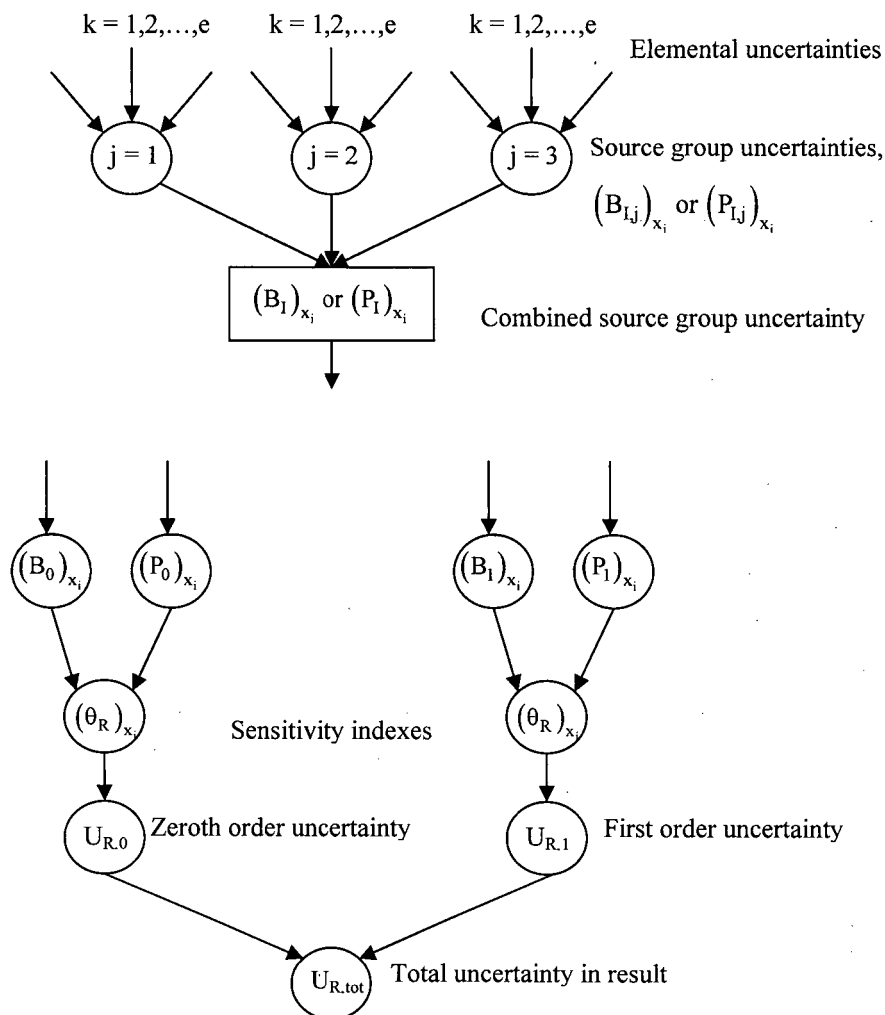


Figure B-3: Propagation of uncertainty into a result

The top half of Figure B-3 is repeated for each of the parameters in Equation (B.13) and each order of uncertainty. The orders of uncertainty are defined below

Zeroth order uncertainty, $I = 0$

This uncertainty would be the minimum possible uncertainty, since at this level only the uncertainties inherent to the instrumentation or method are considered.

First order uncertainty, $I = 1$

Measurements in the test facility are taken over time. All time dependent factors that contribute to the unsteadiness of the experiment are incorporated.

N'th order uncertainty

This is the appropriate uncertainty to report in an uncertainty analysis. This uncertainty includes both the effects of the instrumentation itself as well as the unsteadiness of parameters being measured, i.e. the total uncertainty in a result.

Each source group consists of elemental uncertainties. The three source groups are given below

- Calibration uncertainties, $j = 1$
- Data acquisition uncertainties, $j = 2$
- Data reduction uncertainties, $j = 3$

Examples of elemental uncertainties are

- Curve fitting, $k = 1$
- Calibration technique, $k = 2$
- Instrument resolution, $k = 3$
- Spatial effects, $k = 4$
- Variation in parameter, $k = 5$

These terms are explained in the fill performance uncertainty analysis in Appendix D. The working of Figure B-3 is explained by first considering the zeroth order systematic uncertainties for the parameter x_i . The source group systematic uncertainty is determined by combining the elemental uncertainties in each source group and is given as

$$(B_{0,j})_{x_i} = \sqrt{\sum_{k=1}^e (B_{0,j,k})_{x_i}^2} \quad (\text{B.14})$$

where

$B_{0,j}$ = zeroth order systematic uncertainty for the j 'th source group

$B_{0,j,k}$ = zeroth order k 'th elemental uncertainty in the j 'th source group

e = number of elemental uncertainties

The zeroth order systematic uncertainty is determined by combining the source group systematic uncertainties

$$(B_0)_{x_i} = \sqrt{\sum_{j=1}^3 (B_{0,j})_{x_i}^2} \quad (\text{B.15})$$

where

B_0 = zeroth order systematic uncertainty

In exactly the same manner the zeroth order random uncertainty is calculated as

$$(P_0)_{x_i} = \sqrt{\sum_{j=1}^3 (P_{0,j})_{x_i}^2} \quad (\text{B.16})$$

where

$P_{0,j}$ = zeroth order random uncertainty for the j 'th source group

The sensitivity index is given as

$$\begin{aligned} (\theta_R)_{x_i} &= \left. \frac{\partial R}{\partial x_i} \right|_{WP} \approx \frac{f_R(x_1, x_2, x_i + \delta x_i, \dots, x_n) - f_R(x_1, x_2, x_i - \delta x_i, \dots, x_n)}{(x_i + \delta x_i) - (x_i - \delta x_i)} \\ &= \frac{f_R(x_1, x_2, x_i + \delta x_i, \dots, x_n) - f_R(x_1, x_2, x_i - \delta x_i, \dots, x_n)}{2\delta x_i} \end{aligned} \quad (\text{B.17})$$

where

$i = 1, 2, 3, \dots, n$

δx_i = small change in x_i

The first order derivatives were approximated with the central differencing formula that has an error of $O(h^2)$, (Gerald and Wheatley (1999)). Although Figure B-3 indicates that Equation (B.17) should be calculated near the end of the analysis, this should actually be one of the first steps. It was found that almost more time is required to estimate uncertainties than to do the actual experiments. This way one can

identify which parameters will need closer investigation. The zeroth order uncertainty can now be calculated by combining the zeroth order random and systematic uncertainties of all the parameters

$$U_{R,0} = \sqrt{\sum_{i=1}^n (\theta_R P_0)_{x_i}^2} + \sqrt{\sum_{i=1}^n (\theta_R B_0)_{x_i}^2 + 2 \sum_{i=1}^{n-1} \sum_{z=i+1}^n (\theta_R)_{x_i} (\theta_R)_{x_z} B_{x_i, x_z}} \quad (\text{B.18})$$

where

B_{x_i, x_z} = correlated systematic uncertainties in x_i and x_z

n = number of parameters, see Equation (B.13)

Correlated systematic uncertainties arise from measurements that share a common elemental uncertainty source. In these situations the common error source will either increase or decrease the total uncertainty. Coleman and Steele (1999) and ASME PTC (2003) suggests the following estimate for correlated systematic uncertainties,

$$B_{x_i, x_z} = \sum_{\alpha=1}^L (B_{x_i})_{\alpha} (B_{x_z})_{\alpha} \quad (\text{B.19})$$

where L is the number of systematic uncertainties that are common to measurements x_i and x_z .

The first order uncertainty is calculated similar as to the zeroth order uncertainty

$$U_{R,1} = \sqrt{\sum_{i=1}^n (\theta_R P_1)_{x_i}^2} + \sqrt{\sum_{i=1}^n (\theta_R B_1)_{x_i}^2 + 2 \sum_{i=1}^{n-1} \sum_{z=i+1}^n (\theta_R)_{x_i} (\theta_R)_{x_z} B_{x_i, x_z}} \quad (\text{B.20})$$

Finally, the total or N 'th order uncertainty is given as

$$U_{R,tot} = \sqrt{(U_{R,0})^2 + (U_{R,1})^2} \quad (\text{B.21})$$

APPENDIX C. PROCESSING OF EXPERIMENTAL DATA

C.1. Introduction

In this appendix the processing of experimental data for the fill performance test is presented. The test setup and test procedure is described in Chapter 3 and 4. It is assumed that the air pressure drop from the inlet of the tunnel to the ASHRAE 51-75 nozzles is negligible, hence $p_{up} = p_{atm}$. The sample calculation refers to the last entry of Table H-2 on page H-6.

MEASUREMENTS

Averaged measurements

Atmospheric pressure	$p_{atm} = 101000 \text{ Pa}$
Air temperature at water trough air inlet	$T_{ai} = 288.0883 \text{ K (14.9383 } ^\circ\text{C)}$
Wet bulb temperature at water trough air inlet	$T_{wbi} = 286.2517 \text{ K (13.1017 } ^\circ\text{C)}$
Static air pressure at water trough air inlet	$p_{ai} = 1.3400 \text{ V}$
Air pressure drop: fill + water troughs	$\Delta p_{fiTOT} = 1.2592 \text{ V}$
Fill water inlet temperature	$T_{wi} = 294.4631 \text{ K (21.3131 } ^\circ\text{C)}$
Trough water outlet temperature	$T_{wo} = 291.0910 \text{ K (17.9410 } ^\circ\text{C)}$
Water pressure drop: orifice plate	$\Delta p_{or} = 5.5921 \text{ V}$
Air static pressure before ASHRAE 51-75 nozzles	$p_{up} = 101000 \text{ Pa}$
Wet bulb temperature: ASHRAE 51-75 nozzles	$T_{wbn} = 285.4689 \text{ K (12.3189 } ^\circ\text{C)}$
Air temperature: ASHRAE 51-75 nozzles	$T_{an} = 287.0902 \text{ K (13.9402 } ^\circ\text{C)}$
Air pressure drop: ASHRAE 51-75 nozzles	$\Delta p_{nth} = 2.5380 \text{ V}$

Zero readings

Air static pressure at water trough air inlet	$p_{ai0} = 1.00145 \text{ V}$
Air pressure drop – fill plus water troughs	$\Delta p_{fiTOT0} = 1.0017 \text{ V}$
Air pressure drop – ASHRAE 51-75 nozzles	$\Delta p_{nth0} = 0.9797 \text{ V}$

Other data

Fill frontal area	$A_{fr} = 2.25 \text{ m}^2$
Diameter of nozzle throat	$d_n = 0.3 \text{ m}$
Upstream area of nozzles	$A_{tus} = 4 \text{ m}^2$
Length of fill	$L_{fi} = 1.524 \text{ m}$

CALIBRATION DATA

Unit	Parameter	Curve: $y = mx + c$		Calibrated zero reading, V	Measured zero reading, V
		m, Pa/V	c, Pa		
0 L	Δp_{fiTOT}	462.8223	- 463.5870	1.0029	1.0017
1 L	p_{ai}	620.7888	- 616.1144	0.9936	1.00145
2 H	Δp_{nth}	381.3774	- 371.7136	0.9752	0.9797
m_{wHIGH}	Δp_{or}	4801.56446	- 4808.53259		

WATER MASS FLOW RATE

The water mass flow rate is determined by measuring the water pressure drop over an orifice plate according to British Standard 1042 (1981). The water mass flow rate is calculated following an iterative procedure. It will be shown that $m_w = 12.4551$ kg/s gives a converged solution.

The diameter ratio of the orifice plate is

$$\beta = \frac{0.062}{0.13} = 0.4769231$$

From Appendix A determine the following properties at T_{wi} : $\rho_{wi} = 997.8829$ kg/m³ and $\mu_{wi} = 9.7052 \times 10^{-4}$ kg/ms. The velocity of the water in the pipe is given as

$$\begin{aligned} v_w &= 4 \frac{m_w}{\rho_{wi} \pi 0.13^2} \\ &= 4 \frac{12.4551}{997.8829 \times \pi \times 0.13^2} = 0.9404 \text{ m/s} \end{aligned}$$

The corresponding Reynolds number is

$$\begin{aligned} Re_D &= \frac{\rho_{wi} v_w 0.13}{\mu_{wi}} \\ &= \frac{997.8829 \times 0.9404 \times 0.13}{9.7052 \times 10^{-4}} = 125698.8 \end{aligned}$$

The coefficient of discharge is given by

$$\begin{aligned} C_d &= 0.5959 + 0.0312\beta^{2.1} - 0.1840\beta^8 + 0.0029\beta^{2.5} \left(\frac{1 \times 10^6}{Re_D} \right)^{0.75} + 0.09 \times 0.0390L_1 - 0.0377L_2\beta^3 \\ &= 0.5959 + 0.0312(0.4769231)^{2.1} - 0.1840(0.4769231)^8 + 0.0029(0.4769231)^{2.5} \left(\frac{1 \times 10^6}{125698.8} \right)^{0.75} + \\ &\quad 0.09 \times 0.0390 \times 1 - 0.0377 \times 0.47(0.4769231)^3 \\ &= 0.6057 \end{aligned}$$

where $L_1 = 1$ and $L_2 = 0.47$ according to the orifice plate setup. The approach velocity factor is given by

$$Y = (1 - \beta^4)^{-0.5} = (1 - 0.4769231^4)^{-0.5} = 1.026917$$

The water pressure drop reading over the orifice plate must be converted to pascals using the calibration curves

$$\Delta p_{or} (\text{Pa}) = 4801.56446 \Delta p_{or} (V) - 4808.53259 = 22042.3 \text{ Pa}$$

The mass flow rate can now be calculated as

$$\begin{aligned} m_w &= \frac{C_d Y \pi d^2}{4} (2 \rho_w \Delta p_{or})^{0.5} \\ &= \frac{0.6057 \times 1.026917 \times \pi \times 0.062^2}{4} (2 \times 997.8829 \times 22042.3)^{0.5} = 12.4552 \text{ kg/s} \end{aligned}$$

This confirms that $m_w = 12.4551$ kg/s.

AIR MASS FLOW RATE

The air mass flow rate is calculated using Equation (F.2). First the air pressure drop over the nozzles is calculated as

$$\Delta p_{nth} = 381.3774 \times (2.5380 + 0.9752 - 0.9797) - 371.7136 = 594.4984 \text{ Pa}$$

From Appendix A find the following properties: $p_{vwb} = 1431.2526 \text{ Pa}$, $w_n = 0.008318 \text{ kg/kg}$ and $\rho_{avn} = 1.2193 \text{ kg/m}^3$. The air-vapour mass flow rate through the nozzles is given by Equation (F.2) as

$$m_{avn} = \frac{3 \left(2 \frac{\Delta p_{nth}}{\rho_{avn}} \right)^{0.5}}{\frac{1}{\rho_{avn}} \left(\frac{1}{A_n} - \frac{1}{A_{tus}} \right)} = \frac{3 \left(2 \frac{594.4984}{1.2193} \right)^{0.5}}{1.2193 \left(\frac{1}{0.0707} - \frac{1}{4} \right)} = 8.2211 \text{ kg/s}$$

The mass flow rate of dry air through the tunnel can be calculated as follows:

$$m_a = \frac{m_{avn}}{1 + w_n} = \frac{8.2211}{1 + 0.008318} = 8.1533 \text{ kg/s}$$

MERKEL NUMBER

The enthalpy of the air below the water troughs is found according to Equation (A.17). At the specified air inlet temperature of $T_{ai} = 288.0883 \text{ K}$, wet bulb temperature of $T_{wbi} = 286.25172 \text{ K}$ and static air pressure of $p_{ai} = 101210.8694 \text{ Pa}$ find the following: $c_{pai} = 1006.4353 \text{ J/kgK}$, $c_{pvi} = 1868.9853 \text{ J/kgK}$, $p_{vbi} = 1506.6398 \text{ Pa}$, $w_i = 0.008688 \text{ kg/kg}$ and $i_{mai} = 37011.3432 \text{ J/kg dry air}$. Merkel's relation is evaluated using the four point Chebyshev integral, where Me_{fitOT} includes both the water trough, spray zone and fill section.

$$Me_{fitOT} = \frac{h_d a L_{fitOT}}{G_w} = \int_{T_{wo}}^{T_{wi}} \frac{c_{pw}}{i_{masw} - i_{ma}} dT_w = c_{pwm} \frac{T_{wi} - T_{wo}}{4} \left(\frac{1}{\Delta i_1} + \frac{1}{\Delta i_2} + \frac{1}{\Delta i_3} + \frac{1}{\Delta i_4} \right)$$

Enthalpy differentials are evaluated at the following intermediate temperatures

$$T_{w1} = T_{wo} + 0.1(T_{wi} - T_{wo}) = 291.4282 \text{ K}$$

$$T_{w2} = T_{wo} + 0.4(T_{wi} - T_{wo}) = 292.4399 \text{ K}$$

$$T_{w3} = T_{wo} + 0.6(T_{wi} - T_{wo}) = 293.1143 \text{ K}$$

$$T_{w4} = T_{wo} + 0.9(T_{wi} - T_{wo}) = 294.1259 \text{ K}$$

The enthalpy of saturated air at $T_{w1} = 291.4282 \text{ K}$ and $p_m = 2/(1/p_{atm} + 1/p_{ai}) = 101107.1230 \text{ Pa}$ is evaluated similar to that of the inlet air and is calculated as $i_{masw1} = 52006.4252 \text{ J/kg dry air}$. From Equation (A.19) find $c_{pwm} = 4185.4723 \text{ J/kgK}$ at $0.5(T_{wi} + T_{wo})$. The enthalpy of unsaturated air at T_{w1} is found from the energy equation as given by Equation (2.4)

$$\begin{aligned} i_{maw1} &= c_{pwm} m_w \frac{T_{w1} - T_{wo}}{m_a} + i_{mai} \\ &= 4181.4723 \times 12.4551 \frac{291.4282 - 291.0910}{8.1533} + 37011.3432 \\ &= 39165.2683 \text{ J/kg dry air} \end{aligned} \quad (C.1)$$

With both enthalpies known, Δi_1 can be calculated as $i_{masw1} - i_{maw1} = 52006.4252 - 39165.2683 = 12841.1569 \text{ J/kg dry air}$. Similarly find $\Delta i_2 = 9659.3246 \text{ J/kg dry air}$, $\Delta i_3 = 7615.7987 \text{ J/kg dry air}$ and $\Delta i_4 = 4670.1486 \text{ J/kg dry air}$. Substitute these values into Merkel's relation and find

$$\begin{aligned} Me_{fitOT} &= c_{pwm} \frac{T_{wi} - T_{wo}}{4} \left(\frac{1}{\Delta i_1} + \frac{1}{\Delta i_2} + \frac{1}{\Delta i_3} + \frac{1}{\Delta i_4} \right) \\ &= 4181.4723 \frac{294.4631 - 291.0910}{4} \left(\frac{1}{12841.1569} + \frac{1}{9659.3246} + \frac{1}{7615.7987} + \frac{1}{4670.1486} \right) \\ &= 1.8571 \end{aligned}$$

The Merkel number of the water troughs and spray zone must now be subtracted from above Merkel number to get the Merkel number of fill. The Merkel number of the water troughs and spray zone is given by Equation (3.12) as

$$\begin{aligned} Me_{tr} &= 0.6589 G_w^{0.2214} G_a^{0.3814} T_{wi}^{-0.4187} \\ &= 0.6589 \left(\frac{12.4551}{2.25} \right)^{0.2214} \left(\frac{8.1533}{2.25} \right)^{0.3814} (294.4631 - 273.15)^{-0.4187} \\ &= 0.4368 \end{aligned}$$

The fill Merkel number per unit length is thus $(1.8571 - 0.4368)/1.524 = 0.9340 \text{ m}^{-1}$.

AIR PRESSURE LOSS COEFFICIENT

The air pressure loss coefficient of the fill in the absence of momentum changes is given by Equation (3.3) as

$$K_{fdm} = \frac{2 \left[\Delta p_{fi} - (\rho_{avo} v_{avo}^2 - \rho_{avi} v_{avi}^2) + (\rho_{avi} - \rho_{avm}) g L_{fi} \right] \rho_{avm} A_{fr}^2}{m_{avm}^2}$$

The air pressure drop over the fill, Δp_{fi} , is found by subtracting the air pressure drop of the water troughs, Δp_{tr} , from the total measured air pressure drop, Δp_{FITOT} . The air pressure drop over the water troughs is given by Equation (3.14) as

$$\begin{aligned} \Delta p_{tr} &= \left(0.7609 G_w^{0.6419} G_a^{1.1371} + 0.7609 G_w^{0.6419} G_a^{1.1371} \right) (T_{wi})^{-0.0803} \\ &= \left[0.7609 (5.5356)^{0.6419} (3.6237)^{1.1371} + 0.7609 (5.5356)^{0.6419} (3.6237)^{1.1371} \right] (294.4631 - 273.15)^{-0.0803} \\ &= 15.4354 \text{ Pa} \end{aligned}$$

From this the air pressure drop over the fill is calculated as $\Delta p_{fi} = 119.7542 - 15.4354 = 104.3188 \text{ Pa}$. To find v_{avi} , first calculate the air-vapour mass flow rate at the water trough inlet,

$$\begin{aligned} m_{avi} &= m_a + w_i m_a \\ &= 8.1533 + 0.008688 \times 8.1533 = 8.2241 \text{ kg/s} \end{aligned}$$

From Appendix A find $\rho_{avi} = 1.2174 \text{ kg/m}^3$, v_{avi} can now be calculated

$$\begin{aligned} v_{avi} &= \frac{m_{avi}}{\rho_{avi} A_{fr}} \\ &= \frac{8.2241}{1.2174 \times 2.25} = 3.0024 \text{ m/s} \end{aligned}$$

To find the fill air outlet conditions, first calculate the fill air outlet temperature. This must be done following an iterative procedure. It will be shown that $T_{ao} = 293.5374 \text{ K}$ gives a converged solution.

Because Merkel assumes the fill outlet air to be saturated find w_{so} from Equation (A.15) evaluated at $T_{wbo} = T_{ao} = 293.5374 \text{ K}$ and $p_{atm} = 101000 \text{ Pa}$ to be 0.015176 kg/kg . The enthalpy of the fill outlet air can be calculated by using an energy balance

$$\begin{aligned} i_{mao} &= c_{pwm} m_w \frac{T_{wi} - T_{wo}}{m_a} + (w_{so} - w_i) c_{pwm} (T_{wo} - 273.15) + i_{mai} \\ &= 4181.4723 \times 12.4551 \frac{294.4631 - 291.0910}{8.1533} + \\ &\quad (0.015176 - 0.008688) 4181.4723 \times (291.0910 - 273.15) + 37011.3432 \\ &= 21539.8892 + 486.7284 + 37011.3432 \\ &= 59037.9608 \text{ J/kg dry air} \end{aligned}$$

Unlike the energy balance used in Equation (C.1), the above energy balance includes evaporation loss. It is included here because we want to predict the fill air outlet temperature, i.e. a physical phenomenon, as good as possible. Whereas in Equation (C.1) it is used to represent experimental data as a dimensionless number, i.e. Merkel number, which in turn will be used in predicting a physical phenomenon, i.e. water outlet temperature. The enthalpy can also be calculated from Appendix A, since Merkel assumes saturated fill outlet conditions. From Appendix A find: $\rho_{avo} = 1.1878 \text{ kg/m}^3$, $c_{pao} = 1006.4865 \text{ J/kgK}$, $c_{pvo} = 1871.2670 \text{ J/kgK}$ and $i_{maos} = 59062.4517 \text{ J/kg dry air}$. The two enthalpy values are close enough to accept that the fill outlet air temperature is 295.4724 K.

Following along the same lines as m_{avi} and v_{avi} find $m_{avo} = 8.2757 \text{ kg/s}$ and $v_{avo} = 3.0967 \text{ m/s}$. The mean air-vapour mass flow rate is given as $m_{avm} = 0.5(8.2241 + 8.2757) = 8.2499 \text{ kg/s}$ and the harmonic mean density as $\rho_{avm} = 2/(1/1.2174 + 1/1.1878) = 1.2024 \text{ kg/m}^3$. These values can now be substituted back into the loss coefficient equation to give

$$K_{fdm} = \frac{2 \left[\Delta p_{fi} - (\rho_{avo} v_{avo}^2 - \rho_{avi} v_{avi}^2) + (\rho_{avi} - \rho_{avm}) g L_{fi} \right] \rho_{avm} A_{fr}^2}{m_{avm}^2}$$

$$K_{fdm} = \frac{2 \left[104.3188 - (1.1878 \times 3.0967^2 - 1.2174 \times 3.0024^2) + (1.2174 - 1.2024) 9.81 \times 1.524 \right] 1.2024 \times 2.25^2}{8.2499^2}$$

$$= 18.6256$$

Or per unit length, $K_{fdm1} = 18.6256/1.524 = 12.2215 \text{ m}^{-1}$.

APPENDIX D. FILL PERFORMANCE UNCERTAINTY ANALYSIS

D.1. Introduction

In this section an uncertainty analysis of the fill performance test data is presented using the theory of Appendix B. This uncertainty is then propagated into the performance of a NDWCT, see Chapter 5. Some calculations have been omitted in order to keep the analysis clear and understandable. The uncertainty of the water troughs and spray zone performance has not been included. This was done to prevent the process from becoming too complex. Also, the uncertainty in the water mass flow rate is only due to the uncertainty in the pressure transducer and does not include the uncertainty in the performance of the orifice plate itself. The total uncertainty can thus be considered smaller than what it really is. The sensitivity indexes are presented first, followed by a zeroth order analysis, first order analysis and then an N'th order analysis. All estimates are based on a 95 % confidence interval. A table summarising all the uncertainties is given at the end of each order of analysis.

D.2. Sensitivity indexes

The sensitivity indexes for the fill performance test were determined according to Equation (B.17). Fill performance test data was used to evaluate functional values. Each parameter was offset by a $+\delta$ and $-\delta$ amount while the other parameters were held constant. The corresponding Me_{fi}/L_{fi} and K_{fdm}/L_{fi} values were then calculated using the method described in Appendix C. The partial derivatives could then be estimated with the central differencing formula as per Equation (B.17). The experimental data, or WP, was chosen to be as close as possible to the operating point of the NDCWT used to generate the results of Table 2-2 and is as follows: $p_{atm} = 101000$ Pa, $T_{ai} = 284.380$ K, $T_{wbi} = 283.899$ K, $p_{ai} = 1.067$ V, $\Delta p_{fitOT} = 1.066$ V, $T_{wi} = 313.139$ K, $T_{wo} = 291.778$ K, $\Delta p_{or} = 1.301$ V ($G_w = 1.415$ kg/sm²), $p_{up} = 101000$ Pa, $T_{wbn} = 283.412$ K, $T_{an} = 283.794$ K and $\Delta p_{nth} = 1.373$ V ($G_a = 1.834$ kg/sm²). The relationship between the measured parameters and the air pressure loss coefficient as well as the fill Merkel number is given below in functional form.

$$R_K = \frac{K_{fdm}}{L_{fi}} = f_K(p_{atm}, T_{ai}, T_{wbi}, p_{ai}, \Delta p_{fitOT}, T_{wi}, T_{wo}, \Delta p_{or}, p_{up}, T_{wbn}, T_{an}, \Delta p_{nth}, L_{fi})$$

$$= f_K(x_1, x_2, \dots, x_{13})$$

and

$$R_M = \frac{Me_{fi}}{L_{fi}} = f_M(p_{atm}, T_{ai}, T_{wbi}, p_{ai}, T_{wi}, T_{wo}, \Delta p_{or}, p_{up}, T_{wbn}, T_{an}, \Delta p_{nth}, L_{fi})$$

$$= f_M(x_1, x_2, \dots, x_{12})$$

where the subscripts K and M refer to whether the result of interest is the air pressure loss coefficient or Merkel number respectively. From previous work it was found that the length of fill does not play a big role in comparison with other parameters and it is thus omitted from the rest of analysis. Table D-1 on the next page shows the sensitivity indexes of each parameter for both the Merkel number and fill air pressure loss coefficient. The third column shows the offset amount, δ_{xi} , for each parameter. Some of the

parameters in Table D-1 are given in volts and pascals. This is done to give the reader a better feeling of the sensitivity index.

Table D-1: Sensitivity indexes for fill test facility

Parameter, x_i	WP	δ_{x_i}	$\frac{\delta_{x_i}}{x_i} \times 100\%$	Air pressure loss coefficient			Merkel number		
				$\frac{K_{fdm}}{L_{fi}} \Big _{WP-\delta_{x_i}}$	$\frac{K_{fdm}}{L_{fi}} \Big _{WP+\delta_{x_i}}$	$(\theta_K)_{x_i}$	$\frac{Me_{fi}}{L_{fi}} \Big _{WP-\delta_{x_i}}$	$\frac{Me_{fi}}{L_{fi}} \Big _{WP+\delta_{x_i}}$	$(\theta_M)_{x_i}$
p_{atm} , Pa	101000	200	0.20	12.350	12.400	0.0001	1.713	1.723	0.0000
T_{ai} , K	284.380	1	0.35	12.402	12.350	-0.0260	1.719	1.717	0.0010
T_{wbi} , K	283.899	1	0.35	12.408	12.342	-0.0330	1.577	1.893	0.1581
p_{ai} , V	1.067	0.01	0.94	12.376	12.377	0.0576	1.718	1.718	0.0036
p_{ai} , Pa	101041	6.208	0.01			0.0001			0.0000
Δp_{fTOT} , V	1.06639	0.01	0.94	10.308	14.444	206.7915	1.718	1.718	0.0000
Δp_{fTOT} , Pa	30.516	4.628	15.45			0.4468			0.0000
T_{wi} , K	313.139	1	0.32	12.400	12.352	-0.0236	1.675	1.758	0.0417
T_{wo} , K	291.778	1	0.34	12.351	12.399	0.0241	2.101	1.423	0.3388
Δp_{or} , V	1.3005	0.01	0.77	12.384	12.366	-0.8988	1.693	1.743	2.4911
Δp_{or} , Pa	1435.921	48.016	3.34			-0.0002			0.0005
p_{up} , Pa	101000	200	0.20	12.402	12.348	-0.0001	1.719	1.716	0.0000
T_{wbn} , K	283.412	1	0.35	12.343	12.408	0.0325	1.716	1.720	0.0019
T_{an} , K	283.794	1	0.35	12.342	12.408	0.0330	1.716	1.720	0.0019
Δp_{nth} , V	1.373	0.01	0.73	12.725	12.044	-34.0509	1.738	1.699	1.9590
Δp_{nth} , Pa	150.320	3.814	0.73			-0.0893			0.0051

From the sensitivity index of p_{up} in Table D-1 it can be seen that the uncertainty of p_{up} will be negligible, hence this parameter was also omitted from the analysis.

D.3. Zeroth order analysis, $i = 0$

The uncertainties associated with this analysis are due to errors inherent in the instrumentation or measuring method used. Zeroth order uncertainty does not incorporate time dependent effects. One can thus say that the zeroth order uncertainty is the uncertainty that will exist if the test conditions were absolutely stable, i.e. the minimum uncertainty we can expect. Two uncertainty source groups were defined, namely calibration and data acquisition source groups.

D.3.1. Calibration uncertainty source group, $j = 1$

CURVE FITTING, $k = 1$

These elemental uncertainties are given in Table F-1. Although they will be listed in this analysis as elemental systematic uncertainties, $B_{0,1,1}$, one should realise that they can be reduced as discussed in Appendix F.

D.3.2. Data acquisition uncertainty source group, $j = 2$

INSTRUMENT RESOLUTION, $k = 3$

These uncertainties are considered to be systematic since they cannot be changed by taking more measurements. The specifications of the data logging system according to the IMP installation guide

(1990) are given in Table D-2 on the next page. FS stands for Full Scale. The first row is applicable to the T-type thermocouples ($0.589 \text{ mV} \approx 15 \text{ }^\circ\text{C}$) and the second to all pressure transducers. All values in volts.

Table D-2: Data logger specifications, all units in volts (DC)

Range	FS	Resolution	WP	Expression for uncertainty	$B_{0,2,3}$
0.02	0.022	1×10^{-6}	0.589×10^{-3}	$[(0.02 \% \times \text{WP} + 5 \times 10^{-6})^2 + (0.5 \times 1 \times 10^{-6})^2]^{0.5}$	5.142×10^{-6}
12	12	0.001	2.00	$[(0.05 \% \times \text{WP} + 0.01 \% \times \text{FS})^2 + (0.5 \times 0.001)^2]^{0.5}$	2.256×10^{-3}

In addition to the above uncertainties, the thermocouples themselves have the following elemental uncertainties (in $^\circ\text{C}$) as well: 0.4 due to automatic cold junction compensation, 0.5×0.1 due to resolution and an additional 0.3. The origin of the 0.3 $^\circ\text{C}$ is not explained in the guide. This uncertainty might be due to curve fit and other calibration errors. The additional $B_{0,2,3}$ value is thus equal to $(0.4^2 + 0.05^2 + 0.3^2)^{0.5} = 0.5025 \text{ }^\circ\text{C}$. From the equations supplied by ITS-90 (1990) find that $\pm 5.142 \times 10^{-6} \text{ V} \approx \pm 5.142 \times 10^{-6} / 4.000 \times 10^{-5} = \pm 0.1286 \text{ }^\circ\text{C}$ at $15 \text{ }^\circ\text{C}$. Hence the combined $B_{0,2,3}$ value for the thermocouples is equal to $(0.1286^2 + 0.5025^2)^{0.5} = 0.5187 \text{ }^\circ\text{C}$. Atmospheric pressure was measured with a mercury barometer. The barometer's elemental uncertainty, $B_{0,2,3}$, due to resolution is estimated to be $0.2 \text{ hPa} = 20 \text{ Pa}$.

SPATIAL EFFECTS, $k = 4$

Only temperature measurements are considered. Recall that a fill test consists of three sets of data, one for each range of water inlet temperatures. Each set consists again of twenty data points per instrument: four water mass flow rates and five air mass flow rates per water mass flow rate. The data set used to analyse the spatial effects was the set represented by Figure H-1 (e) and (f). The following procedure was used to determine the spatial uncertainty. The process was repeated for all six temperatures listed in Table D-3. First the S_{spatial} value for a given temperature in Table D-3 and data point was calculated using Equation (B.10).

$$\left[(S_{\text{spatial}})_{T_i} \right]_{\text{dp}} = \sqrt{\frac{\sum_{k=1}^M (\bar{T}_{i_k} - \langle \bar{T}_i \rangle)_{\text{dp}}^2}{M-1}} \quad (\text{D.1})$$

where

T_i = temperature in Table D-3

M = number of instruments used to determine the specific temperature, T_i

dp = data point

This process was repeated for each of the twenty data points. The twenty $[(S_{\text{spatial}})_{T_i}]_{\text{dp}}$ values were then grouped to give an average $\langle (S_{\text{spatial}})_{T_i} \rangle$ value using Equation (B.6)

$$\langle (S_{\text{spatial}})_{T_i} \rangle = \sqrt{\frac{\sum_{\text{dp}=1}^{20} \left[(S_{\text{spatial}})_{T_i} \right]_{\text{dp}}^2}{20}} \quad (\text{D.2})$$

Finally the $(B_{0,2,4})_{T_i}$ value is calculated as

$$(B_{0,2,4})_{T_i} = 2 \langle (S_{\text{spatial}})_{T_i} \rangle \quad (\text{D.3})$$

Table D-3 on the next page shows the results. All values in $^\circ\text{C}$ or K.

Table D-3: Spatial uncertainties of thermocouples.

Statistic	T_{wbn} , K	T_{an} , K	T_{ai} , K	T_{wbi} , K	T_{wi} , K	T_{wo} , K
N	20 or 21	20 or 21	20 or 21	20 or 21	20 or 21	20 or 21
M	3	2	4	4	2	3
$\langle S_{\text{spatial}} \rangle_{T_i}$	0.0329	0.1240	0.1579	0.2424	0.1509	0.0525
$(B_{0,2,4})_{T_i}$	0.0659	0.2480	0.3158	0.4848	0.3019	0.1050

D.3.3. Zeroth order uncertainty summary

Table D-4 gives a summary of the zeroth order analysis. The $(u_{K,0})_{x_i}$ value refers to the uncertainty in K_{fdm1} due to the zeroth order systematic uncertainty, B_0 , of the parameter x_i in the first column. Columns two to four have the same units as the corresponding parameter. The last two columns have units of m^{-1} .

For a specific parameter $(u_{K,0})_{x_i}$ is given as

$$(u_{K,0})_{x_i} = \sqrt{\left(\left. \frac{\partial K_{fdm1}}{\partial x} \right|_{WP} B_0 \right)_{x_i}^2} = \sqrt{(\theta_K B_0)_{x_i}^2} \quad (D.4)$$

The uncertainty in the Merkel number, $(u_{M,0})_{x_i}$, is calculated similarly as to Equation (D.4). The sensitivity indexes are found in Table D-1. The pressure transducer reference number is given in brackets in column one.

Table D-4: Summary of zeroth order analysis

Parameter, x_i	$(B_{0,1})_{x_i} = (B_{0,1,1})_{x_i}$	$(B_{0,2})_{x_i} = \left[(B_{0,2,3})_{x_i}^2 + (B_{0,2,4})_{x_i}^2 \right]^{0.5}$	$(B_0)_{x_i}$	$(u_{K,0})_{x_i}$	$(u_{M,0})_{x_i}$
p_{atm} , Pa	0	20	20	0.0025	0.0005
T_{ai} , K	0	0.6073	0.6073	0.0158	0.0006
T_{wbi} , K	0	0.7100	0.7100	0.0235	0.1122
p_{ai} , V (1L)	0.0003	0.0023	0.0023	0.0001	0.0000
Δp_{fiTOT} , V (0L)	0.0004	0.0023	0.0023	0.4738	0.0000
T_{wi} , K	0	0.6001	0.6001	0.0142	0.0250
T_{wo} , K	0	0.5292	0.5292	0.0128	0.1793
Δp_{or} , V (m_{wHIGH})	0.0101	0.0023	0.0103	0.0093	0.0258
T_{wbn} , K	0	0.5229	0.5229	0.0170	0.0010
T_{an} , K	0	0.5749	0.5749	0.0190	0.0011
Δp_{nth} , V (2H)	0.0043	0.0023	0.0049	0.1653	0.0095

From Equation (B.18) the total zeroth order uncertainty in a result R (with no random uncertainties), is given as

$$\begin{aligned}
U_{R,0} &= \sqrt{\sum_{i=1}^n (\theta_R P_0)_{x_i}^2 + \sum_{i=1}^n (\theta_R B_0)_{x_i}^2 + 2 \sum_{i=1}^{n-1} \sum_{z=i+1}^n (\theta_R)_{x_i} (\theta_R)_{x_z} B_{x_i, x_z}} \\
&= \sqrt{\sum_{i=1}^n (\theta_R B_0)_{x_i}^2 + 2 \sum_{i=1}^{n-1} \sum_{z=i+1}^n (\theta_R)_{x_i} (\theta_R)_{x_z} B_{x_i, x_z}}
\end{aligned} \tag{D.5}$$

The $B_{0,2,3}$ uncertainties for the thermocouples are considered correlated because the same data logging system is used to log the data, i.e. it shares a common elemental uncertainty source. The same holds for the $B_{0,2,3}$ uncertainties of the pressure readings. These values are $0.1286 \text{ }^\circ\text{C}$ and $2.256 \times 10^{-3} \text{ V}$ respectively. The B_{x_i, x_z} term is calculated according to Equation (B.19). The second term under the square root of Equation (D.5) is given below for the case where the result of interest is the air pressure loss coefficient. The same applies when the Merkel number is the result of interest.

$$\begin{aligned}
u_{K, \text{cor}} &= 2 \sum_{i=1}^9 \sum_{z=i+1}^{10} (\theta_R)_{x_i} (\theta_R)_{x_z} B_{x_i, x_z} = 2 \sum_{i=1}^9 \sum_{z=i+1}^{10} (\theta_K)_{x_i} (\theta_K)_{x_z} B_{x_i, x_z} \\
&= 2 \left[(\theta_K)_{T_{ai}} (\theta_K)_{T_{wbi}} (B_{0,2,3})_{T_{ai}} (B_{0,2,3})_{T_{wbi}} + (\theta_K)_{T_{ai}} (\theta_K)_{T_{wi}} (B_{0,2,3})_{T_{ai}} (B_{0,2,3})_{T_{wi}} + \dots \right] \\
&\quad + (\theta_K)_{\Delta p_{or}} (\theta_K)_{\Delta p_{nh}} (B_{0,2,3})_{\Delta p_{or}} (B_{0,2,3})_{\Delta p_{nh}}
\end{aligned}$$

After the above equation was solved it was found that $u_{K, \text{cor}} = -0.0732 \text{ m}^{-2}$ for the air pressure loss coefficient and $u_{M, \text{cor}} = -0.002 \text{ m}^{-2}$ for the Merkel number. When replaced in Equation (D.5) the zeroth order uncertainty for the air pressure loss coefficient, $U_{K,0}$ was calculated as 0.4248 m^{-1} and for the Merkel number $U_{M,0}$ was calculated as 0.2100 m^{-1} . Although both u_{cor} values are very small when compared to total uncertainty, it confirms that ignoring correlated systematic uncertainties does not automatically result in a smaller uncertainty value. This conclusion is supported by Coleman and Steele (1999).

D.4. First order analysis, $i = 1$

In this analysis time dependent effects are evaluated. Two uncertainty source groups are defined, namely data acquisition and data reduction source groups

D.4.1. Data acquisition uncertainty source group, $j = 2$

VARIATION IN PARAMETER, $k = 5$

This elemental uncertainty is due to the time varying nature of the parameters being measured. It is considered a random uncertainty since it is affected by time and number of measurements. The same data set and procedure was followed as with the calculation of the spatial effects, Equations (D.1) to (D.3). The $P_{1,2,5}$ value for a given temperature in Table D-3 and one data point is calculated using Equation (B.8)

$$\left[(P_{1,2,5})_{T_i} \right]_{\text{dp}} = 2 \left[\frac{\langle S_{T_i} \rangle}{\sqrt{MN}} \right]_{\text{dp}} = 2 \left[\langle S_{T_i} \rangle \right]_{\text{dp}}$$

where M is the number of instruments used and N the number of measurements taken over time. This calculation is repeated for each of the twenty data points per temperature in Table D-3. The $P_{1,2,5}$ value for a given temperature is then determined by combining its twenty $P_{1,2,5}$ values, using Equation (B.6)

$$(P_{1,2,5})_{T_i} = 2 \sqrt{\frac{\sum_{dp=1}^{20} \langle S_{T_i} \rangle^2}{20}} = 2 \langle \langle S_{T_i} \rangle \rangle \quad (D.6)$$

Table D-5 shows the results.

Table D-5: First order uncertainty due to variation in parameters

Statistic	T_{wbn} K	T_{an} K	T_{ai} K	T_{wbi} K	p_{ai} V	Δp_{nth} V	Δp_{or} V	Δp_{fitTOT} V	T_{wi} K	T_{wo} K
N	20 or 21	20 or 21	20 or 21	20 or 21	20 or 21	20 or 21	20 or 21	20 or 21	20 or 21	20 or 21
M	3	2	4	4	1	1	1	1	3	3
$2 \langle \langle S_{T_i} \rangle \rangle$	0.0018	0.0036	0.0014	0.0015	0.0002	0.0009	0.0122	0.0001	0.0045	0.0065
$(P_{1,2,5})_{T_i}$	0.0037	0.0073	0.0028	0.0029	0.0004	0.0018	0.0244	0.0003	0.009	0.0147

D.4.2. Data reduction error source group, $j = 3$

CURVE FITTING, $k = 1$

This elemental uncertainty is due to the curve fit errors of Equations (3.20) to (3.23). The data representing all the graphs of Figure H-1 were used to determine this uncertainty. From Equation (B.9) the S_{xy} values were calculated and multiplied by 2, yielding the $P_{1,3,1}$ value for the Merkel number as 0.1834 m^{-1} and 0.1818 m^{-1} for the air pressure loss coefficient.

D.4.3. First order uncertainty summary

Table D-6 provides a summary of the first order analysis, similar as to Table D-4.

Table D-6: Summary of first order analysis

Parameter	$(P_1)_{x_i} = (P_{1,2,5})_{x_i}$	$(u_{K,1})_{x_i}$	$(u_{M,1})_{x_i}$
p_{atm} , Pa	0.0000	0.0000	0.0000
T_{ai} , K	0.0028	0.0001	0.0000
T_{wbi} , K	0.0029	0.0001	0.0005
p_{ai} , V	0.0004	0.0000	0.0000
Δp_{fitTOT} , V	0.0003	0.0558	0.0000
T_{wi} , K	0.0090	0.0002	0.0004
T_{wo} , K	0.0147	0.0004	0.0050
Δp_{or} , V	0.0244	0.0219	0.0607
T_{wbn} , K	0.0037	0.0001	0.0000
T_{an} , K	0.0073	0.0002	0.0000
Δp_{nth} , V	0.0018	0.0605	0.0035

The first order uncertainty is calculated similar as to Equation (D.5) but is written here to accommodate for the curve fit uncertainty, $P_{1,3,1}$, discussed in Section D.4.2. No correlated uncertainties were found in the first order of analysis.

$$U_{R,1} = \sqrt{\sum_{i=1}^{10} (\theta_R P_1)_{x_i}^2 + (P_{1,3,1})^2} \quad (D.7)$$

The first order uncertainty is thus $U_{K,1} = 0.2008 \text{ m}^{-1}$ and $U_{M,1} = 0.1933 \text{ m}^{-1}$ for the air pressure loss coefficient and Merkel number respectively.

D.5. N'th order analysis

The total uncertainty for the fill performance test is given by Equation (B.20) as

$$U_{R,tot} = \sqrt{(U_{R,0})^2 + (U_{R,1})^2} \quad (D.8)$$

The total uncertainty for the air pressure loss coefficient based on 95 % confidence interval is

$$U_{K,tot} = \sqrt{(0.4248)^2 + (0.2008)^2} = 0.4699 \text{ m}^{-1} \quad (D.9)$$

The total uncertainty for the Merkel number based on 95 % confidence interval is

$$U_{M,tot} = \sqrt{(0.2100)^2 + (0.1933)^2} = 0.2854 \text{ m}^{-1} \quad (D.10)$$

APPENDIX E. AIR PRESSURE DROP EQUATION

E.1. Introduction

In this appendix the equation describing the air pressure drop over the fill for the counter flow test section, described in Chapter 3, is derived. The equation is derived for non-uniform air flow and is then simplified for uniform air flow. The effect of the buoyancy force due to the density differences of hot air inside the test section and that of the colder air inside a pressure transducer tube external to the test facility is also described.

E.2. Air pressure drop over the fill

Consider the force and momentum diagram of an elementary control volume (to the right) for steady incompressible air moving through the counter flow test section (to the left) in Figure E-1. The control volume consists of a differential height dz , frontal area dA , friction and drag force dF_{fd} and gravitational force $\rho_m dzg dA$ where ρ_m is the harmonic mean density of the inlet and outlet conditions. The static pressure forces and momentum flows are shown in solid and broken lines respectively.

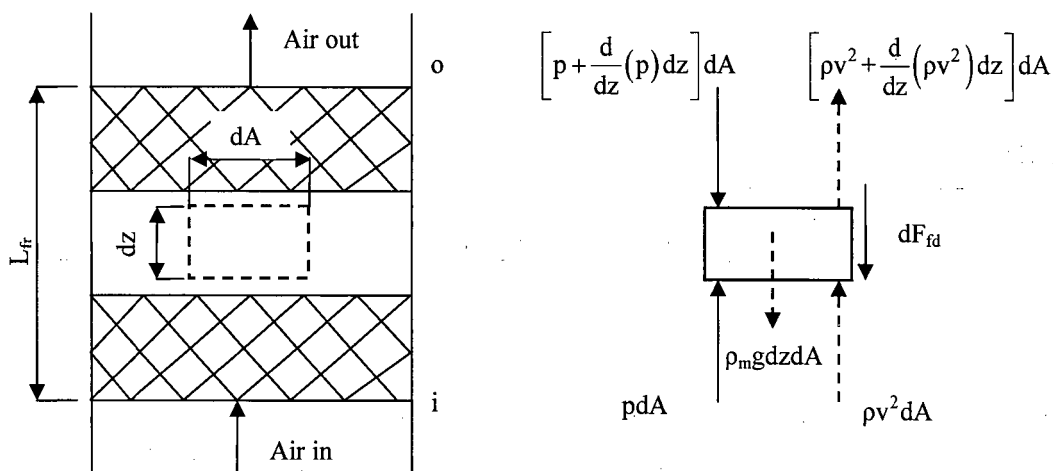


Figure E-1: Elementary control volume in the vertical fill test section

From continuity

$$m = \int \rho v dA = \rho v_m A = \text{constant} \quad (\text{E.1})$$

It follows from Newton's second law of motion that the sum of the forces acting on the air inside the control volume is equal to the change in momentum of the air.

$$p dA - \left(p + \frac{dp}{dz} dz \right) dA - \rho_m dz g dA - \frac{dF_{fd}}{dz} dz = \frac{d}{dz} (\rho v^2) dz dA \quad (\text{E.2})$$

Simplifying Equation (E.2) and integrating over the cross sectional area leads to

$$\begin{aligned} -dp dA - \rho_m dz g dA - dF_{fd} &= d(\rho v^2) dA \\ \therefore -dp A - \rho_m dz g A - dF_{fd} A &= d \left(\int \rho v^2 dA \right) \\ &= d(\alpha_m \rho v_m^2 A) \\ &= \rho v_m A d(\alpha_m v_m) dz + \alpha_m v_m d(\rho v_m A) dz \end{aligned} \quad (\text{E.3})$$

where the momentum velocity correction factor, α_m is given as

$$\alpha_m = \frac{\int v^2 dA}{v_m^2 A} \quad (\text{E.4})$$

Simplifying Equation (E.3) and realising that from continuity the second term on the right hand side is equal to zero, yields

$$-dp - \rho_m dzg - dF_{fd} = \rho v_m d(\alpha_m v_m) \quad (\text{E.5})$$

Integrating above equation between the inlet and outlet section, yields

$$-(p_o - p_i) - \rho_m L_{fi}g - F_{fd} = \rho v_m (\alpha_{mo} v_{mo} - \alpha_{mi} v_{mi}) \quad (\text{E.6})$$

Realising that $\rho v_m = \rho_o v_{mo} = \rho_i v_{mi} = \text{constant}$, yields

$$\Delta p_{fi} = \Delta p_{fd} + (\alpha_{mo} \rho_o v_{mo}^2 - \alpha_{mi} \rho_i v_{mi}^2) + \rho_m L_{fi}g \quad (\text{E.7})$$

where Δp_{fd} is the pressure drop due to friction and drag effects.

For uniform air flow the α_m value from Equation (E.4) is equal to unity and the air pressure drop equation reduces to

$$\Delta p_{fi} = \Delta p_{fd} + (\rho_o v_{mo}^2 - \rho_i v_{mi}^2) + \rho_m L_{fi}g \quad (\text{E.8})$$

E.3. Using a pressure transducer

Figure E-2 shows the setup when measuring the static air pressure drop, Δp_{fi} , with a pressure transducer.

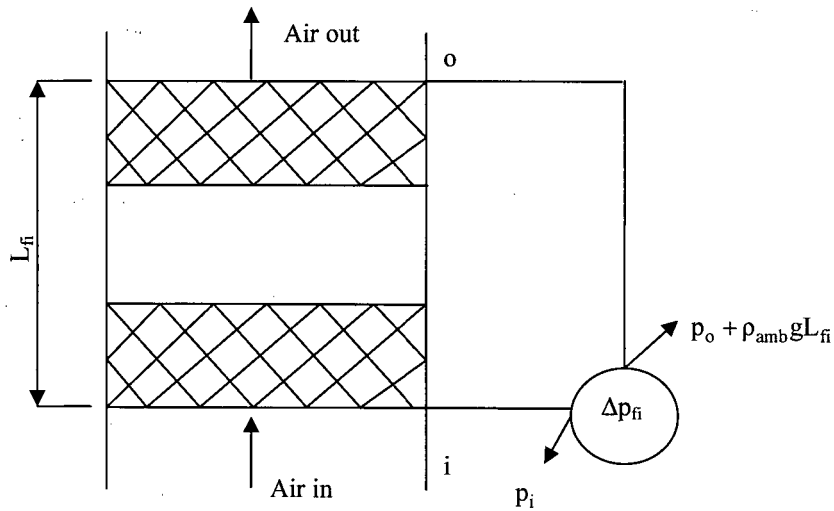


Figure E-2: Setup for measuring Δp_{fi}

Equation (E.8) is now given as

$$\Delta p_{fi} = (p_o + \rho_{amb} L_{fi}g) - p_i = \Delta p_{fd} + (\rho_o v_{mo}^2 - \rho_i v_{mi}^2) + \rho_m L_{fi}g \quad (\text{E.9})$$

where ρ_{amb} is the density of the ambient air. Rearranging Equation (E.9) gives

$$\Delta p_{fi} = \Delta p_{fd} + (\rho_o v_{mo}^2 - \rho_i v_{mi}^2) - (\rho_{amb} - \rho_m) L_{fi}g \quad (\text{E.10})$$

APPENDIX F. CALIBRATION OF MEASUREMENT EQUIPMENT

F.1. Introduction

In this appendix the calibration curve of each pressure transducer is presented, accompanied by a description of the calibration method and an estimate of the uncertainty. The current methods used to calculate the air and water mass flow rates are also compared to other methods. Lastly, the results of the water trough catchment ratio test are discussed. In this experiment an attempt was made to try and quantify how much water is drained by the upper and lower set of water troughs, respectively.

F.2. Pressure transducers

The pressure transducers used to measure Δp_{nth} , Δp_{FITOT} and p_{ai} were calibrated with the use of a Betz manometer. A pressure was applied to both the pressure transducer and the Betz up to a point where the measurement reference line on the Betz was exactly on a marker of its measurement scale (in mm). This eliminates the uncertainty due to resolution. The pressure of the water height was then calculated and plotted against the volt signal of the pressure transducer as per Figure F-1 (a) to (f) on the next page. The only significant uncertainty is thus due to the curve fit and is equal to $2S_{yx}$, where S_{yx} is given by Equation (B.9). This is a random uncertainty and can be reduced by taking more measurements. Table F-1 shows the results of the calibration for each unit.

Table F-1: Calibration data of pressure transducers

Unit	Curve: $y = mx + c$		Zero reading V	Calibration range Pa	$P_{0,1,1}$ V
	m, Pa/V	c, Pa			
0 H	466.5408	- 468.1393	1.0025	0 -1000	0.0034
0 L	462.8223	- 463.5870	1.0029	0-100	0.0004
1 H	625.9734	- 622.2271	0.9934	0-1000	0.0021
1 L	620.7888	- 616.1144	0.9936	0-100	0.0003
2 H	381.3774	- 371.7136	0.9752	0-1000	0.0043
m_{wHIGH}	4801.5645	-4808.5326	1.0000	0-17000	0.0101

The m_{wHIGH} pressure transducer was calibrated with the use of a water manometer. The total uncertainty of m_{wHIGH} includes the 3 mm resolution uncertainty of the water manometer which constitutes a systematic uncertainty. This uncertainty is due to scale of the manometer and the shape of the meniscus.

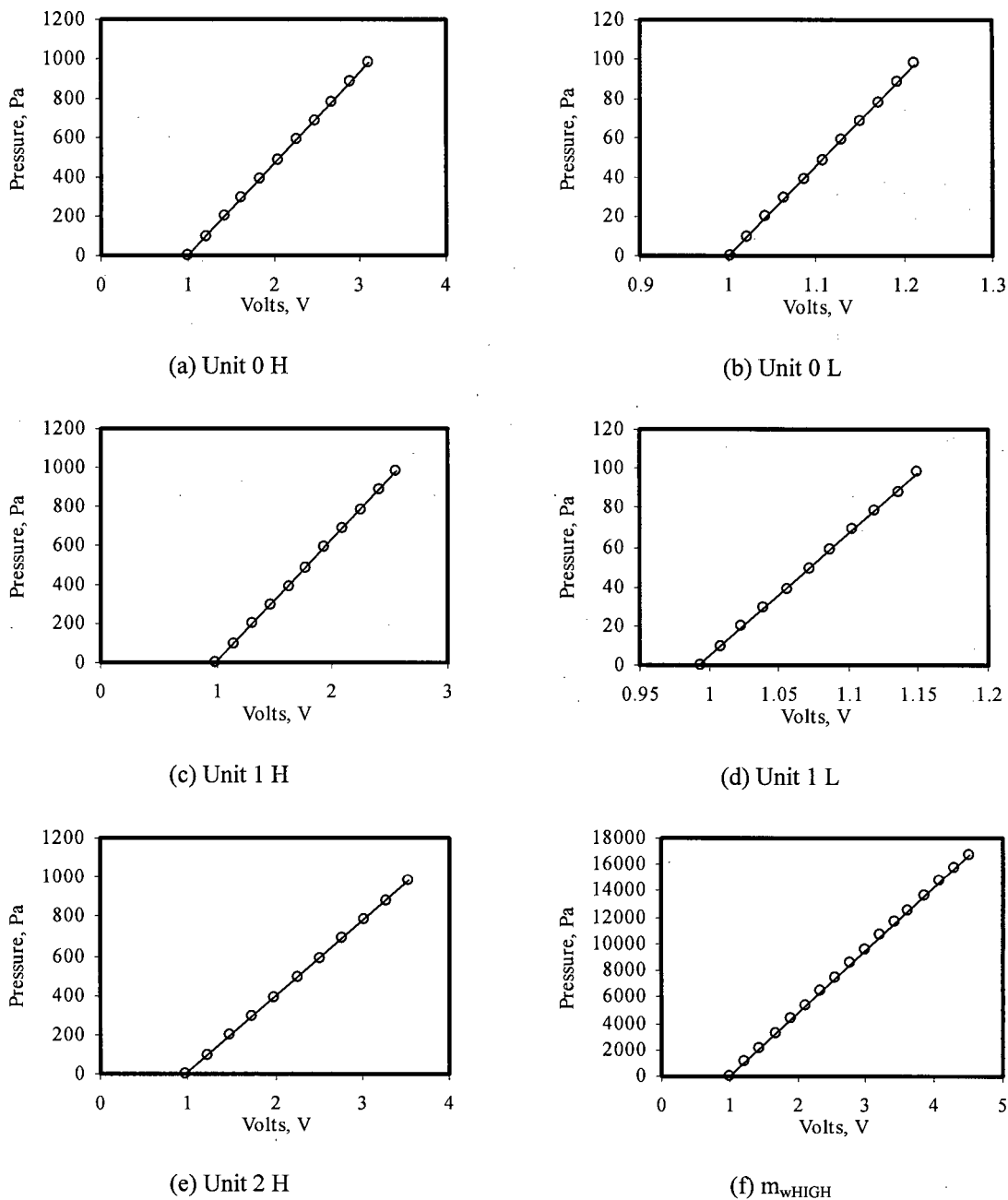


Figure F-1: Calibration curves of pressure transducers

F.3. Water mass flow rate

It was decided to compare the water mass flow rate through the orifice plate, predicted by the British Standard (BS) method, to that of a calibration test. In this test, the orifice plate was calibrated by connecting the water inlet pipe directly to a calibration tank and taking the time needed to fill the tank to a certain water level indicated by a transparent PVC pipe, see Figure F-2 on next page. The width of the tank is 700 mm. Using the dimensions of the tank, the volume of water could be calculated and ultimately the water mass flow rate. This water flow rate was then compared to the water flow rate through the orifice plate as determined according to the British Standard 1042 (1981).

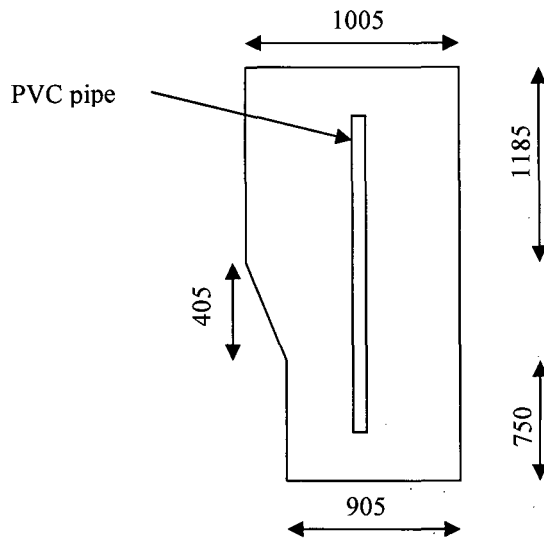


Figure F-2: Calibration tank for orifice plate, all dimensions in mm

The water pressure drop over the orifice plate was measured with the m_{wHIGH} electronic pressure transducer while the tank was filling up. The water mass flow rate could then be correlated with the volt or pressure signal of the pressure transducer. Figure F-3 compares the values of the BS method to that of the calibration tank

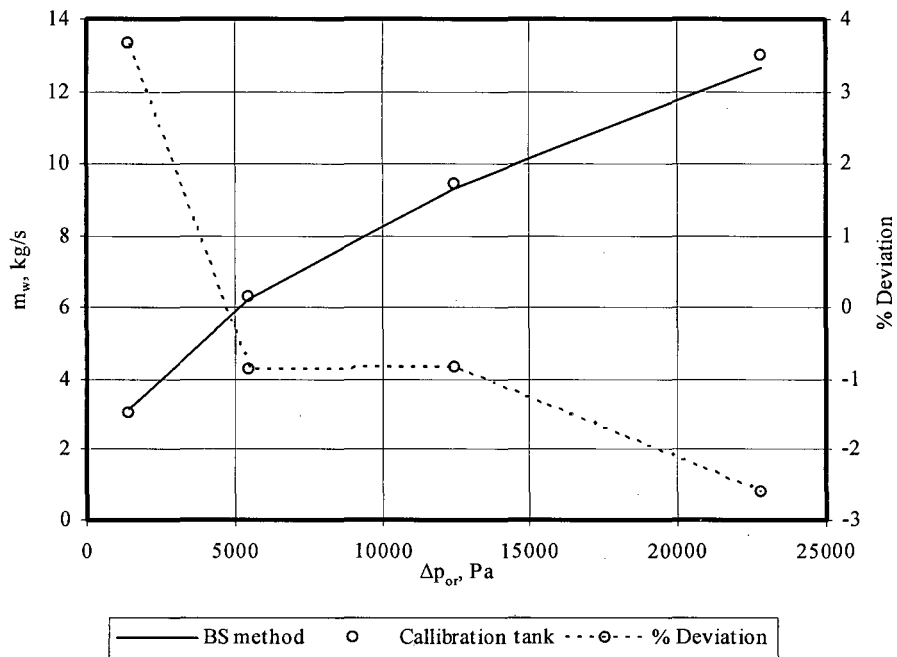


Figure F-3: Water mass flow rate determined with orifice plate and calibration tank.

From Figure F-3 one can see that the BS method predicts water mass flow rates that are very close the calibrated values. The method is thus acceptable.

F.4. Air-vapour mass flow rate

In the past, the air-vapour mass flow rate through one nozzle was determined using the equation given by Kröger (1998 and 2004),

$$m_{avn} = C_n \theta_g Y A_n (2\rho_{avn} \Delta p_{nwl})^{0.5} \quad (\text{F.1})$$

where

m_{avn} = air-vapour mass flow rate through the nozzle, kg/s

C_n = nozzle coefficient

θ_g = gas expansion coefficient

Y = approach velocity coefficient

A_n = nozzle throat area, m²

ρ_{avn} = air-vapour density inside the nozzle, kg/m³

Δp_{nwl} = air pressure drop over the nozzle measured at the walls of the duct, Pa

The mass flow rate is calculated for one nozzle and then multiplied by the number of nozzles (if the inside diameters are the same). This method was compared to the mass flow rate predicted by the equation given below

$$m_{avn} = \frac{\left(2 \frac{\Delta p_{nth}}{\rho_{avn}}\right)^{0.5}}{\frac{1}{\rho_{avn}} \left(\frac{1}{A_n} - \frac{1}{A_{tus}}\right)} \quad (\text{F.2})$$

where the air pressure drop, Δp_{nth} (Pa), is measured as shown in Figure F-4 and A_{tus} is the duct area upstream of the nozzles, in m². Equation (F.2) is derived by applying Bernoulli's equation along a stream line between a point in the settling chamber upstream of the nozzles and a point in the centre of the nozzle's throat (where the velocity distribution is assumed to be uniform). The required air mass flow rates for the fill performance tests were such that only the top three nozzles had to be used.

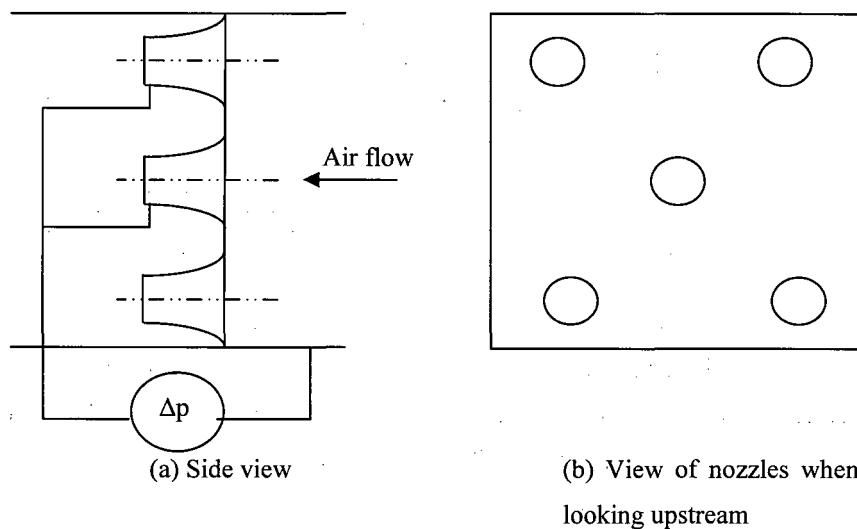


Figure F-4: Nozzle pressure drop measurement used to determine air-vapour mass flow rate

Common to both Equation (F.1) and (F.2) is the assumption that the air pressure drop over the three nozzles is equal. To confirm this assumption the air pressure drop over each nozzle was measured at three mass flow settings. The air pressure drop was measured as shown in Figure F-4, except that each nozzle

was connected to a separate pressure transducer. Table F-2 shows the air pressure drop for each nozzle at three air-vapour velocities. These are the approximate velocities in the vertical test section.

Table F-2: Air pressure drop over each nozzle, Pa

Nozzle Location	Air-vapour velocities		
	1.5 m/s	2.5 m/s	3.5 m/s
Top left	153.7938	423.8797	837.7432
Middle	154.9915	425.8769	840.1669
Top right	156.2959	429.4831	847.1337
Max deviation, %	1.61	1.31	1.11

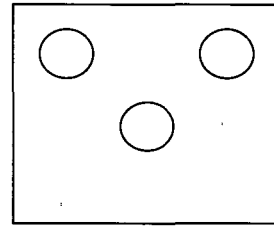


Figure F-5: View of nozzles when looking upstream

The maximum air pressure drop deviation over the entire range of mass flow rate occurs at 1.5 m/s and is 1.61 % which translates to $(1.61)^{0.5} = 1.27$ % maximum deviation on mass flow rate per nozzle. Considering measurement and instrumentation uncertainties, this can be assumed negligible and the assumption of equal air pressure drops is acceptable. An additional experiment was conducted where the air-vapour mass flow rates calculated with Equation (F.1) and (F.2) were evaluated. The setup was as shown in Figure F-4. Table F-3 shows the results.

Table F-3: Comparison of Equation (F.2) and (F.3)

Δp_{nwl} Pa	Δp_{nth} Pa	Equation (F.1) m_{avn} kg/s	Equation (F.2) m_{avn} kg/s	Max deviation, %
157.1494	153.5670	4.0258	4.0789	1.30
419.2207	406.3275	6.5719	6.6400	1.03
810.3104	781.3699	9.1084	9.1985	0.98

The difference in mass flow rate decreases from 1.30 % at low flow rates up to 0.98 % at higher flow rates. Equation (F.1) is solved using an iterative procedure where as Equation (F.2) can be solved with a hand calculation. Due to its simplicity and comparative accuracy, it was decided to use Equation (F.2).

F.5. Water trough catchment ratio

In this test, the water mass flow rate in the lower water trough section was determined. The water mass flow rate was measured with a calibration tank and stop watch. The test was first done with the water distribution system (WDS) 200 mm above the upper water trough and then repeated for 1.524 m of fill installed. Each setting of the WDS was tested with no air flow and repeated with maximum air flow. The results are shown in Figure F-6 and F-7. See Chapter 3 for conclusions.

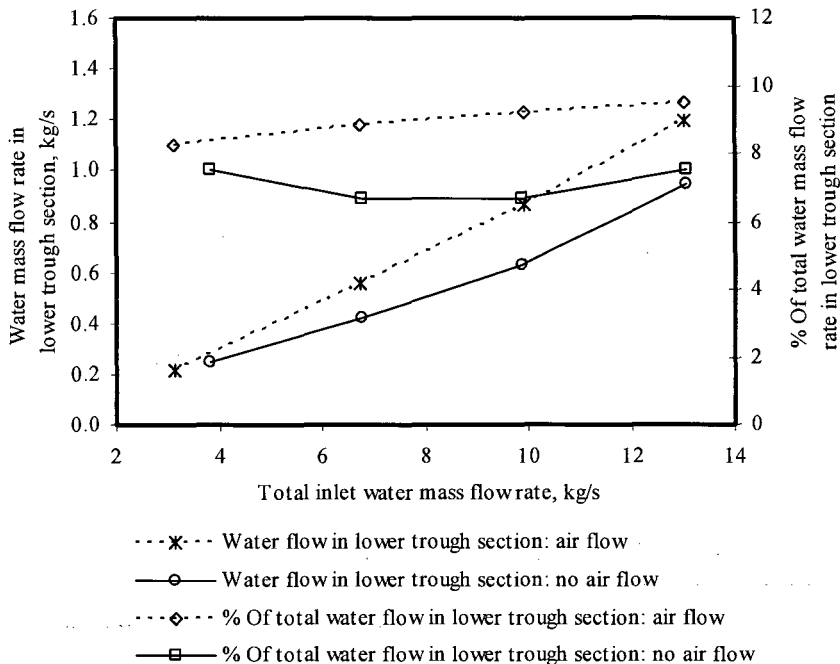


Figure F-6: Water trough catchment ratio with WDS 200 mm above troughs

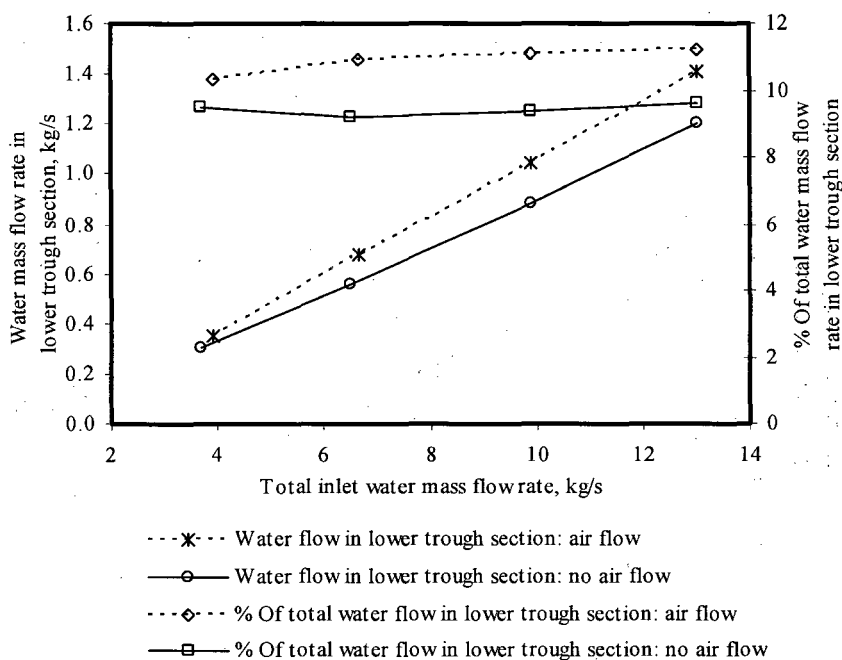


Figure F-7: Water trough catchment ratio with 1.524 m of fill installed

APPENDIX G. WATER TROUGH AND SPRAY ZONE PERFORMANCE TEST DATA

G.1. Introduction

The results of the water trough and spray zone performance tests are presented in this appendix. Figure G-1 indicates how the current test data compares with Equation (3.8) and (3.9). Figure G-2 gives a comparison between the current test data and Equation (3.11) to (3.14). Each row of graphs includes the Merkel number and air pressure drop over the water troughs for a specific range of water inlet temperatures. The figures are shown for an increase in water inlet temperature range with the coldest range at the top. Each corresponding set of curves in Figure G-1 and G-2 has the same legend as shown in Table G-1. The water inlet temperature ranges are shown at the top of each column in Table G-1. The first column of Table G-1 indicates the symbol (experimental data) and the line type (correlation) used for each G_w value. All values in kg/sm^2 .

Table G-1: Legend for Figure G-1 and G-2

Symbol	Water inlet temperature ranges				
	15.9 – 16.0 °C	20.0 – 20.9 °C	21.5 – 23.4 °C	24.0 – 26.1 °C	30.0 – 32.5 °C
◇ — — —	5.526	5.504	5.535	5.541	5.561
□ — — —	4.155	4.139	4.118	4.184	4.174
△ - - - - -	2.731	2.701	2.705	2.748	2.752
○ - - - -	1.386	1.360	1.413	1.394	1.350

For Figure G-1 and G-2 the water outlet temperature was calculated according to Equation (3.7)

$$T_{wo} = 0.1T_{wob} + 0.9T_{wot} \quad (\text{G.1})$$

Figure G-3 (a), (c), (e), (g) and (i) show the deviation in Merkel number when the water outlet temperature is calculated according to

$$T_{wo} = 0.5(T_{wob} + T_{wot}) \quad (\text{G.2})$$

and Figure G-3 (b), (d), (f), (h) and (j) show the deviation in Merkel number when the water outlet temperature is calculated according to

$$T_{wo} = T_{wot} \quad (\text{G.3})$$

The legend for Figure G-3 is the same as in Table G-1. Both y-axes are % deviation and is calculated as

$$\% \text{ Deviation} = (Me' - Me_{10/90}) / Me_{10/90} \times 100 \quad (\text{G.4})$$

where

Me' = Merkel number calculated using Equation (G.2) or (G.3)

$Me_{10/90}$ = Merkel number calculated using Equation (G.1)

Figure G-4 and G-5 shows the results of the dry test (air only), i.e. Equation (3.10). The % deviation is given as

$$\% \text{ Deviation} = [\text{Experimental} - \text{Eqn}(3.10)] / \text{Eqn}(3.10) \times 100 \quad (\text{G.5})$$

All the experimental data is given in Table G-2

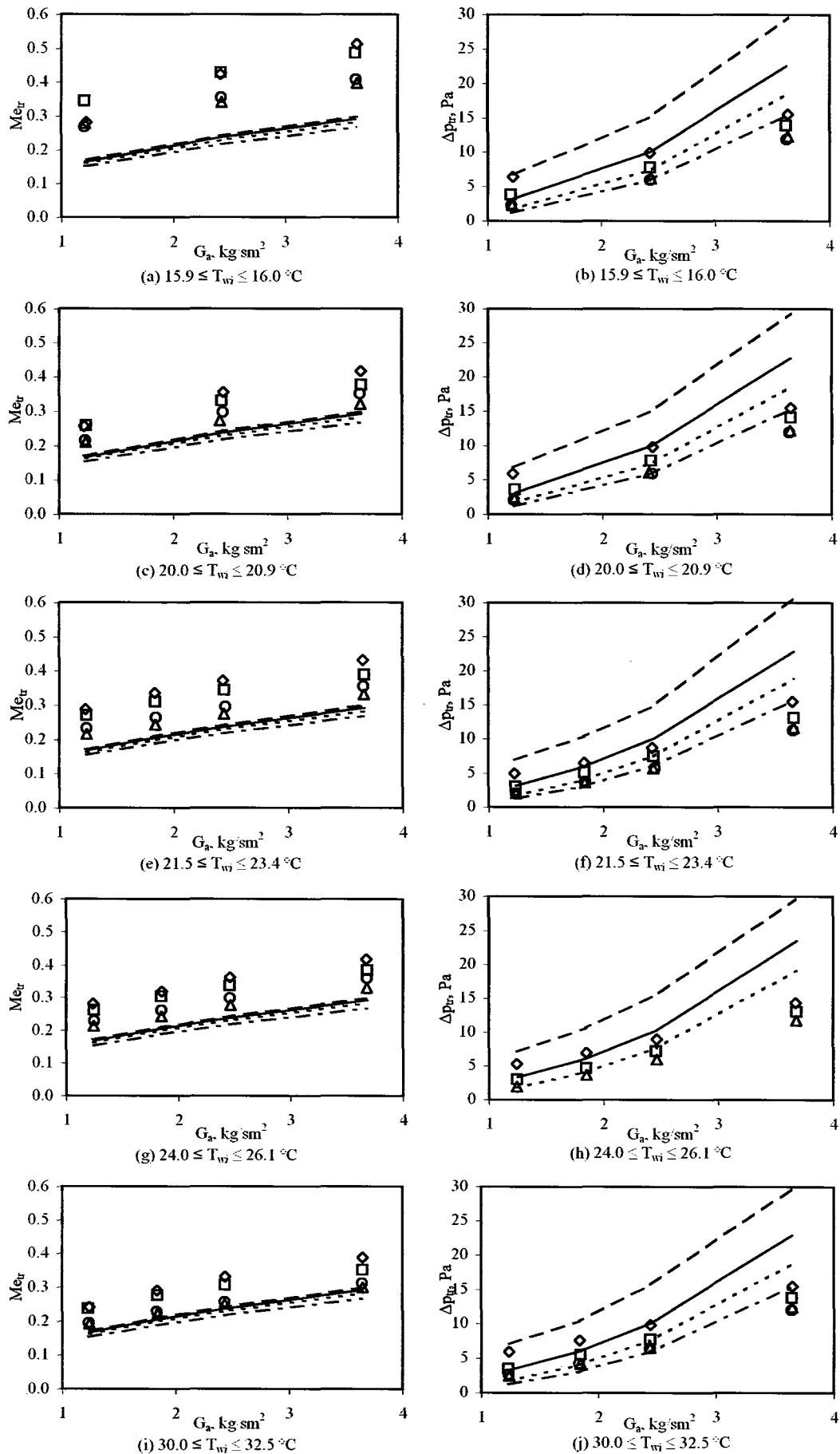


Figure G-1: Water trough and spray zone performance characteristic data compared to Equation (3.8) and (3.9)

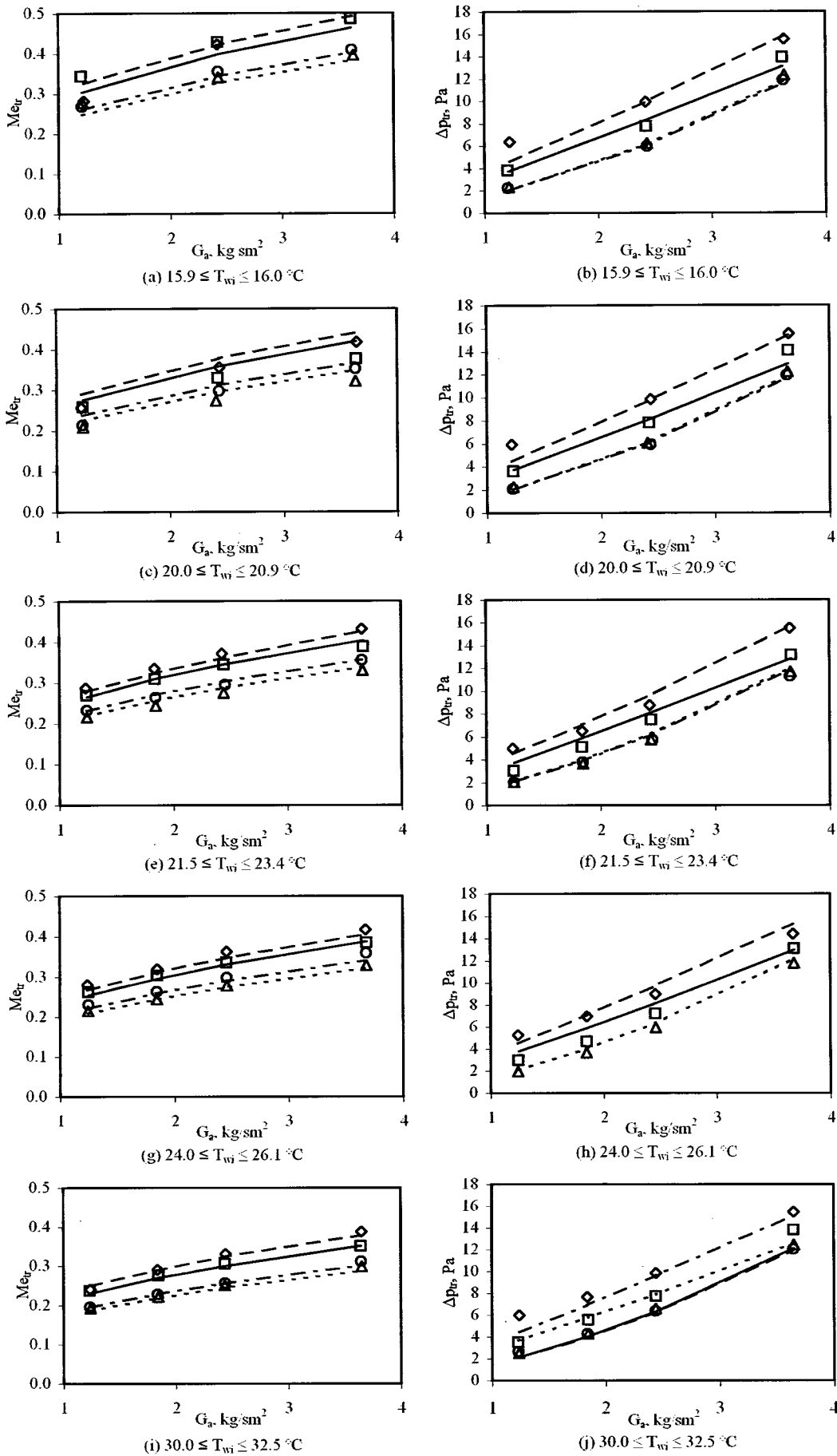


Figure G-2: Water trough and spray zone performance characteristic data compared to Equation (3.11) to (3.14)

APPENDIX G. WATER TROUGH AND SPRAY ZONE PERFORMANCE TEST DATA

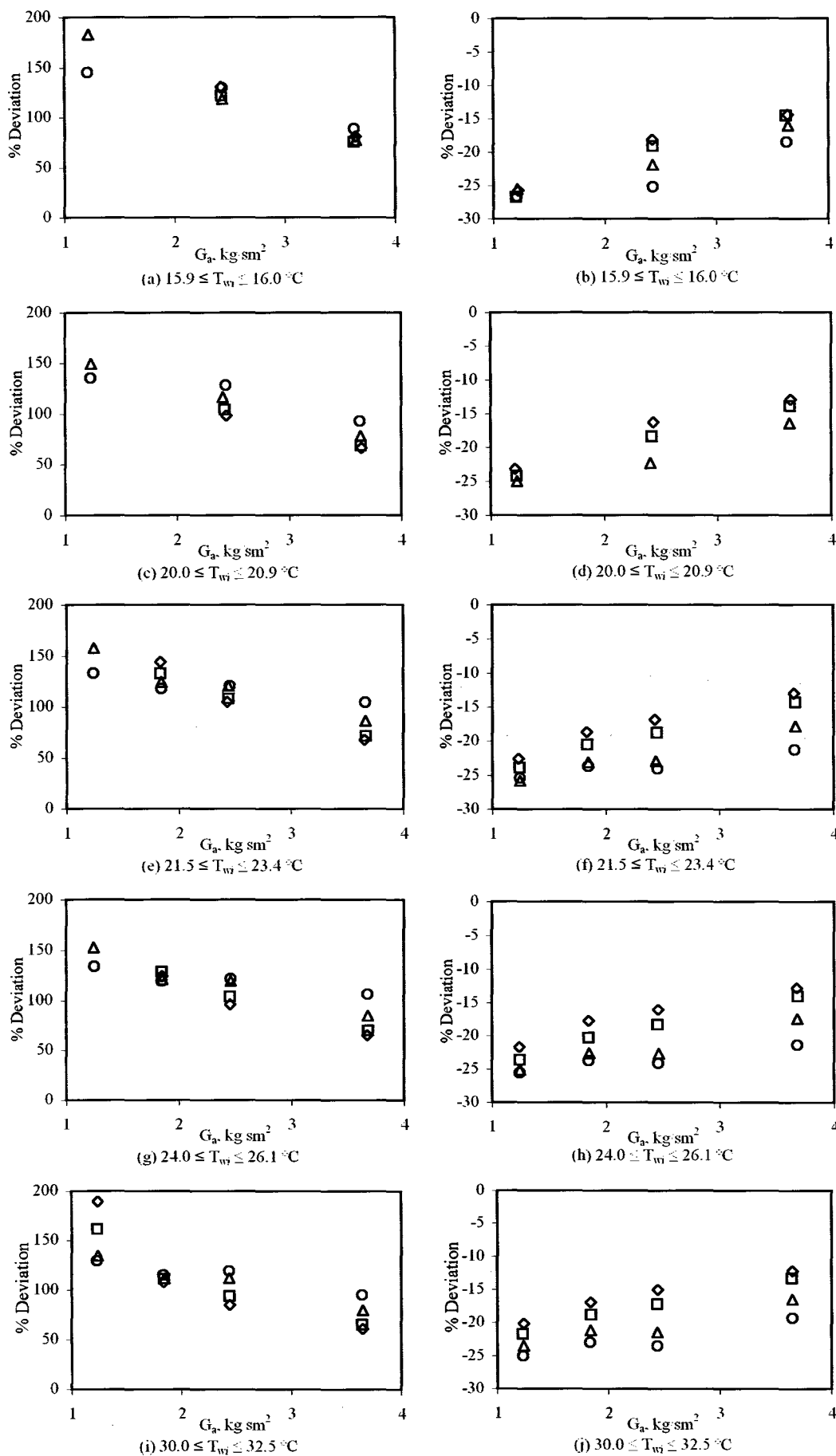


Figure G-3: Effect on water trough and spray zone Merkel number using Equation (G.2) and (G.3) to determine T_{wo}

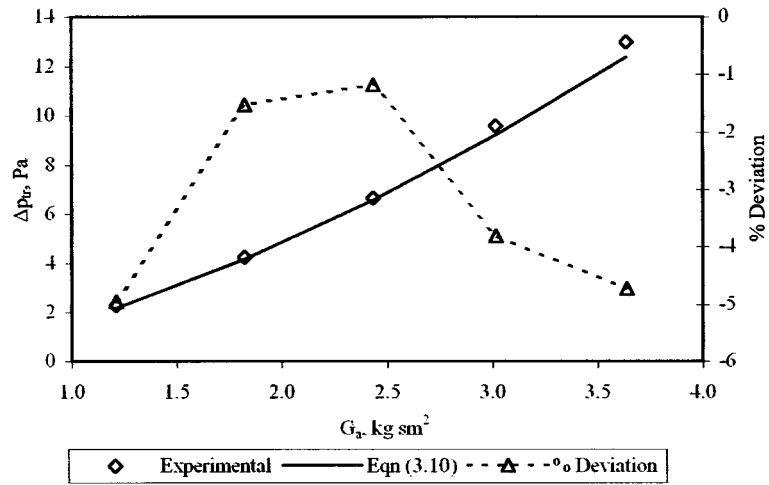


Figure G-4: Air pressure drop over water troughs – dry test with WDS at 200 + 1524 mm above water troughs

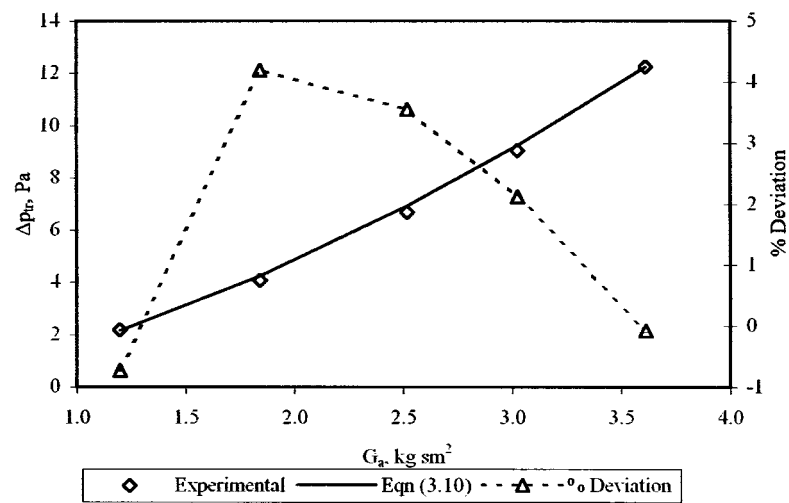


Figure G-5: Air pressure drop over water troughs – dry test with WDS at 200mm above water troughs

APPENDIX G. WATER TROUGH AND SPRAY ZONE PERFORMANCE TEST DATA

Table G-2: Water trough and spray zone performance test data

T _{non} (°C)	T _{in} (°C)	T _{wtr} (°C)	T _{ai} (°C)	ΔP _{inh} (V)	ΔP _{inh} (Pa)	ΔP _{tr} (V)	ΔP _{tr} (Pa)	P _{ai} (V)	P _{ai} (Pa)	ΔP _{or} (V)	ΔP _{or} (Pa)	m _w (kg/s)	T _{wtr} (°C)	T _{wo} (°C)	T _{to} (°C)	G _w (kg/sm ²)	G _a (kg/sm ²)	M _{cr}
12.41	15.29	12.95	15.24	1.15	67.57	1.02	6.40	1.03	101520.57	5.53	21761.71	12.39	16.01	15.70	15.16	5.51	1.22	0.28
12.27	15.13	12.78	15.38	1.67	264.86	1.03	9.97	1.08	101547.82	5.57	21927.04	12.44	16.01	15.47	14.74	5.53	2.42	0.42
12.17	14.98	12.84	15.71	2.54	597.10	1.04	15.56	1.16	101602.46	5.59	22035.11	12.47	16.00	15.33	14.49	5.54	3.64	0.51
12.25	15.01	12.58	14.79	1.15	65.38	1.01	3.81	1.02	101513.89	3.54	12194.86	9.29	15.90	15.48	14.87	4.13	1.20	0.34
12.17	14.90	12.56	15.01	1.67	265.62	1.02	7.77	1.06	101538.64	3.61	12508.04	9.40	15.89	15.28	14.25	4.18	2.43	0.43
12.18	14.89	12.77	15.56	2.53	592.47	1.04	13.90	1.13	101581.29	3.58	12390.18	9.36	15.88	15.20	14.04	4.16	3.62	0.49
12.23	14.89	12.48	14.63	1.15	66.26	1.01	2.32	1.02	101510.32	2.12	5375.87	6.18	15.89	15.46	14.08	2.74	1.21	0.28
12.23	14.86	12.54	14.96	1.68	266.35	1.02	6.24	1.05	101530.50	2.11	5311.35	6.14	15.88	15.32	13.59	2.73	2.43	0.34
12.03	14.77	12.77	15.50	2.54	596.70	1.03	12.34	1.10	101565.49	2.10	5282.99	6.12	15.87	15.24	13.54	2.72	3.64	0.40
12.22	14.78	12.50	14.62	1.15	65.54	1.01	2.23	1.01	101508.96	1.28	1337.85	3.09	15.87	15.40	13.39	1.38	1.20	0.27
12.25	14.83	12.54	14.95	1.67	265.79	1.02	5.99	1.04	101525.97	1.28	1333.76	3.09	15.88	15.24	13.13	1.37	2.43	0.36
12.25	14.78	12.79	15.54	2.53	593.28	1.03	11.91	1.09	101555.06	1.29	1406.61	3.17	15.93	15.24	13.24	1.41	3.63	0.41
12.80	13.42	13.47	13.99	1.15	66.51	1.02	5.95	1.03	101520.01	5.57	21957.00	12.44	20.92	20.13	18.74	5.53	1.21	0.26
12.74	13.41	13.38	14.12	1.68	267.52	1.03	9.86	1.08	101548.13	5.54	21798.65	12.39	20.79	19.57	17.53	5.51	2.44	0.36
12.66	13.25	13.49	14.47	2.55	597.92	1.04	15.53	1.17	101603.83	5.49	21557.39	12.32	20.71	19.24	16.84	5.48	3.64	0.42
12.77	13.34	13.37	13.88	1.16	68.22	1.01	3.62	1.02	101513.84	3.52	12098.78	9.24	20.36	19.54	17.52	4.11	1.23	0.26
12.78	13.34	13.40	14.06	1.67	264.01	1.02	7.83	1.06	101538.05	3.58	12388.59	9.35	20.31	19.16	16.43	4.16	2.42	0.33
12.79	13.33	13.60	14.52	2.54	597.18	1.04	14.08	1.13	101582.91	3.58	12380.41	9.35	20.24	18.92	15.92	4.15	3.64	0.38
12.81	13.24	13.32	13.76	1.16	68.03	1.01	2.29	1.01	101510.04	2.10	5268.41	6.11	20.16	19.38	15.98	2.71	1.23	0.21
12.83	13.33	13.37	13.97	1.66	260.51	1.02	6.09	1.05	101530.01	2.09	5228.08	6.09	20.11	19.07	15.21	2.70	2.40	0.27
12.65	13.27	13.56	14.42	2.54	594.37	1.03	12.22	1.10	101565.40	2.07	5151.40	6.04	20.06	18.86	14.95	2.68	3.63	0.32
12.78	13.25	13.18	13.63	1.15	67.65	1.01	2.09	1.01	101508.40	1.28	1323.41	3.07	20.00	19.14	14.71	1.37	1.23	0.21
12.81	13.28	13.28	13.88	1.68	266.26	1.02	5.95	1.04	101526.20	1.28	1313.97	3.06	20.02	18.83	14.34	1.36	2.43	0.30
12.81	13.27	13.42	14.26	2.53	593.52	1.03	11.92	1.09	101555.98	1.27	1292.56	3.04	20.06	18.67	14.24	1.35	3.63	0.35
9.29	13.11	10.12	12.87	1.15	67.14	1.02	4.98	1.03	101917.26	5.59	22052.11	12.46	23.36	21.89	20.21	5.54	1.23	0.29
9.23	13.09	9.91	12.89	1.37	149.77	1.02	6.54	1.05	101928.72	5.56	21878.12	12.41	23.28	21.38	18.86	5.52	1.84	0.34
9.28	13.23	9.82	13.11	1.66	262.07	1.02	8.77	1.07	101944.73	5.44	21302.10	12.25	23.10	20.90	17.74	5.44	2.43	0.37
9.16	12.99	9.85	13.49	2.53	592.93	1.04	15.50	1.17	102005.18	5.77	22908.94	12.70	22.83	20.22	16.46	5.64	3.65	0.43
8.96	12.82	9.44	12.34	1.16	68.09	1.01	3.03	1.02	101912.36	3.51	12023.08	9.21	22.42	20.89	17.63	4.09	1.24	0.27
8.96	12.77	9.35	12.42	1.37	149.98	1.02	5.09	1.04	101922.63	3.55	12032.63	9.30	22.37	20.49	16.35	4.13	1.84	0.31
8.85	12.96	9.19	12.64	1.67	265.17	1.02	7.47	1.06	101936.95	3.57	12318.29	9.32	22.27	20.11	15.40	4.14	2.44	0.34
8.70	12.54	9.21	12.83	2.54	596.01	1.03	13.12	1.13	101981.83	3.52	12084.81	9.23	22.05	19.56	14.07	4.10	3.67	0.39
8.64	12.56	8.98	11.95	1.15	67.82	1.01	2.05	1.01	101908.75	2.09	5207.13	6.07	21.90	20.47	14.41	2.70	1.24	0.22
8.69	12.27	8.94	11.98	1.37	150.19	1.01	3.65	1.03	101917.73	2.10	5275.76	6.11	21.78	20.12	13.30	2.72	1.84	0.24
8.65	12.20	8.95	12.12	1.67	263.20	1.02	5.75	1.05	101929.42	2.09	5221.43	6.08	21.69	19.81	12.71	2.70	2.44	0.27
8.63	12.07	9.15	12.59	2.53	593.33	1.03	11.72	1.10	101965.01	2.09	5217.05	6.08	21.66	19.41	12.15	2.70	3.66	0.33
8.55	11.93	8.76	11.55	1.16	67.83	1.01	3.78	1.05	101907.97	1.30	1420.69	3.18	21.57	19.93	12.17	1.41	1.24	0.23
8.54	11.92	8.70	11.65	1.37	150.09	1.01	3.78	1.02	101915.41	1.29	1397.96	3.16	21.53	19.63	11.38	1.40	1.84	0.26
8.61	12.03	8.78	11.96	1.68	266.23	1.02	5.69	1.04	101925.30	1.30	1424.84	3.19	21.52	19.41	11.06	1.42	2.45	0.30
8.55	11.85	9.02	12.47	2.53	591.60	1.03	11.30	1.09	101953.46	1.30	1425.82	3.19	21.49	19.01	10.82	1.42	3.66	0.36

APPENDIX G. WATER TROUGH AND SPRAY ZONE PERFORMANCE TEST DATA

Table G-2: (continued) Water trough and spray zone performance test data

T_{in} (°C)	T_{out} (°C)	T_{wet} (°C)	T_{air} (°C)	ΔP_{inh} (V)	ΔP_{inh} (Pa)	ΔP_{ur} (V)	ΔP_{ur} (Pa)	ΔP_{ur} (V)	P_{in} (V)	P_{in} (Pa)	ΔP_{ur} (V)	m_w (kg/s)	T_{wi} (°C)	T_{wo} (°C)	T_{bo} (°C)	G_w (kg/m ²)	G_t (kg/m ²)	M_{e_0}
7.33	9.30	8.60	10.12	1.15	67.38	1.02	5.30	5.67	1.03	101817.56	5.67	22432.17	26.07	24.09	22.01	5.58	1.24	0.28
7.19	9.14	8.30	9.90	1.37	150.08	1.02	6.98	5.64	1.05	101829.67	5.64	22822.63	25.82	23.34	20.01	5.56	1.85	0.32
7.14	9.04	8.25	9.92	1.67	264.96	1.02	8.98	5.63	1.08	101846.15	5.63	22927.67	25.70	22.79	18.83	5.55	2.46	0.36
7.11	9.05	8.18	10.17	2.53	591.82	1.04	14.42	5.48	1.17	101903.60	5.48	21503.85	22.30	25.52	22.01	16.91	3.67	0.42
6.98	8.77	8.02	9.47	1.16	67.94	1.01	2.96	3.65	1.02	101812.32	3.65	12478.48	25.18	23.14	19.07	4.20	1.25	0.26
6.86	8.70	7.80	9.31	1.37	149.65	1.01	4.68	3.60	1.04	101822.18	3.60	12478.48	25.04	22.52	17.28	4.17	1.85	0.30
6.89	8.78	7.75	9.43	1.67	264.05	1.02	7.20	3.60	1.06	101837.04	3.60	12478.48	24.88	22.03	16.04	4.16	2.46	0.34
6.88	8.64	7.88	9.79	2.53	593.58	1.03	13.08	3.64	1.14	101883.45	3.64	12478.48	24.73	21.41	14.54	4.20	3.68	0.38
6.61	8.57	7.47	8.85	1.15	67.30	1.01	1.97	2.14	1.01	101808.19	2.14	5447.95	24.50	22.58	14.99	2.76	1.24	0.21
6.94	8.81	7.54	9.11	1.37	149.46	1.01	3.66	2.14	1.03	101817.52	2.14	5447.95	24.48	22.22	13.62	2.76	1.85	0.24
6.71	8.62	7.41	9.14	1.67	264.63	1.02	5.99	2.13	1.05	101828.68	2.13	5396.04	24.37	21.78	12.73	2.74	2.46	0.28
6.68	8.51	7.54	9.54	2.53	591.71	1.03	11.80	2.11	1.11	101865.21	2.11	5333.53	24.29	21.23	11.77	2.73	3.68	0.33
6.65	8.43	7.17	8.67	1.16	67.71	1.00	-0.47	1.29	1.01	101807.16	1.29	1389.29	24.14	21.93	11.82	1.40	1.24	0.23
6.72	8.60	7.18	8.79	1.37	149.15	1.01	3.90	1.29	1.02	101814.55	1.29	1403.70	24.04	21.50	10.86	1.41	1.85	0.26
6.57	8.37	7.16	8.89	1.67	263.63	1.01	3.69	1.29	1.04	101825.02	1.29	1389.38	24.02	21.14	10.32	1.40	2.46	0.30
6.46	8.24	7.28	9.29	2.53	590.65	1.03	11.53	1.28	1.09	101853.56	1.28	1339.37	23.96	20.56	9.74	1.37	3.68	0.36
10.52	12.40	10.96	12.62	1.16	67.43	1.01	2.65	1.29	1.01	101806.89	1.29	1370.00	32.38	29.32	16.54	1.39	1.23	0.20
10.48	12.31	11.00	12.76	1.37	149.92	1.01	4.28	1.26	1.02	101814.86	1.26	1277.03	32.47	28.86	15.28	1.31	1.83	0.23
10.36	12.13	10.95	12.78	1.67	263.77	1.02	6.38	1.27	1.04	101825.10	1.27	1290.54	32.30	28.30	14.67	1.34	2.43	0.26
10.21	11.94	10.97	13.06	2.53	590.43	1.03	12.05	1.28	1.09	101854.86	1.28	1317.35	32.14	27.43	13.96	1.36	3.64	0.31
10.30	12.02	11.02	12.44	1.16	67.93	1.01	2.50	2.14	1.01	101808.23	2.14	5474.54	32.06	29.35	20.14	2.76	1.24	0.19
10.32	12.00	10.99	12.47	1.37	150.57	1.01	4.26	2.14	1.03	101817.04	2.14	5482.12	31.95	28.77	18.43	2.76	1.84	0.22
10.36	12.02	11.07	12.66	1.67	263.56	1.02	6.29	2.14	1.05	101829.18	2.14	5358.16	31.76	28.20	17.48	2.76	2.43	0.25
10.34	11.96	11.16	13.02	2.53	592.03	1.03	12.49	2.12	1.11	101865.69	2.12	5350.90	31.69	27.46	16.28	2.73	3.65	0.30
9.87	11.58	11.23	12.39	1.15	67.22	1.01	3.48	3.62	1.02	101811.70	3.62	12567.95	31.37	28.68	23.89	4.18	1.23	0.24
9.97	11.51	10.98	12.23	1.37	150.99	1.02	5.54	3.64	1.04	101822.38	3.64	12656.43	31.21	27.92	21.83	4.19	1.84	0.28
10.01	11.53	10.95	12.28	1.67	263.79	1.02	7.74	3.58	1.06	101836.75	3.58	12392.59	31.08	27.36	20.42	4.15	2.44	0.31
9.99	11.41	10.92	12.53	2.53	590.43	1.03	13.82	3.62	1.14	101883.91	3.62	12574.14	30.88	26.56	18.60	4.18	3.65	0.35
9.98	11.39	11.38	12.35	1.16	67.93	1.02	6.01	5.66	1.03	101818.94	5.66	22380.48	30.49	28.19	25.26	5.57	1.24	0.24
9.99	11.41	11.13	12.22	1.37	150.00	1.02	7.68	5.61	1.05	101831.34	5.61	22115.02	30.37	27.41	23.56	5.54	1.84	0.29
9.99	11.48	11.05	12.31	1.67	264.05	1.02	9.86	5.71	1.08	101848.68	5.71	22631.31	30.14	26.72	22.31	5.60	2.44	0.33
9.94	11.42	11.02	12.59	2.53	591.56	1.04	15.47	5.60	1.17	101908.45	5.60	22768.27	29.96	25.83	20.37	5.53	3.65	0.39

APPENDIX H. FILL PERFORMANCE TEST DATA

H.1. Introduction

The results of the fill performance tests are presented in this appendix. All the results in this appendix were generated by using the water trough performance correlations of Equation (3.11) to (3.14). Figure H-1 indicates how the current test data compares with Equation (3.15) and (3.16). Figure H-2 gives a comparison between the current test data and Equation (3.20) to (3.23). Each row of graphs includes the Merkel number and loss coefficient of the fill for a specific range of water inlet temperatures. The figures are shown for an increase in water inlet temperature range with the coldest range at the top. Each corresponding set of curves in Figure H-1 and H-2 has the same legend as shown in Table H-1. The water inlet temperature ranges are shown at the top of each column in Table H-1. The first column of Table H-1 indicates the symbol (experimental data) and the line type (correlation) used for each G_w value. All values in kg/sm^2 .

Table H-1: Legend for Figures H-1 and H-2

Symbol	Water inlet temperature ranges		
	21.3 – 24.8 °C	25.5 – 32.3 °C	32.6 – 40.8 °C
◇ — — —	5.548	5.488	5.557
□ — — —	4.134	4.147	4.159
△ - - - - -	2.745	2.739	2.766
◇ - - - -	1.364	1.346	1.374

For Figures H-1 and H-2 the water outlet temperature was calculated according to Equation (3.7)

$$T_{wo} = 0.1T_{wob} + 0.9T_{wot} \quad (\text{H.1})$$

Figure H-3 (a), (c) and (e) show the deviation in Merkel number when the water outlet temperature is calculated according to

$$T_{wo} = 0.5(T_{wob} + T_{wot}) \quad (\text{H.2})$$

and Figure H-3 (b), (d) and (f) show the deviation in Merkel number when the water outlet temperature is calculated according to

$$T_{wo} = T_{wot} \quad (\text{H.3})$$

The legend for Figure H-3 is the same as in Table H-1. Both y-axes are % deviation and is calculated as

$$\% \text{ Deviation} = (Me' - Me_{10/90}) / Me_{10/90} \times 100 \quad (\text{H.4})$$

where

Me' = Merkel number calculated using Equation (H.2) or (H.3)

$Me_{10/90}$ = Merkel number calculated using Equation (H.1)

Figure H-4 shows the results of the dry test (air only), i.e. Equation (3.17). The air pressure drop over the water troughs for the particular test was determined with Equation (3.10). The % deviation is given as

$$\% \text{ Deviation} = \left[\text{Experimental} - \text{Eqn (3.17)} \right] / \text{Eqn (3.17)} \times 100 \quad (\text{H.5})$$

All the experimental data is given in Table H-2.

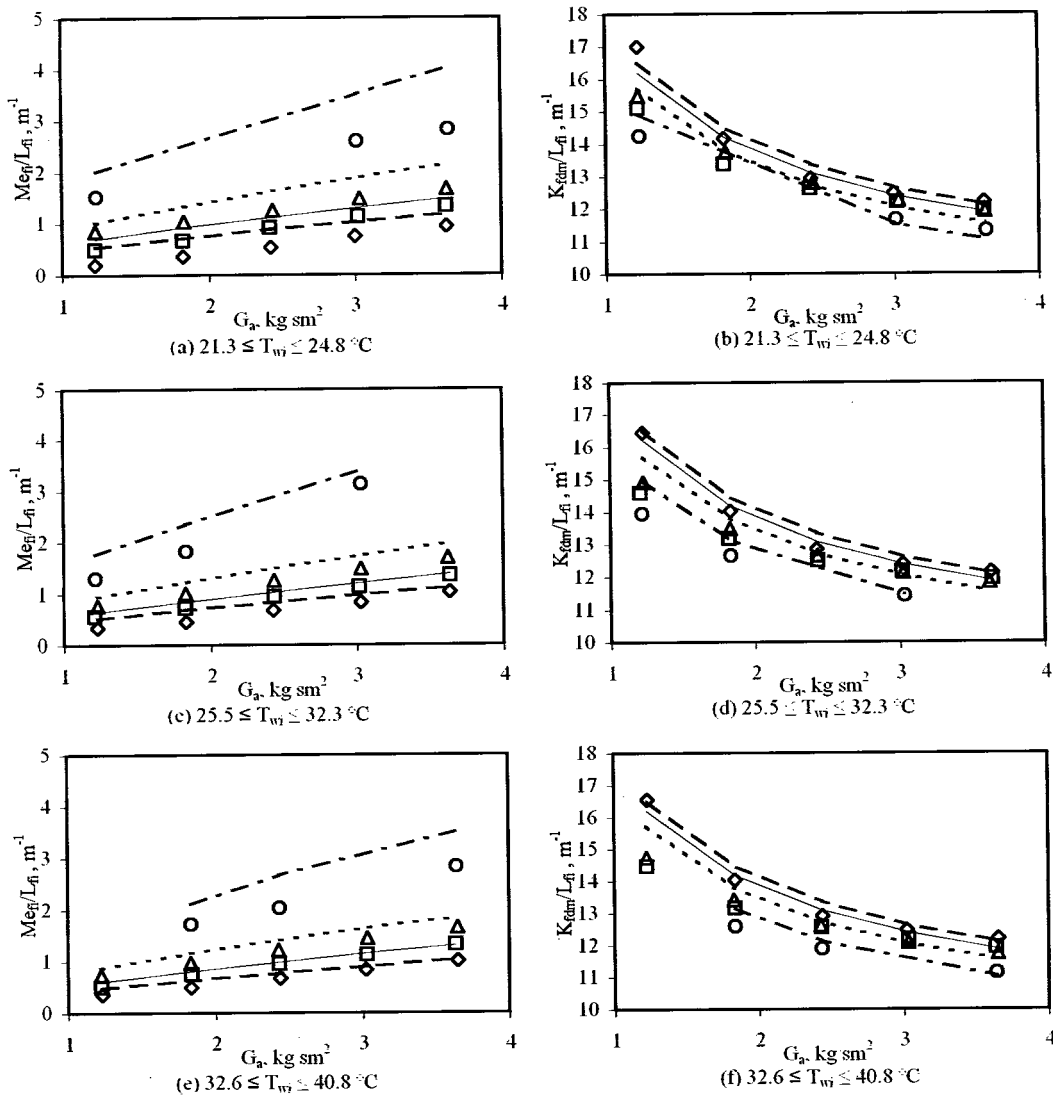


Figure H-1: Fill performance characteristic data compared to Equation (3.15) and (3.16)

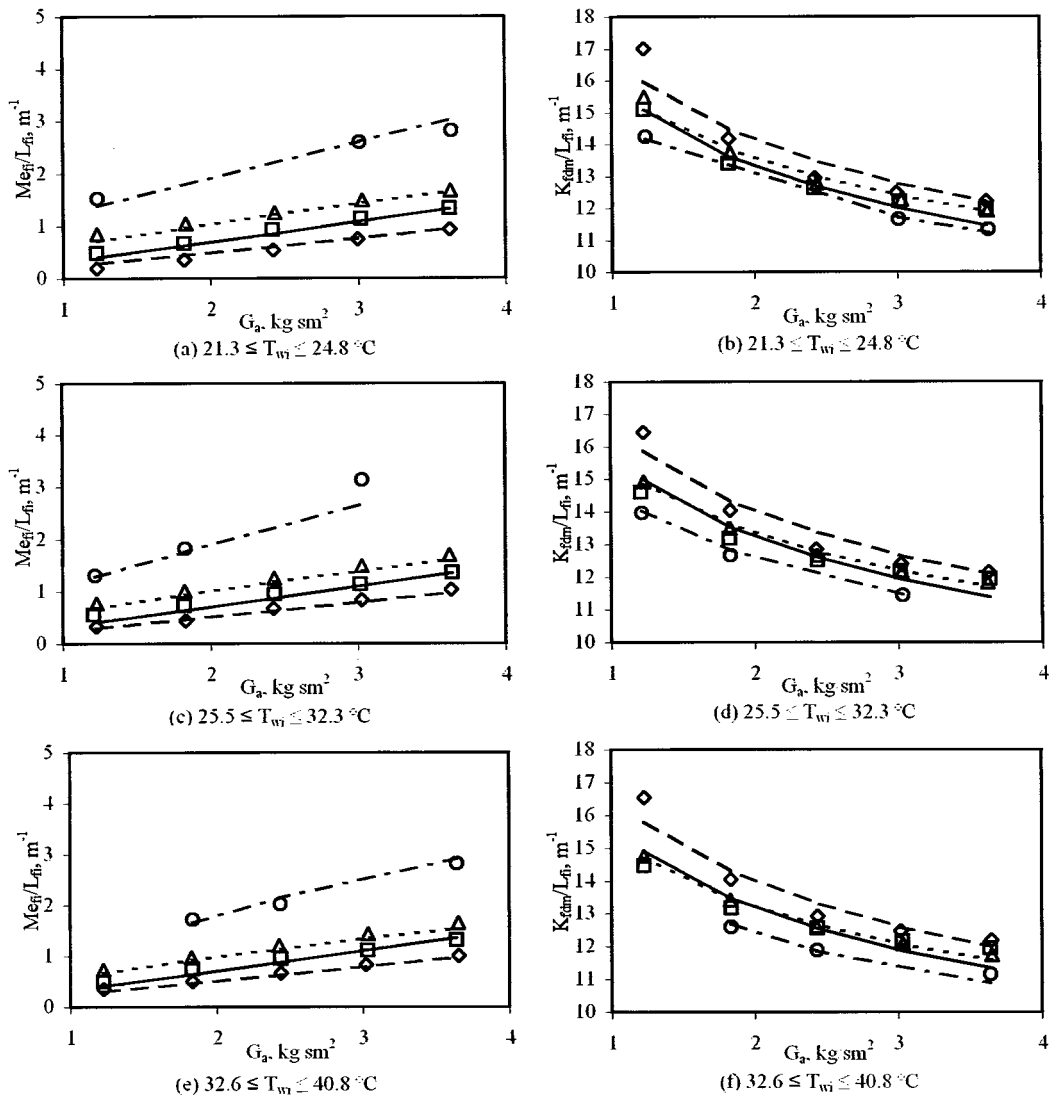


Figure H-2: Fill performance characteristic data compared to Equation (3.20) to (3.23)

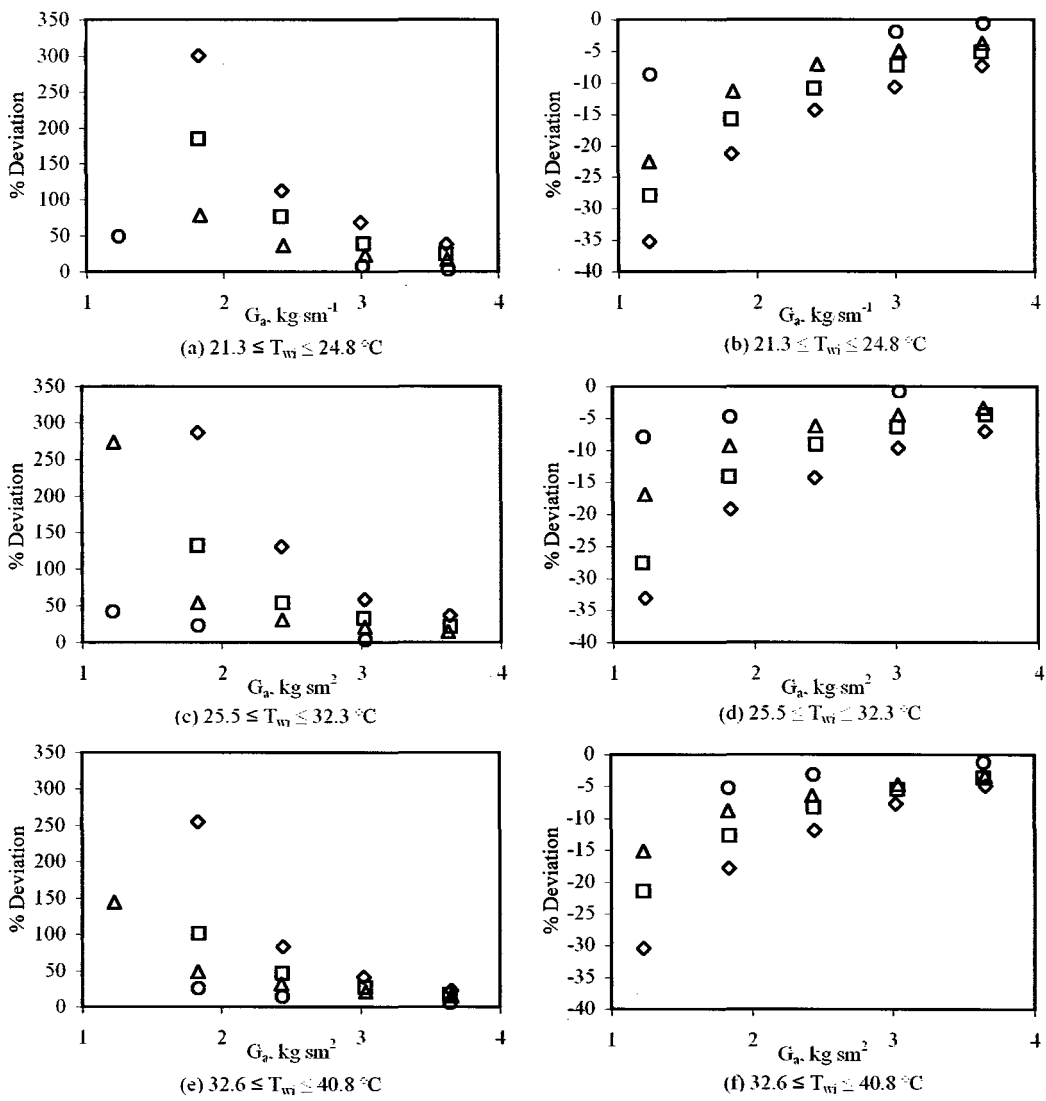


Figure H-3: Effect on fill Merkel number using Equation (H.2) and (H.3) to determine T_{w0}

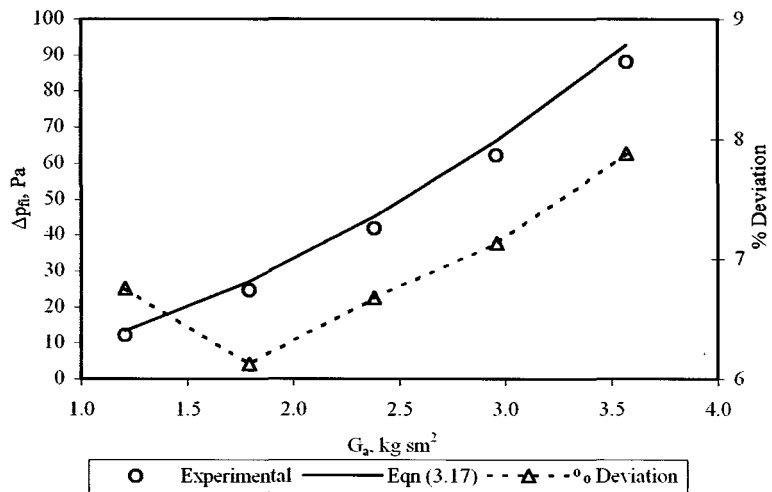


Figure H-4: Air pressure drop over fill only – dry test

Table H-2: Fill performance test data

T _{amb} (°C)	T _{in} (°C)	T _{fwl} (°C)	T _{sl} (°C)	ΔP _{wh} (V)	ΔP _{rot} (V)	ΔP _{rot} (Pa)	P _u (V)	P _u (Pa)	ΔP _{ur} (V)	ΔP _{ur} (Pa)	m _w (kg/s)	T _{sl} (°C)	T _{sw} (°C)	T _{so} (°C)	G _w (kg/min)	G _s (kg/min)	M _{sc} (Pa)	ΔP _{sc} (Pa)	K _{fm} /L _q (m ⁻¹)		
10.00	10.37	10.63	10.87	1.15	66.01	14.52	1.03	101018.59	1.28	1340.02	3.08	32.25	20.10	27.86	1.37	1.22	0.19	1.38	1.30	13.96	
9.86	10.37	10.52	10.99	1.37	149.48	1.07	30.15	1.07	101040.95	1.27	1305.51	32.12	16.88	25.47	1.35	1.83	0.23	2.68	1.83	12.66	
10.08	10.46	10.66	11.22	1.68	266.20	1.11	50.32	1.11	101069.80	1.22	1112.23	3.94	14.60	21.02	1.25	2.44	0.26	4.26	2.19	11.93	
10.22	10.62	10.85	11.53	2.05	410.07	1.16	74.14	1.17	101103.87	1.26	1232.20	2.86	31.83	13.32	1.22	3.03	0.28	6.04	3.14	11.53	
10.29	10.68	11.10	11.95	2.52	586.14	1.22	105.29	1.24	101146.13	1.24	148.35	2.86	31.89	13.45	1.27	3.62	0.30	8.04	2.80	11.23	
10.30	10.66	10.92	11.30	1.16	67.18	1.03	15.84	1.03	101021.34	2.13	5409.75	6.17	31.84	24.57	30.27	2.74	1.23	4.33	0.77	14.93	
10.44	10.91	11.03	11.51	1.37	148.98	1.07	32.15	1.07	101044.63	2.14	5461.04	6.20	31.76	22.14	28.84	2.76	1.82	2.71	1.01	13.48	
10.52	11.02	11.17	11.75	1.67	264.74	1.12	53.64	1.12	101076.58	2.12	5367.21	6.15	31.74	20.16	27.52	2.73	2.43	4.31	1.26	12.66	
10.56	10.96	11.27	11.97	2.05	408.89	1.17	79.31	1.17	101115.73	2.13	5397.62	6.17	31.69	18.69	26.42	2.74	3.02	6.12	1.49	12.15	
10.46	10.86	11.34	12.20	2.52	585.87	1.24	110.21	1.27	101164.38	2.11	5317.63	6.12	31.59	17.47	25.29	2.72	3.62	8.18	1.69	11.84	
10.49	10.88	11.28	11.72	1.15	65.43	1.04	17.30	1.04	101056.23	3.60	12496.43	9.37	31.64	26.64	31.21	4.16	1.21	3.58	0.56	14.59	
10.48	10.85	11.34	11.75	1.37	148.92	1.08	34.58	1.08	101052.35	3.58	12391.94	9.33	31.46	24.53	30.04	4.15	1.82	0.27	5.70	0.72	13.17
10.42	10.84	11.35	11.87	1.67	265.36	1.12	57.06	1.14	101087.72	3.59	12414.08	9.34	30.84	22.46	28.78	4.15	2.44	7.93	0.94	12.51	
10.25	10.68	11.25	11.91	2.05	407.00	1.18	83.48	1.21	101130.99	3.38	12363.24	9.32	30.17	20.75	27.51	4.14	3.02	10.12	1.14	12.17	
10.25	10.66	11.31	12.15	2.53	591.87	1.25	116.92	1.31	101189.45	3.56	12262.01	9.29	29.47	19.23	26.28	4.13	3.64	12.52	1.35	11.94	
10.26	10.62	11.49	11.81	1.16	67.19	1.04	20.31	1.06	101035.12	5.63	22208.74	12.49	28.54	25.55	28.27	5.55	1.23	0.26	4.41	0.34	16.44
10.31	10.68	11.37	11.74	1.37	149.77	1.08	37.55	1.10	101063.19	5.42	21033.99	12.21	27.81	23.73	26.82	5.43	1.83	0.30	6.86	0.45	14.04
10.21	11.17	11.80	12.55	1.67	263.93	1.13	59.27	1.16	101000.21	5.56	21877.51	12.40	26.85	22.06	25.86	5.51	2.43	0.34	9.58	0.68	12.85
10.29	11.23	11.86	12.42	2.05	409.53	1.19	86.60	1.24	101127.66	5.45	21648.57	12.26	26.89	20.67	24.77	5.45	3.02	0.37	12.23	0.84	12.41
10.85	11.33	11.94	12.76	2.53	593.33	1.26	120.31	1.35	101215.67	5.54	21782.14	12.38	25.48	19.53	24.01	5.50	3.63	0.41	13.20	1.04	12.16
10.88	11.25	11.38	11.78	1.16	68.05	1.03	13.18	1.03	101019.92	1.26	1238.28	2.97	24.78	17.38	22.46	1.32	1.23	1.44	1.52	14.25	

Table H-2: (continued) Fill performance test data

T _{min} (°C)	T _{in} (°C)	T _{wti} (°C)	T _{ai} (°C)	ΔP _{inh} (V)	ΔP _{inh} (Pa)	ΔP _{tot} (V)	ΔP _{tot} (Pa)	P _{ai} (V)	P _{ai} (Pa)	ΔP _{air} (V)	ΔP _{air} (Pa)	m _{in} (kg/s)	T _{ai} (°C)	T _{se} (°C)	T _{ss} (°C)	C _{se} (kg/m ³)	C _s (kg/m ³)	M _{se} (Pa)	AP _{se} (Pa)	M _{se} /L _g (m ⁻³)	K _{se} /L _g (m ⁻³)
11.00	11.52	11.44	12.00	1.37	148.98	1.07	30.13	1.07	101040.23	1.24	1166.92	2.88	24.69	15.47	20.80	1.28	1.82	2.71	2.71	1.96	12.86
11.08	11.64	11.58	12.29	1.67	263.80	1.11	50.55	1.11	101069.17	1.37	1764.17	3.54	24.47	15.16	20.37	1.57	2.42	4.32	4.32	2.06	12.20
11.22	11.87	11.83	12.76	2.05	407.33	1.16	74.23	1.17	101103.04	1.29	1381.27	3.14	24.55	14.00	19.07	1.39	3.01	6.11	6.11	2.60	11.66
11.11	11.72	11.90	13.00	2.54	593.64	1.23	104.72	1.24	101147.38	1.28	1348.59	3.10	24.54	13.55	18.18	1.38	3.64	8.28	8.28	2.82	11.34
11.04	11.67	11.58	12.25	1.16	67.30	1.04	16.28	1.04	101021.68	2.13	5430.54	6.20	24.54	20.51	23.88	2.75	1.22	0.21	1.45	0.85	15.49
11.20	11.99	11.71	12.49	1.37	150.10	1.07	32.48	1.07	101044.86	2.14	5461.67	6.21	24.61	19.15	23.05	2.76	1.83	0.24	2.77	1.05	13.75
11.09	11.87	11.71	12.61	1.68	266.25	1.12	53.63	1.12	101075.30	2.12	5366.09	6.16	24.58	17.91	22.19	2.74	2.43	0.27	4.41	1.25	12.80
10.97	11.91	11.81	12.87	2.06	411.73	1.17	79.27	1.19	101114.87	2.12	5368.08	6.16	24.51	16.92	21.51	2.74	3.03	0.30	6.27	1.49	12.26
11.26	12.19	12.01	13.33	2.53	591.09	1.24	110.08	1.26	101162.59	2.12	5365.71	6.15	24.48	16.25	20.88	2.73	3.63	0.32	8.38	1.67	11.92
11.41	12.32	12.08	12.87	1.16	67.31	1.04	18.20	1.04	101026.33	3.60	12466.53	9.37	24.46	21.82	24.09	4.17	1.22	0.26	3.71	0.48	13.10
11.48	12.38	12.05	13.01	1.37	149.26	1.08	34.53	1.08	101031.44	3.54	12168.07	9.26	24.39	20.65	23.51	4.12	1.84	0.30	3.77	0.67	13.98
11.66	12.77	12.25	13.35	1.67	263.58	1.12	56.13	1.14	101085.23	3.58	12398.01	9.35	24.39	19.67	23.25	4.15	2.42	0.33	8.02	0.92	12.62
11.60	12.64	12.38	13.61	2.06	411.11	1.18	82.95	1.21	101128.30	3.53	12153.66	9.26	24.34	18.69	22.71	4.11	3.02	0.36	10.27	1.13	12.20
11.64	12.77	12.47	13.91	2.53	591.60	1.25	115.18	1.30	101184.43	3.54	12185.94	9.27	24.13	17.89	22.24	4.12	3.62	0.39	12.64	1.34	11.97
11.79	12.94	12.64	13.57	1.16	67.62	1.05	20.85	1.06	101094.83	5.64	22270.81	12.52	23.46	21.82	22.80	5.56	1.22	0.28	4.47	0.20	17.01
12.07	13.49	12.71	13.85	1.37	149.82	1.08	37.47	1.10	101061.73	5.64	22259.58	12.52	22.64	20.47	21.90	5.56	1.82	0.33	7.05	0.36	14.17
12.29	13.87	12.92	14.30	1.68	265.65	1.13	59.07	1.16	101097.99	5.59	22046.67	12.46	21.89	19.34	21.11	5.54	2.42	0.37	9.75	0.54	12.95
12.29	13.80	13.00	14.51	2.05	407.14	1.18	85.37	1.23	101143.54	5.59	22029.23	12.46	21.51	18.55	20.72	5.54	3.00	0.40	12.44	0.75	12.48
12.32	13.94	13.10	14.94	2.54	594.52	1.26	119.75	1.34	101210.85	5.59	22042.48	12.46	21.31	17.94	20.40	5.54	3.62	0.44	15.44	0.94	12.22

APPENDIX I. PERFORMANE CURVE GENERATOR (PCG)

I.1. Introduction

All NDWCT performance test standards require that suppliers of cooling towers must submit performance curves. ASME requires a minimum of nine sets of performance curves. Each set must show cold water temperatures on the y-axis and wet bulb temperature on the x-axis with lines of constant relative humidity as parameter, 25 %, 40 %, 65 % and 100 %. The performance curves must include three main groups at 90 %, 100 % and 110 % of the design water flow rate. A minimum of three sets of curves with each flow rate group shall be for a constant cooling range including 80 %, 100 % and 120 % of design cooling range. Based on these curves and the test data, five more curves must be generated by the test engineer in order to determine the predicted water flow rate. This is a very cumbersome and clumsy method to determine off-design tower performance. Probably the biggest disadvantage of this method is that not all the information is displayed at once. This makes it very hard to understand and try and predict how the tower will operate at off-design conditions. With this in mind it was decided to develop the PCG software in order to meet the following requirements: (a) it must be user friendly, (b) all relevant data must be available immediately, (c) it must be flexible to incorporate different tower configurations and performance characteristics, such as fill, spray zone and rain zone performance. The ideal situation would be to have a computer program analyse the test conditions in order to determine what the output should be. This output can then be compared to the measured output to see if the tower meets its guarantee. This is the idea on which the PCG software is build. It uses the output of the one dimensional Improved Merkel method discussed in Chapter 2 to generate performance curves. This appendix then discusses the method followed to generate these performance curves, the potential error involved by using these curves compared to the one dimensional Improved Merkel method and the features of the PCG package.

I.2. Generating performance curves

The input parameters are T_{a1} , RH_1 , p_{a1} , dT_a/dz , T_{wi} and m_w . Note that dT_a/dz is in fact not an independent input parameter as discussed in Appendix K. However in the PCG software, the user still has the option to specify it as if it were an independent input parameter. This was done to accommodate future studies that might require dT_a/dz to be an independent input parameter. The output, T_{wo} is determined with the one dimensional Improved Merkel method discussed in Chapter 2. First, five 45 ° angle lines are drawn as shown in Figure I.1. These lines represent the design parameters.

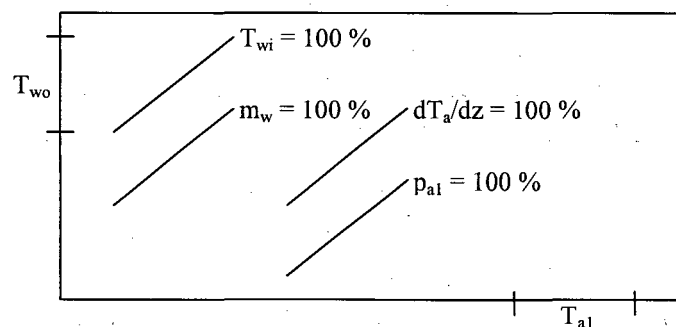


Figure I-1: Step 1 of generating performance curves

The design values of T_{a1} , p_{a1} , dT_a/dz , T_{wi} , m_w and RH_1 are then used to calculate T_{wo} over a range of T_{a1} values. The T_{wo} values are then projected backwards to give the intersection points of the design RH_1 line.

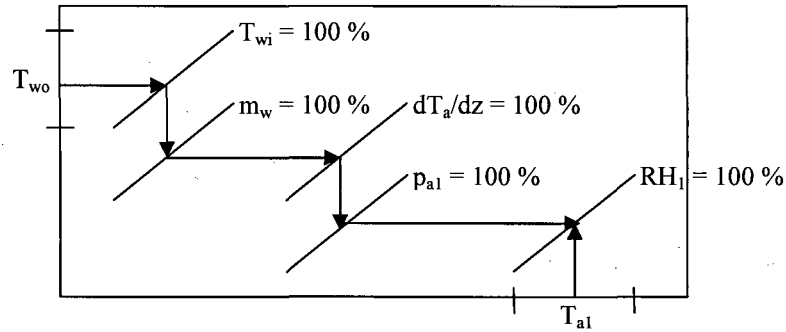


Figure I-2: Step 2 of generating performance curves

This process is repeated for all the RH_1 values required by the user. Determining the off-design lines for the other parameters are similar. Consider the m_w case. With all the other parameters held at the design value, T_{wo} is calculated over the range of T_{a1} for a specific value of m_w , say 110 % of design value. The T_{wo} values are then projected backwards to determine the intersection points of the 110 % m_w line. See Figure I-3.

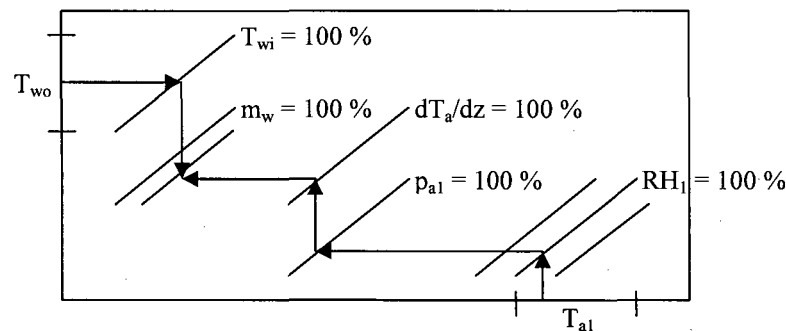


Figure I-3: Step 3 of generating performance curves

This process is repeated until all the necessary curves have been generated. As long as four of the five parameters are at the design value, the performance curve method predicts T_{wo} values identical to those of the one dimensional model over the entire range of T_{a1} values. However, when more parameters are not at the design value the T_{wo} values of the two methods will differ slightly. Figure I-4 shows a typical distribution of errors found in T_{wo} when employing the performance curve method over the range of inputs defined in Figure I-7. The subscripts PC and 1D indicate the performance curve method and one dimensional model output respectively. From Figure I-4 one can conclude that the PC output compares well with the 1D output.

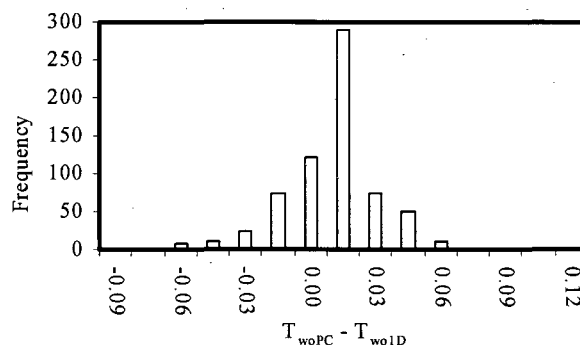


Figure I-4: Histogram for difference in T_{wo} values

I.3. PCG

This section serves as a user manual for the PCG package and also highlights some of its features. Figure I-5 indicates the first tab of the user interface for PCG. The user can define the dimensions of the tower in this window. Options are also available to model the tower using the effective frontal area or not. Reduction in frontal area happens in cooling tower because of flow separation at the tower inlet. Another option is whether the known input is constant water inlet temperature, T_{wi} , or constant cooling range, z .

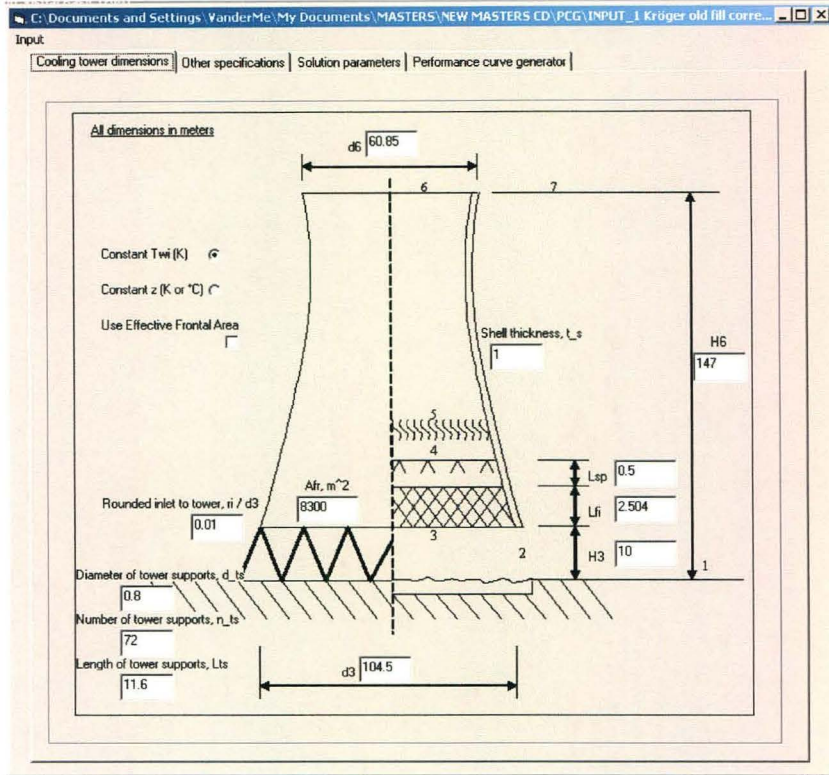


Figure I-5: PCG – Cooling tower dimensions tab

Figure I-6 shows the other specifications, as well as fill performance characteristics, that can be defined by the user.

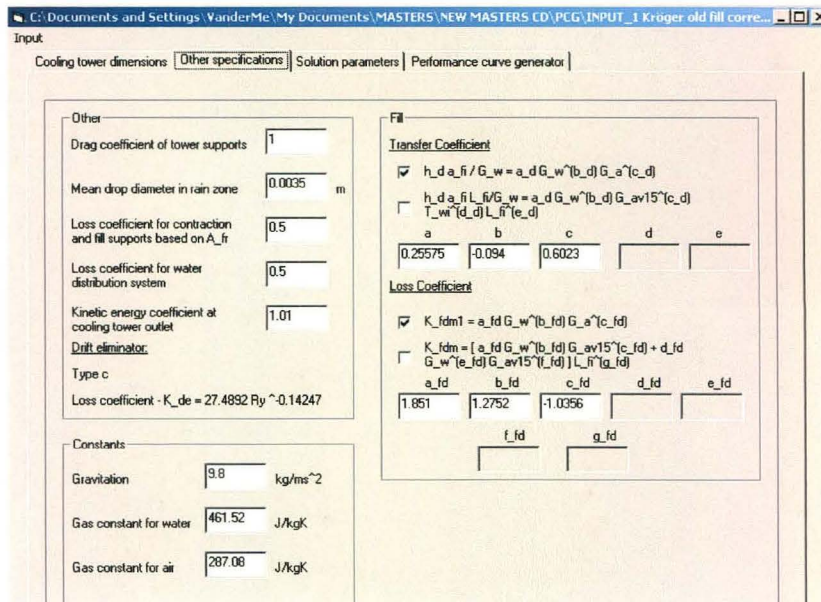


Figure I-6: PCG – Other specifications tab

The Solution parameters tab allows the user to adjust the relaxation factors and the maximum allowable residual. Figure I-7 shows the parameters that can be adjusted to generate the performance curves.

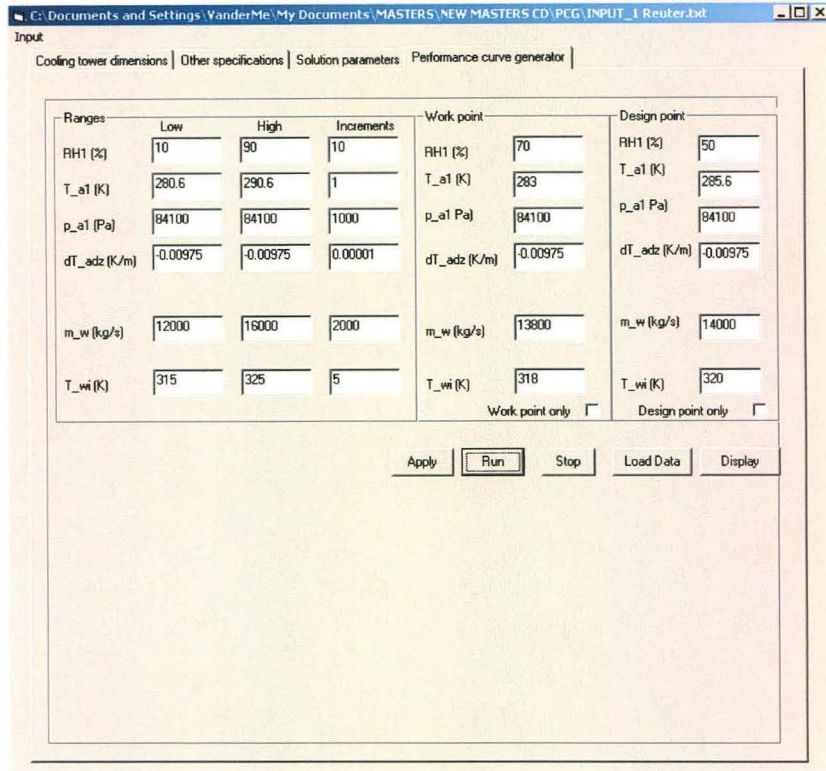


Figure I-7: PCG – Performance curve generator tab

The performance curves generated from the inputs of Figure I-7 are shown in Figure I-8, along with the location of the work point, design point and deviations from the one dimensional model. The work point is equivalent to as tested conditions

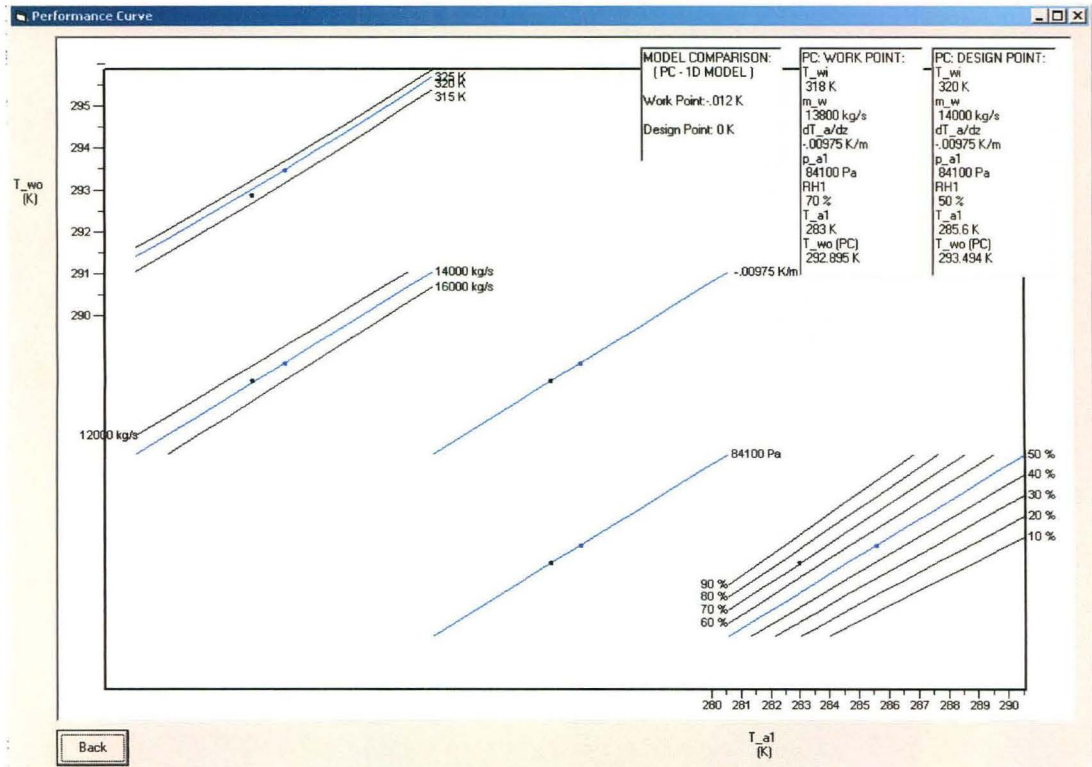


Figure I-8: PCG – performance curves

With these performance curves it is now possible to easily and effectively adjust the off-design test results in order to determine whether the NDWCT has met its guarantee or not. For instance, if one wants to know what the water outlet temperature should be at the test conditions, simply enter the performance curves at the test conditions and read of the water outlet temperature. If the result of interest is water mass flow rate, then enter the performance curves at the test T_{wo} value and the other test conditions. The intersection of these lines will indicate what the water mass flow rate should be. In this case, use horizontal interpolation if intersection point lies between lines. Other features of the PCG package include the following:

- Thermophysical properties of both the work point and design point at all the locations of the tower.
- Tower performance, i.e. loss coefficients, Merkel numbers, heat rejection rate and mass water evaporated, at work point and design point.
- Displaying invalid data on the performance curves. These data points indicate the sections of the performance curves that lie outside the valid domain of the one dimensional model. This situation should be avoided by changing the range of the input parameters.
- Tower configurations can be saved or imported using the Input drop-down menu.

Table I-1 indicates the additional files that can be accessed by the user. The first column indicates the name of the file used to process the data. The second column gives a short description of what the processing file does and the last column indicates the name of the data file that has to be imported by the user.

Table I-1: Files included in the PCG package

Processing file	Description	Data file
Sensitivity at WP.xls	Determines the sensitivity indexes of the six work point parameters.	Sensitivity at WP.rpt
Convergence analyses for 1D MODEL.xls	Shows how the residuals of the iteration variables converged. Is activated by checking the Work point and Design point only check boxes in Figure I-7	WP iteration data.rpt or DP iteration data.rpt
PC and 1D MODEL comparison.xls	Generates the histogram of Figure I-4	PC-D1.rpt
RH tool.xls	Relates T_{a1} , T_{wb1} , p_{a1} and RH_1	Not applicable
Validity 1D Model over range.rpt	Reports whether or not any equation was used outside its valid region.	Not applicable

Note that the two .pcg files supplied with the PCG package must not be deleted or edited by the user.

APPENDIX J. CONFIGURATION OF NDWCT'S

J.1. Introduction

In this appendix the configuration of the NDWCT's used in this thesis is given. The configuration of each tower is given by Kröger (1998 and 2004) and Kloppers (2003) respectively.

KRÖGER (1998)

Cooling tower specifications:

Tower height	H_6	= 147 m
Tower inlet height	H_3	= 10 m
Tower inlet diameter	d_3	= 104.5 m
Tower outlet diameter	d_6	= 60.85 m
Number of tower supports	n_{ts}	= 72
Length of tower supports	L_{ts}	= 11.6 m
Diameter of support	d_{ts}	= 0.8 m
Drag coefficient of tower support (round)	C_{Dts}	= 1.0
Shell thickness (inlet)	t_s	= 1.0 m

Fill specifications:

Length of fill	L_{fi}	= 2.504 m
Transfer coefficient	$h_{dfi}a_{fi}/G_w$	= $0.25575G_w^{-0.094}G_a^{0.6023}$
Loss coefficient	K_{fdm1}	= $1.851G_w^{1.2752}G_a^{1.0356}$
Frontal area of fill	A_{fr}	= 8300 m ²

Other specifications:

Depth of spray zone above fill	L_{sp}	= 0.5 m
Mean drop diameter in rain zone	d_d	= 0.0035 m
Loss coefficient for contraction and fill supports based on A_{fr}	$K_{fs} + K_{ctc}$	= 0.5
Loss coefficient for water distribution system	K_{wd}	= 0.5
Kinetic energy coefficient at cooling tower outlet	α_{c6}	= 1.01
Loss coefficient for drift eliminator (type c)	K_{de}	= $27.4892Ry^{-0.14247}$
Rounded inlet of tower shell	r_i/d_3	= 0.01

KRÖGER (2004)

The configuration of this tower is the same as for Kröger (1998), the only difference being a r_i/d_3 value of 0.02.

KLOPPERS (2003)

The configuration of this tower is the same as for Kröger (2004).

APPENDIX K. AMBIENT TEMPERATURE GRADIENT

K.1. Introduction

The objective of this appendix is to show the reader that the ambient temperature gradient, as used in this thesis, is not an independent input parameter. This is done by presenting the derivation of the pressure difference between ground level and a point at an elevation z external to the tower. The derivation is based on the work of Kröger (1998 and 2004).

K.2. Derivation of the pressure difference between ground level and a point at an elevation z external to the tower

Consider a small parcel of moist air that is moved up or down in an atmospheric pressure field. The pressure gradient in a gravity field is given as

$$\frac{dp_a}{dz} = -\rho_{av}g \quad (K.1)$$

The expansion and compression processes of a gas, i.e. parcel of moist air, is termed a polytropic process. In such a process the relation between pressure and density is given by

$$\frac{p_a}{\rho_{av}^n} = C \quad (K.2)$$

where n is the polytropic exponent. From Equation (A.10) the density of air containing water vapour is expressed as

$$\rho_{av} = (1 + w) [1 - w/(w + 0.62198)] p_a / (287.08 T_a) \quad (K.3)$$

Equation (K.3) can be rearranged to give

$$\rho_{av} = \frac{1 + w}{R_{av}} \frac{p_a}{T_a} \quad (K.4)$$

where

$$R_{av} = R + wR_v, \text{ J/kgK}$$

$$R = \text{gas constant of dry air, } 287.08 \text{ J/kgK}$$

$$R_v = \text{gas constant for water vapour, } 461.52 \text{ J/kgK}$$

Substitute Equation (K.4) into (K.2) and find upon rearranging

$$p_a^{1-n} \left(\frac{R_{av}}{1+w} \right)^n T_a^n = C \quad (K.5)$$

Differentiate both sides with respect to altitude and find

$$\begin{aligned} \frac{d}{dz} \left[p_a^{1-n} \left(\frac{R_{av}}{1+w} \right)^n T_a^n \right] &= \frac{d}{dz} C = 0 \\ \therefore \left[(1-n) p_a^{-n} \frac{dp_a}{dz} \right] \left(\frac{R_{av}}{1+w} \right)^n T_a^n &+ p_a^{1-n} \left[n \left(\frac{R_{av}}{1+w} \right)^{n-1} \frac{(1+w) \frac{dR_{av}}{dz} - R_{av} \frac{dw}{dz}}{(1+w)^2} \right] T_a^n + \\ p_a^{1-n} \left(\frac{R_{av}}{1+w} \right)^n \left[n T_a^{n-1} \frac{dT_a}{dz} \right] &= 0 \end{aligned} \quad (K.6)$$

In order solve Equation (K.6), Kröger (1998 and 2004) suggests a constant humidity ratio, implying that $dw/dz = 0$ as well as $dR_{av}/dz = 0$. Equation (K.6) then reduces to

$$\left[(1-n)p_a^{-n} \frac{dp_a}{dz} \right] \left(\frac{R_{av}}{1+w} \right)^n T_a^n + p_a^{1-n} \left(\frac{R_{av}}{1+w} \right)^n \left[nT_a^{n-1} \frac{dT_a}{dz} \right] = 0 \quad (K.7)$$

Multiplying Equation (K.7) with $n^{-1}p_a^{-1+n}T_a^{-n+1}[R_{av}/(1+w)]^{-n}$ and substituting for dp_a/dz from Equation (K.1) yields

$$\frac{dT_a}{dz} = -\left(\frac{1-n}{n} \right) \frac{T_a}{p_a} (-\rho_{av}g) = -\left(\frac{1-n}{n} \right) \frac{T_a}{p_a} \left(-\frac{1+w}{R_{av}} \frac{p_a}{T_a} g \right) \quad (K.8)$$

Recall that the result of interest is the pressure difference between ground level and a point at an elevation z external to the tower. This is given by Equation (K.1) as

$$\frac{dp_a}{dz} = -\rho_{av}g \quad (K.9)$$

Since ρ_{av} in the above equation is dependent on temperature, Equation (K.8) and (K.9) are coupled. In order to solve for T_a in Equation (K.8), Kröger (1998 and 2004) makes the following assumptions:

- The compression and expansion process of the air-vapour mixture is isentropic, $n = \gamma_{av}$
- The ambient air is assumed to be completely dry air, $w = 0$

For dry air, $n = 1.4$, and Equation (K.8) thus reduces to

$$\frac{dT_a}{dz} = -\left(\frac{1-n}{n} \right) \frac{T_a}{p_a} \left(-\frac{1}{R} \frac{p_a}{T_a} g \right) = -\left(\frac{1-1.4}{1.4} \right) \frac{9.8}{-287.08} = -0.00975 \text{ K/m} \quad (K.10)$$

which is also known as the dry adiabatic lapse rate (DALR). Upon integration of Equation (K.10) between ground level and an elevation z external to the tower find

$$T_{az} = T_{a1} - 0.00975z \quad (K.11)$$

where T_{az} is a dry bulb temperature at some elevation z external to the tower. It is now possible to solve for p_a in Equation (K.9). In solving for p_a , Kröger (1998 and 2004) now assumes that the ambient air has a constant humidity ratio of $w = w_1$, where w_1 is the humidity ratio at ground level. Substitute Equation (K.3) and (K.11) into Equation (K.9) to find

$$\begin{aligned} \frac{dp_a}{dz} &= -(1+w_1) \left[1 - w_1/(w_1 + 0.62198) \right] p_a / \left[287.08(T_{a1} - 0.00975z) \right] g \\ \frac{dp_a}{p_a} &= -g \frac{(1+w_1) \left[1 - w_1/(w_1 + 0.62198) \right]}{\left[287.08(T_{a1} - 0.00975z) \right]} dz \end{aligned} \quad (K.12)$$

Since Kröger (1998 and 2004) assumed a constant humidity ratio, Equation (K.12) can be rewritten as

$$\frac{dp_a}{p_a} = -K \frac{dz}{(T_{a1} - 0.00975z)} \quad (K.13)$$

where

$$K = \frac{g}{287.08} (1+w_1) \left(1 - \frac{w_1}{w_1 + 0.62198} \right) \quad (K.14)$$

Integrating Equation (K.14) between ground level and a point at an elevation z external to the tower yields

$$\begin{aligned}
\ln p_{a|z} &= \frac{K}{0.00975} \ln(T_{a1} - 0.00975z) \Big|_1^z \\
\therefore p_{az} &= p_{a1} \left[1 - \frac{0.00975z}{T_{a1}} \right]^{\frac{K}{0.00975}} \\
&= p_{a1} \left[1 - \frac{0.00975z}{T_{a1}} \right]^{\frac{1}{0.00975} \frac{g}{287.08} (1+w_1) \left(1 - \frac{w_1}{w_1+0.62198} \right)} \\
&= p_{a1} \left[1 - \frac{0.00975z}{T_{a1}} \right]^{3.5(1+w_1) \left(1 - \frac{w_1}{w_1+0.62198} \right)}
\end{aligned} \tag{K.15}$$

The pressure difference between ground level and a point at an elevation z external to the tower is thus given as

$$p_{a1} - p_{az} = p_{a1} \left[1 - \left(1 - 0.00975 \frac{z}{T_{a1}} \right)^{3.5(1+w_1) \left(1 - \frac{w_1}{w_1+0.62198} \right)} \right] \tag{K.16}$$

The draught equation used in this thesis, as discussed in Section 2.2, is based on Equation (K.16).

SUMMARY OF ASSUMPTIONS

- In solving for T_a in Equation (K.8), Kröger (1998 and 2004) assumes that the compression and expansion process of the air-vapour mixture is isentropic, $n = \gamma_{av}$ and that
- the ambient air is completely dry air, $w = 0$
- In solving for p_a in Equation (K.12), Kröger (1998 and 2004) assumes a constant humidity ratio, i.e. $w = w_1$.

Note that Kröger (2004) gives a derivation of the ambient temperature distribution, assuming a constant humidity ratio.

K.3. Ambient temperature gradient as independent input parameter

From a mathematical point of view, the ambient temperature gradient can only be an independent input parameter if it is not a function of other parameters. From Equation (K.6) one can see that this is not the case since dT_a/dz is a function of the humidity distribution, as well as the type of thermodynamic process (value of exponent n).

One might argue that the assumptions leading to Equation (K.16) renders the above statement invalid, which is partially true. However, when looking at Equation (K.16) one can see that the 3.5 value in the exponent is given by

$$\frac{1}{\frac{dT}{dz}} \frac{g}{287.08} = \frac{1}{0.00975} \frac{9.8}{287.08} = 3.5 \tag{K.17}$$

Thus, if one wishes to change the dT_a/dz value of -0.00975 , the 3.5 value in Equation (K.16) has to change as well, which will not happen since the 3.5 value is assumed fixed in solving the draught equation. One can conclude that using the current method to solve the draught equation, dT_a/dz can not be considered an independent input parameter.